NASA/CR-1998-208445

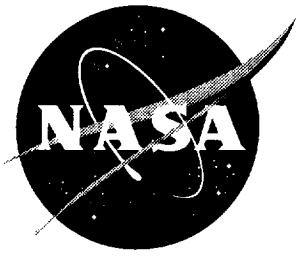

Supersonic Leading Edge Receptivity

Anatoly A. Maslov
Institute of Theoretical and Applied Mechanics, Novosibirsk, Russia

National Aeronautics and
Space Administration

Langley Research Center
Hampton, Virginia 23681-2199

Prepared for Langley Research Center
under Cooperative Agreement NCC1-240

June 1998

Available from the following:

NASA Center for AeroSpace Information (CASI)
7121 Standard Drive
Hanover, MD 21076-1320
(301) 621-0390

National Technical Information Service (NTIS)
5285 Port Royal Road
Springfield, VA 22161-2171
(703) 487-4650

Principal Investigator: Deputy of Director, Professor Anatoly A. Maslov

Head of Laboratory: Dr. S.A.Gaponov

Experimental Group:

Dr. A.D.Kosinov

Dr. N.V.Semionov

Mr. V.E.Novikov

P.G.St. Yu.G.Ermolaev

CONTENTS

List of symbols

M - Mach number,
Nu - Nusselt number,
ρ - density,
x, y, z - cartesian coordinates fixed with respect to the flat plate,
Re_1 - unit Reynolds number, m^{-1},
T - temperature (absolute),
T_w - heating wire temperature,
T_e - wire recovery temperature,
T_o - stagnation temperature,
U - freestream velocity,
η - recovery factor ($\eta = T_e/T_o$),
Re_d - Reynolds number based on the hot-wire diameter,
E - anemometer output voltage,
e, e' - voltage fluctuations across hot wire,
l - length of the hot-wire element,
a_w - overheat ratio of the wire $\left(a_w = \frac{R_w - R_e}{R_e} \right)$,
d - diameter of the wire,
R_w - wire resistance at operating temperature T_w,
R_e - wire resistance at operating temperature T_e,
Q - dimensionless sensitivity to the mass flow fluctuations,
F - dimensionless frequency parameter($F = 2\pi f/(Re_1 U)$),
G - dimensionless sensitivity to the total temperature fluctuations,
k_m - sensitivity factor to the mass flow fluctuations,
k_θ - sensitivity factor to the total temperature fluctuations,
θ - root-mean-square (r.m.s.) value of the hot-wire output, %,
$\langle m \rangle$ - dimensionless r.m.s. mass flow fluctuations,
$\langle T_o \rangle$ - dimensionless r.m.s. stagnation temperature fluctuations,
r - sensitivity ratio,
P_o - stagnation pressure, kg/m^2,
P_{st} - static pressure, kg/m^2,
τ - overheat ratio $\left(\tau = \frac{T_w - T_e}{T_0} \right)$.

Preface

This study «Supersonic Leading Edge Receptivity» is proceeded according to the Research Cooperative Agreement between NASA (USA) and Institute of Theoretical and Applied Mechanics of Siberian Division of Russian Academy of Science (ITAM), signed in 1995 (first year Grant number NCCW-74, second and third years Grant number NCC-1-240).

According to the Agreements, investigations of receptivity problem should be made using controlled disturbances during three years. The field of controlled disturbances were excited using the local disturbance generator placed in the test section of supersonic wind tunnel. During the first year, the levels and modes of natural and artificial fluctuations were determined by the hot-wire measurements in the free stream of ITAM T-325 supersonic wind tunnel at Mach numbers 2 and 3.5. In the second year, sharp leading edge receptivity was studied using controlled disturbances. In the third year, the receptivity was studied for the case of a flat plate with blunted leading edge (bluntness radius was 2.5 mm).

Since ITAM T-325 wind tunnel does not belong to the category of low-noise wind tunnels, the fulfillment of scheduled work was preceded by technical works for reduction of noise level in the test section of T-325. Namely, they were:
(a) a grinding of a surface of settling chamber part behind damping screens and (b) polishing of the surface of the test section and the entrance to the test section. This allowed us to achieve at least 20% reduction of acoustic noise level in T-325 test section for M=2 and 50% — for M=3.5. As for the introduction of controlled disturbances into the free stream, the source of disturbances was improved in comparison with our early works (Kosinov et al. 1994[1]) to study the receptivity problem in controlled conditions. It was made to ensure the smooth adjustment of controlled disturbance intensity and to gain an additional experience in such experiments.

The programs for automated hot-wire measurements with regard to determination of pulsation modes were based on the method, proposed by Kovasznay (1950), and the appropriate programs for data processing were used.

1. Introduction

Now it is common knowledge, that laminar-turbulent transition in boundary layers is associated with receptivity and instability (an amplification of disturbances, which cause transition) processes. Usually the term «receptivity» means the mechanism, through which the various external disturbances excite unstable oscillations inside boundary layer, leading to transition (Morkovin 1969). In particular, the solution of receptivity problem is connected with the development of engineering methods of transition prediction (Bushnell 1990; Reshotko 1976, 1994). Now it is necessary to design a new generation of high-speed airplanes, therefore the receptivity problem is very important.

The majority of theoretical and experimental studies of receptivity problem was carried out for subsonic flows. The first experimental study of the receptivity problem was made by Klebanoff (1971). This pioneer work provided an influence on further experimental studies.

More exhaustive reviews can be found in Nishioka & Morkovin 1986; Kachanov et al. 1981; Goldstein & Hultgren 1989; Kendall 1990, 1998; Heinrich et al 1988. In low speed flows, the wavelengths of free-stream disturbances (acoustic and vortex modes) are much longer than wavelengths of boundary layer instability fluctuations. Therefore, the transformation of external disturbances to the eigenwaves of the boundary layer occurs near the leading edge and is caused by roughness, local separation and other flow inhomogeneities. Here we should cite only some theoretical and experimental studies related to subsonic receptivity problem: (Bushnell 1990; Nishioka & Morkovin 1986; Kachanov et al. 1981; Goldstein & Hultgren 1989; Goldstein 1983; Choudhari & Street 1992; Aizin & Polyakov 1979; Nayfeh & Ashour 1994; Saric et al. 1994; Kosorygin et al. 1995; Kobayashi et al. 1995; Crouch 1994; Bertolotti 1995; Kachanov 1996; Kendall 1990, 1998; Herbert et al. 1993; Westin at al. 1994; Crouch & Spalart 1995).

At supersonic speed the problem is more complicated, and it still was not studied in detail. The first attempt to study theoretically the interaction between sound waves and supersonic boundary layer on the basis of linear stability theory

was undertaken by Mack (1975). It was obtained, that under the action of external sound waves, the growing oscillations appeared in the boundary layer, and that their amplitudes were many times the acoustic waves amplitudes. Similar studies were carried out by Gaponov (1977). The localized generation of Tollmien-Schlicting (TS) waves in supersonic boundary layer was analyzed by Choudhari & Street (1990). They obtained that «receptivity could occur either due to nonparallel effects close to the leading edge and in regions of short-scale variations in wall boundary conditions, or as a result of local resonances between the free-stream unsteadiness and the instability waves». It was found that generation of TS waves by free stream vorticity or entropy modes are an order lower than those due to the action of external acoustic waves. The most effective receptivity mechanism takes place for oblique acoustic waves and streamwise inhomogeneity in geometry (Choudhari & Street 1990).

We should note the theoretical studies (Fedorov & Khohlov 1991; 1992; Duck 1990; Choudhari & Street 1993) of the leading edge receptivity to external sound waves in supersonic boundary layer. An excitation of the first and the second modes by longitudinal sound waves in the vicinity of a sharp leading edge of flat plate was analyzed by Fedorov & Khohlov (1991). An excitation was caused by sound diffraction at the displacement effect of boundary layer. These results were generalized by Fedorov & Khohlov (1992) for any falling angle of an external wave. Two mechanisms of excitation were defined there. *First mechanism was connected with diffraction of the sound waves and the second — with occurrence of sound field sources due to wave interference on the leading edge.* From this point of view it may be obtained, that the generation of unstable waves in the boundary layer depends on the inclination angle of the acoustic wave and on the direction from where the sound waves falls, i.e. from above or below. The excitation of the oscillations by longitudinal sound field in boundary layer was investigated by Gaponov (1995). Strong dependence of disturbance intensity inside boundary layer from spatial orientation of the forced sound wave was obtained in this work. Study of blunted edge receptivity appeared most recently (Xiaolin Zhong 1997). We should note that

the verifications of foregoing conclusions (Fedorov & Khohlov 1992; Gaponov 1995; Duck et al. 1997; Xiaolin Zhong 1997) calls for extended experimental investigations.

In the first experiments the influence of external factors (level of a free stream turbulence, model vibrations, acoustic background disturbances) on laminar-turbulent transition was studied. But for better understanding of transition process it is necessary first of all to study the generation and the development of unstable waves, leading to transition. Such approach was used at Mach number M=1.6÷8.5 by Kendall (1975) who tested the development of natural disturbances in the boundary layer and also measured the correlation coefficients between fluctuations in the free stream and inside the boundary layer. Large intensity of disturbances in the boundary layer in a region close to the leading edge, caused by influence of an external sound field, was found out. It was found that at M>3 the aerodynamic noise in the test section led to the monotonic growth of the disturbances in the boundary layer from the leading edge of model. Correlation measurements have shown, that correlation coefficients increased with increasing Mach number M. Comparison of experimental results (Kendall 1975) with theory developed by Mack (1984) showed a good agreement for M=4.5.

A source of controlled disturbances developed at supersonic speeds by Kosinov et al. (1983) allowed to carry out experimental study of receptivity problem (Maslov & Semionov 1986; 1987[1]; 1989; Kosinov et al. 1990[1]) as well. In Maslov & Semionov (1986; 1987[1]) it was established, that the most intensive generation of eigen oscillations of the supersonic boundary layer by the sound waves takes place in the following areas: the leading edge, lower branch of a neutral stability curve and a "sound" branch. A wave structure of boundary layer disturbances, induced by the sound waves which fell on the flat plate leading edge from above, was investigated in Maslov, Semionov (1989). The obtained data was compared with the structure of wave disturbances, induced by the local source in the boundary layer (Kosinov et al. 1990[1]). The results (Kosinov et al. 1994[1]; 1990[1], Maslov & Semionov 1986; 1987[1]) showed a complicated picture of transformation of acoustic waves into boundary layer unstable disturbances. In particular, the excitation of the unstable disturbances

in the boundary layer can occur in various places and for the different reasons (Bushnell 1990; Nishioka & Morkovin 1986; Maslov & Semionov 1986).

The technique of receptivity researches was modified several years ago (Kosinov et al. 1994[1]). The leading edge receptivity was recently investigated experimentally in Kosinov et al. (1994[1]), Semionov et al. (1996). In this case acoustic waves fell from below and the excitation of unstable waves took place only in the leading edge region. This method allowed to obtain the receptivity coefficients (the ratio of generated disturbance amplitude in the boundary layer to the amplitude of acoustic wave which fell on the leading edge) for the first time. The maximum receptivity coefficients were observed for the waves with inclination angles χ=20÷40°. Experimental investigations of hypersonic leading edge receptivity began only with the help of our method (Maslov et al. 1998). We should note that all our previous receptivity experiments were carried out using surface discharge as the source of controlled disturbances. That source was improved later and now it is based on the discharge in a chamber (Kosinov et al. 1996). It was made to ensure smooth adjustment of intensity of controlled disturbances and to gain an additional experience in such investigations. All data presented in this report were obtained with the new source of controlled disturbances.

However the carried out studies are still insufficient to understand the generation of unstable disturbances in boundary layer by external disturbances. As it follows from a number of papers, the receptivity problem is rather complicated and extensive. There is no all-purpose solution of this problem now. It is necessary to find this solution for each specific case. New additional results connected with this problem should be forthcoming.

The following report presents experimental study of generation of unstable disturbances in supersonic boundary layer by external controlled disturbances in sharp and blunted leading edge of the flat plate.

2. Experimental equipment and data processing

2.1. Wind tunnel

Experiments were carried out in periodic action supersonic wind tunnel T-325 ITAM SD RAS. The main characteristics of wind tunnel T-325 are as follows:

- Range of Mach numbers: from 0.5 up to 4;
- Range of unit Reynolds numbers: $(3.5 \div 160) \times 10^6$ m^{-1};
- Stagnation pressure: up to 14 atm.;
- Sizes of test section: 0.2×0.2×0.6 m;
- Duration of continuous work: - up to 60 minutes.

The working range of Mach numbers was realized by installation of replaceable nozzles with a step in Mach numbers - 0.5.

For the reduction of speed fluctuations, acoustic noise level, vibrations of wind tunnel construction, the following steps have been taken:

- Large reducing degree of a flow (for M=2 reducing degree was 35.7, for M=3.5 reducing degree was 130.8); the reducing degree of a flow was calculated as the ratio of settling chamber cross section before entrance in nozzle to the critical nozzle section;
- Multistep system of noise suppression after constrictors;
- Installation of 8 damping screens and honeycombs in settling chamber;
- Vibration-proof positioning of test section and special vibration suppressing devices.

The non-uniformity of Mach numbers in test section did not exceed 0.8 %.

The diagram of wind tunnel T-325 is shown in Fig.2.1. The wind tunnel is built up with traversing equipment of test section. Traversing equipment of test section represents the gear for moving of models, measuring devices, probes in three mutually perpendicular direction:

- Streamwise axis "x": a travel is 265 mm;
- Crossflow axis "y" and "z": a travel is 160 mm.

The accuracy of a travel makes 0.1 mm.

The wind tunnel is equipped with traversing equipment, which has an accuracy of a travel 0.01 mm, for more precise measurements in the boundary layer of model.

T-325 wind tunnel is equipped by measuring system for pressure and temperature measurements in settling chamber and test section.

Fig.2.2 shows a view of test section and a part of settling chamber.

2.2. Measuring system

The wind tunnel is equipped by automated measuring system for non-stationary and stationary flow parameters as well as probe position measurements. The automated measuring system is based on two Russian-made micro-computers connected with CAMAC. The given equipment permits to apply the input of experimental data in PC, to accumulate the data and to create local archives, to process the data and to output an express information on display, as well as to control the work of wind tunnel. The scheme of automated measurements in supersonic wind tunnel is shown in figs.2.3, 2.4. This scheme was used in experiments.

Constant temperature hot-wire anemometer (or constant current hot-wire anemometer) has been used for disturbance measurements. AC signal from hot-wire output was recorded in PC memory using 10-bit and 1MHz ADC (in the third year — 12-bit 750kHz ADC, thanks to kind gifts from Dr. James. M. Kendall). DC signal from hot-wire output was measured using five decade voltmeter. At mean flow measurements, ADC had impulse start generated by the block of synchronization. At controlled disturbance measurements, the start impulse was time-synchronized with a signal from sine-shaped wave generator that was used to ignite the glow discharge. This procedure provided synchronization of ADC start with phase accuracy better than 1° in sine-shaped wave signal.

Constant temperature hot-wire anemometer, made in ITAM, was used in these experiments. Throughout the first and the second year, hot-wire in use had the Winston bridge with resistance ratio of 1:5 and frequency response up to 200 kHz.

The last year a new hot-wire with resistance ratio of circuit arms 1:10 and frequency response up to 500 kHz was in use. Probes were fabricated of tungsten wire with 5 microns diameter.

2.3. Data processing

For experiments conducting and data processing we used the results, published in Kovasznay (1950), Zinojev & Lebiga (1990), and Kovasznay (1953). Basic formulas, used for the data processing, are given below.

The following relations, that are applied to the interpretation of the hot-wire results in the supersonic flows (Kovasznay 1950, Smits et al. 1983, Zinovjev & Lebiga 1990), are well known:

$$Nu = \frac{E^2 R_w}{\pi \lambda l \left(R_a + R_w\right)^2 \left(T_w - T_e\right)} = A_1 f(\tau) + B_1 g(\tau) \mathrm{Re}^n = \qquad (1)$$

where A, A_1, B, B_1 are certain dimensionless factors, determined by calibration, R_a=23 Ohm, and the functions f and g are defined similar to Smits et al. (1983) by expressions: $f(\tau)=1-f'(\tau)$, $g(\tau)=1-g'(\tau)$.

The relation (1) is usually used in dimensional form:

$$E^2=L+N(\rho U)^n, \qquad (2)$$

where L and N are dimensional calibration coefficients.

As hot-wire in supersonic flow is sensitive to the mass flux $(\rho U)'$ and temperature T_o' fluctuations, we have:

$$e' = \left.\frac{\partial E}{\partial \rho U}\right|_{T_0} (\rho U)' + \left.\frac{\partial E}{\partial T_0}\right|_{\rho U} T_0'$$

or

$$e' = k_m m' + k_\vartheta T_0',$$

where relations $k_m = \left.\frac{\partial E}{\partial \rho U}\right|_{T_0}$, $k_0 = \left.\frac{\partial E}{\partial T_0}\right|_{\rho U}$ define dimensional sensitivity factors.

Following Smits et al. (1983), we can express k_m and k_θ in the form:

$$k_m = \left.\frac{\partial E}{\partial \rho U}\right|_{T_0} = \frac{nM}{2E}\left[\frac{E^2 - L}{M}\right]^{\frac{n-1}{n}},$$

$$k_0 = \frac{1}{2E}\left\{\frac{E^2}{T_0}\left(a - \frac{\eta}{\tau}\right) - \frac{(\tau+\eta)}{T_0}\left[\frac{L\partial f}{f(\tau)\partial\tau} + \frac{(E^2 - L)\partial g}{g(\tau)\partial\tau}\right] - \frac{bn(E^2 - L)}{T_0}\right\} =$$

$$= \frac{E}{2T_0}\left(a - \frac{\eta}{\tau} - \frac{bn(E^2 - L)}{E^2} - \frac{(\tau+\eta)}{E^2}\left[\frac{L}{f(\tau)}\frac{\partial f}{\partial\tau} + \frac{(E^2 - L)}{g(\tau)}\frac{\partial g}{\partial\tau}\right]\right)$$

Here n=0.5, recovery factor is η=0.95±0.01 (η was defined by special measurements), and coefficients a=b=0.768 are taken from power laws for heat conductivity:

$$k = k_1\left(\frac{T}{T_1}\right)^a$$

and viscosity:

$$\mu = \mu_1\left(\frac{T}{T_1}\right)^b.$$

Reynolds number was determined to the wire diameter:

$$\mathrm{Re} = \frac{\rho U d}{\mu},$$

overheat ratio was defined by following expressions:

$$E^2 = \frac{\pi k l (R_a + R_w)^2 (T_w - T_e)}{R_w}\left[Af(\tau) + Bg(\tau)\mathrm{Re}^n\right] = E',$$

$$\tau = \frac{T_w - T_e}{T_0}.$$

Dimensionless factors of sensitivity to fluctuations of the mass flux (Q) and the stagnation temperature (G) were defined by expressions:

$$Q = \frac{k_m \rho U}{E} = \frac{n}{2}\left(1 - \frac{L}{E^2}\right),$$

$$G = \frac{k_\theta T_0}{E}.$$

Dimensionless root-mean-square fluctuations were defined by expressions:

$$\theta = \frac{e'}{k_\theta T_0}.$$

As the fluctuation mode diagrams were linear functions for all measurements, the governing equation can be written like this:

$$\theta = r\langle m' \rangle + \langle T_o' \rangle ,$$

where r is the relative sensitivity, defined by the following ratio:

$$r = \frac{Q}{G} = \frac{k_m \rho U}{k_\theta T_0} .$$

To determine the controlled disturbance level, some assumptions were used: (a) relation between mass flux fluctuations and stagnation temperature fluctuations is constant in the course of every given experiment and (b) this value is large, i.e.

$$\frac{< m >}{< T_0 >} = A_o = const \quad \text{and } A_o >> 1.$$

Then mass flux fluctuations can be expressed in the form:

$$\langle m'(x, y, z) \rangle = \frac{\theta(x,y,z) A_0}{rA_0 + 1} = \frac{e' A_0}{k_\theta T_0 (rA_0 + 1)} = \langle e' \rangle A_{<m>} .$$

Measurements of controlled disturbance field, generated by the source, were carried out at frequency 20 kHz. A selective amplifier with 1% bandwidth and output connected with ADC was used for these measurements. Application of selective amplifier allowed to reduce the number of summations over realizations up to 200 (with the purpose to determine the controlled signal), that sped up the measurement process. Complete length of each realization was 4096 points, but only first 200 points (that corresponds to four periods at frequency 20 kHz) were used for averaging procedure. During experiment was supervised each, from averaged 200 times, oscillograms, and then it was recorded in data file. The source generates disturbances with divisible frequencies by 10 kHz. On the other hand, since controlled disturbances are rather small in free stream, much more summations are needed to select them from complete signal.

Since the purpose of this study was to determine the level of controlled disturbance field, Fourier time-transformation in the form of Fourier series was used for oscillograms processing:

$$e_f(x,y,z)=e_f(x,y,z)e^{i\Phi(x,y,z)} =$$

$$=\frac{2}{T}\int_0^T e(x,y,z,t)e^{-i\omega t}dt = \frac{2}{N}\sum_{j=1}^{N} e(x,y,z,t_j)e^{-i\omega t_j},$$

where T is the length of realization in time, N is the number of points in realization, e_f are amplitudes of Fourier components, and Φ is the phase. Discrete Fourier transformation was used to determine amplitudes $e_f(\beta)$ and phases $\Phi(\beta)$ of pulsation's β-spectra:

$$e_f(x,\beta)\exp(i\Phi(x,\beta))=\Sigma e_f(x,z_j)\ \exp(-i\beta z_j).$$

To determine the absolute value of controlled disturbances at frequency 20 kHz, the root-mean-square value of a signal was used:

$$e_f^{'} = \frac{e_f}{\sqrt{2}}.$$

The transfer coefficient (i.e. a ratio of excited disturbance amplitude inside the boundary layer to the forced oscillation amplitude of the acoustic wave, falling on the leading edge), were found from the relation:

$$K(\beta) = \frac{m_f(\beta)\big|_{x=x_i}}{m_f(\beta)\big|_{x=x_0}}.$$

The total (integrated and dimensionless) controlled pulsation of mass flux was defined by:

$$m_{tot}=\int m_f(\beta)d\beta.$$

Mean transfer factors K were defined using values of m_{tot} by:

$$K=m_{bl}/m_{fs},$$

where m_{bl} and m_{fs} are mass flux pulsations in free stream and in boundary layer, respectively.

2.4. Figures

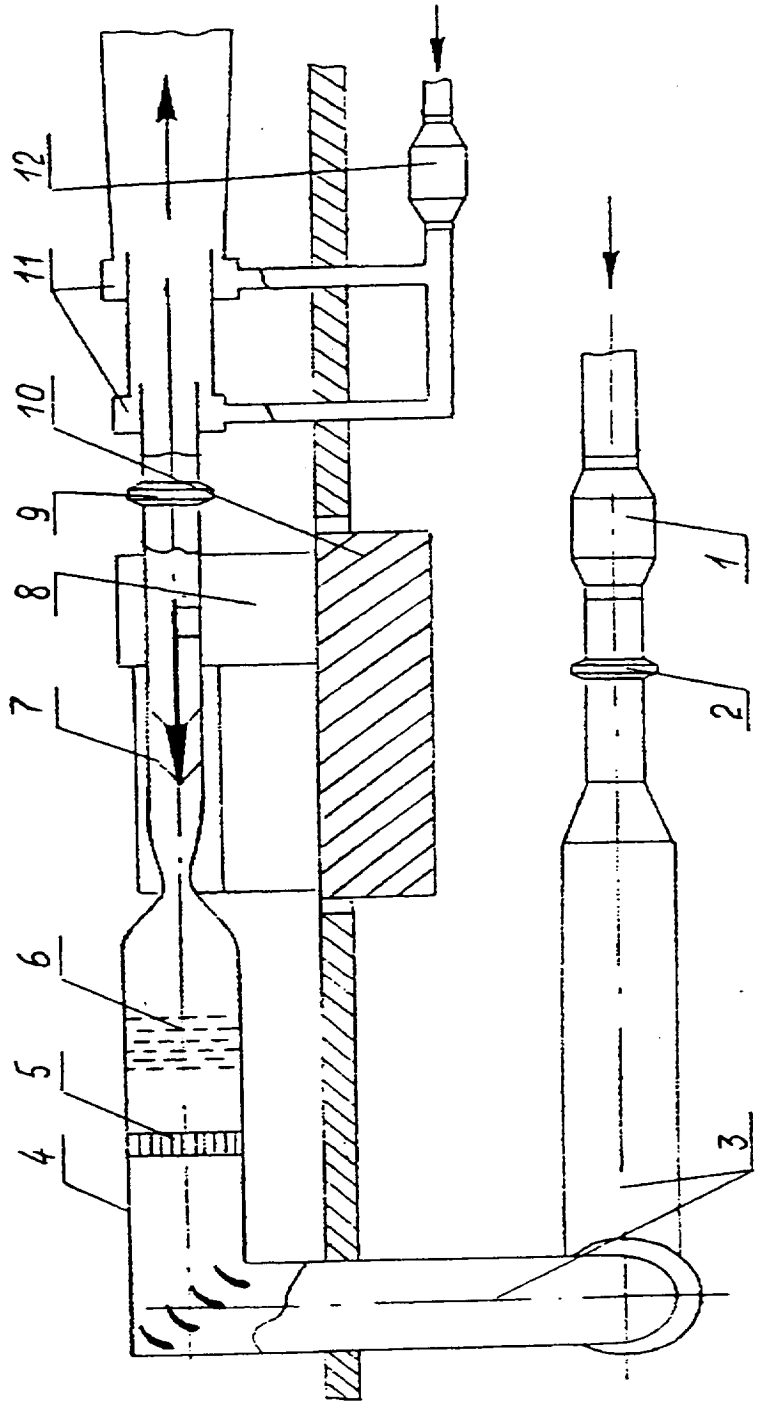

Fig.2.1. Diagram of T-325: 1, 12 - constrictors; 2, 9 - dampers; 3 - noise suppression compartments; 4 - settling chamber; 5 - honeycomb; 6 - damping screens; 7 - test section; 8 - traversing equipment of test section; 10 - vibroisolated foundation; 11 - ejectors.

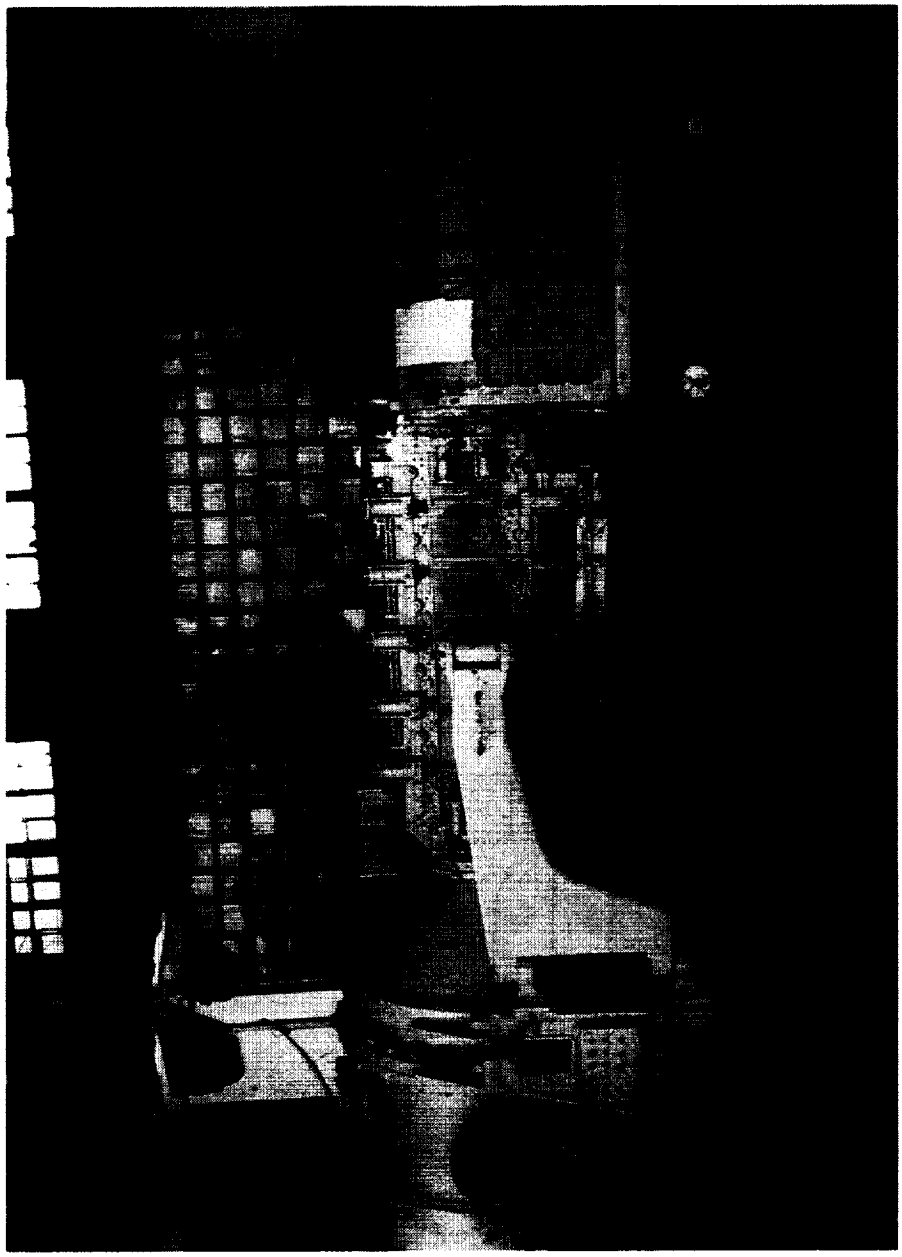

Fig.2.2. Photo of T-325 test section

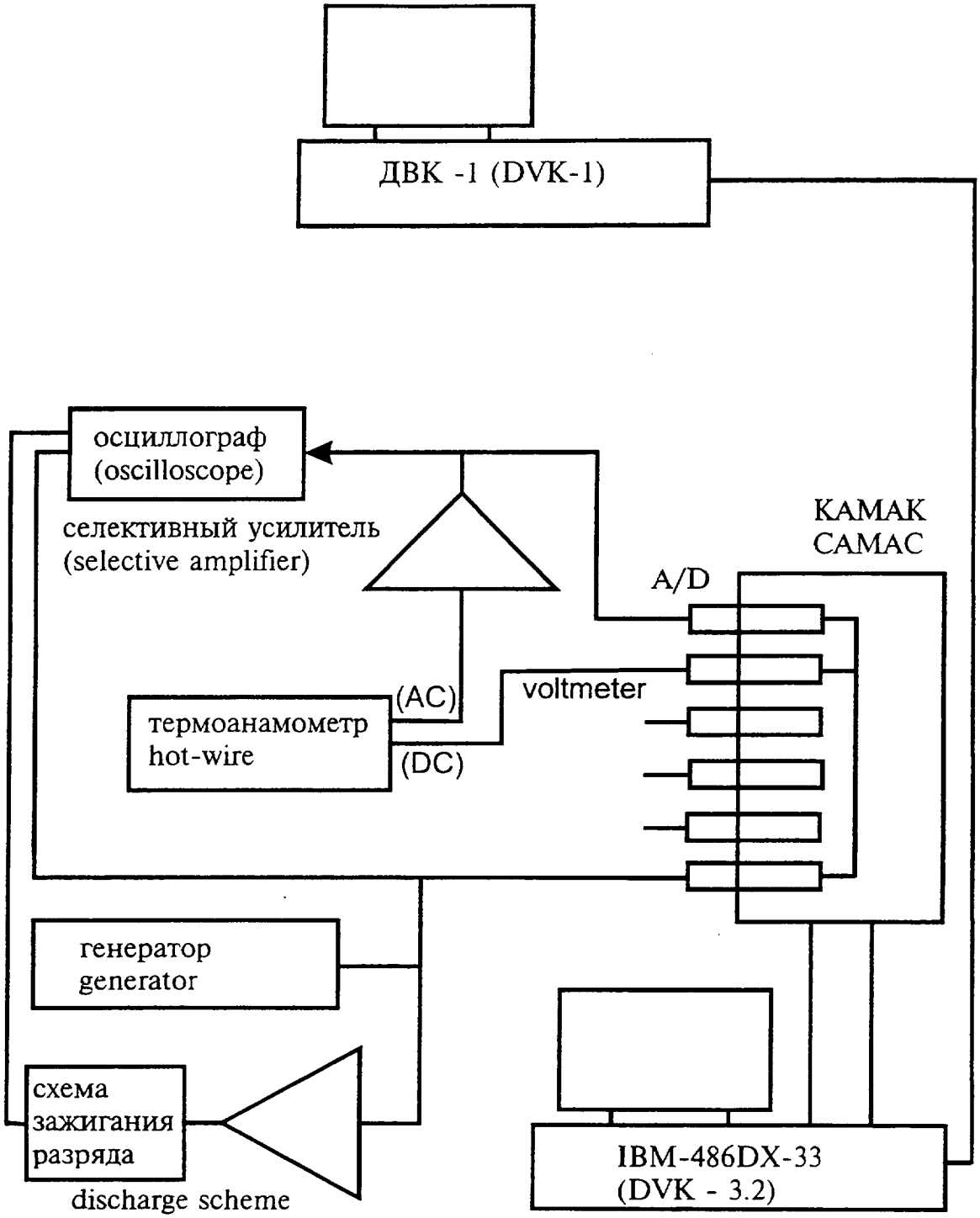

Fig.2.3. Scheme of measurements

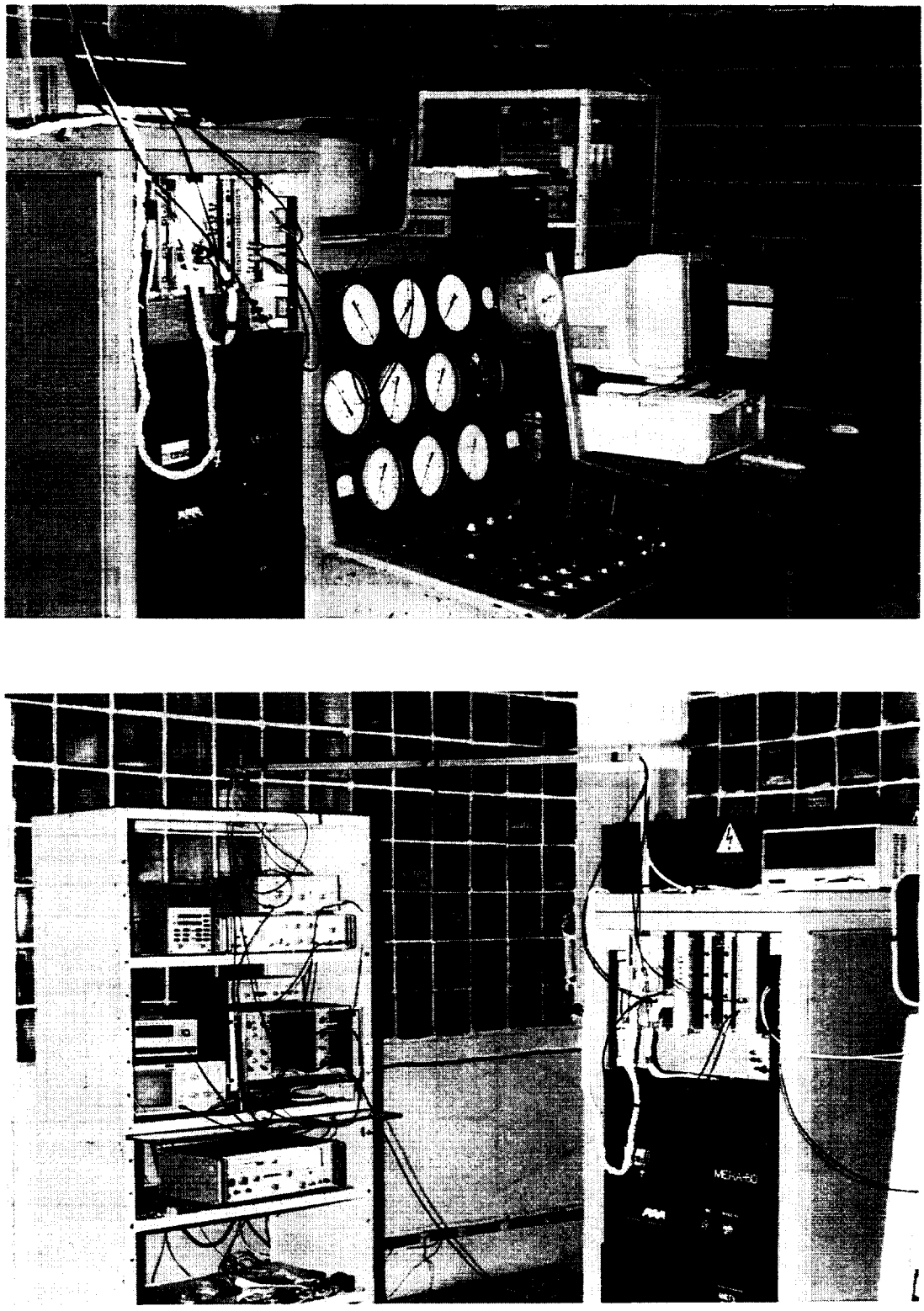

Fig.2.4. Photos of T-325 control panel and measuring equipment

3. On the pulsation level of natural and controlled disturbances in the test section

Following scheduled program, the measurements were carried out to investigate the spectrum and amplitudes of background disturbances in supersonic wind tunnel T-325 free stream at Mach numbers 2 and 3.5. Forced disturbance field in free stream was studied as well at Mach numbers 2 and 3.5.

3.1. Organization of experiments

Glow discharge on the flat plate surface was used earlier as a source of controlled disturbances (Semionov et al. 1996) in our experiments on the leading edge receptivity at Mach number M=2. Increased measurement accuracy allowed to use the less powerful source of controlled disturbances, namely, a glow discharge in the chamber. This source of controlled disturbances has many points in its favour: it is more durable and more stable in time; it produce less electromagnetic noise; it allows to regulate disturbance intensities moor smoothly. Therefore the glow discharge in the chamber instead of the surface glow discharge was used in these experiments.

3.2. Flat plates

The experimental installation is shown in fig.3.1 (and also on photographs, figs.3.2, 3.3). We used two trapezoidal plates, placed under zero angle of attack. The plate *1* with generator of periodic disturbances was mounted on traversing equipment bar and during experiment could moved to vary the distance from the wall of wind tunnel test section. The plate *1* was 80 mm length, 80 mm width at a top and 60 mm at a basis, 5 mm thick. Slope angles of leading edge and lateral sides were 14°30′. The distance a between the plate *1* and the test section wall was different for Mach numbers 2 and 3.5. Namely, a=76 mm (see fig.3.1) for M=2 and a=90 mm for M=3.5. The design of periodic disturbances generator is based on electric discharge

in a chamber and is similar to the source described in Kosinov et al. (1990[2]). The artificial disturbances entered supersonic flow through 0.5 mm aperture in the working surface of the flat plate. Coordinates of the source were: x=18±0.25 mm, z=0, where x is a streamwise coordinate from the leading edge of plate *1*, z is a spanwise coordinate in the symmetry plane of the plate *1*. Disturbances at frequency 20 kHz were generated using high-frequency electric discharge, because it radiates rather intensive acoustic waves in free stream (Maslov & Semionov 1987[2]).

The plate *2* was fastened to pylon at 116 mm from the wall of T-325 test section. The plate *2* was 280 mm length, 160 mm width at top and 80 mm at basis, 7 mm thick. Slope angles of sharp leading edge and lateral sides were 14°30′. The constructional arrangement allowed for remounting the plate *2* at various distances b (see fig. 3.1) in streamwise direction. The leading edge radius was less than 0.03 mm.

3.3. Results

All measurements were carried out using constant temperature hot-wire anemometer. We used probe fabricated of tungsten wire l=0.76 mm length and 5 microns in diameter. Presented in items 3.3.1 and 3.3.2 measurements were made in one point at test section centerline, since dimensional root-mean-square pulsation magnitudes were constant when hot-wire probe moved (as far as it was possible) in x, y, z-directions. Controlled disturbance field in free stream was studied in the plane of plate *2*, except when a structure of radiation in normal direction from the plane of plate *1* (see fig.3.1) was investigated.

3.3.1. Level of fluctuations in the test section of T-325 at M=2

Fig.3.4 shows dimensional calibrating dependencies at different wire heating (here $0.54<a_w<1.0$ and $0.46<\tau<0.86$). Corresponding dimensional values of calibrating constants as the functions of τ are presented in fig.3.5. The change of stagnation temperature at these measurements comprised T_0=283±0.2°K with

exception of separate points. It is seen that stagnation temperature was stable, since the scatter of points is basic stacked in error of definition T_0 (0.1%). Fig.3.6 shows dimensionless calibrating dependence $Nu\left(\sqrt{\mathrm{Re}_d}\right)$ at different overheat ratio of the wire, and dependence $Nu(\tau)$ is shown in fig.3.7 at different Re_d. Presented in fig.3.8 data show relative changing of Nusselt number from overheat loading τ at different Re_d. Variation of dimensionless calibrating factors A, B on τ are shown in fig.3.9. The functions $f(\tau)$ and $g(\tau)$ were determined from this data and are shown in fig.3.10. These functions were used at further processing of measurement data.

It was obtained that

$$g(\tau)=1-0.015\tau \quad \text{and} \quad f(\tau)=1-0.76\tau,$$

which is quite similar to the data presented in Smits et al.(1983), where at n=0.55 it was obtained that

$$g(\tau)=1-0.085\tau \quad \text{and} \quad f(\tau)=1-0.65\tau.$$

The dimensionless values of sensitivity to the mass flux fluctuations Q and to the stagnation temperature fluctuations G are presented in fig.3.11 and 3.12. Let us not that $L>0$, if $n>2Q$ and $L<0$, if $n<2Q$. In the experiments it was obtained Q=0.24 and for n=0.5 it was defined $L>0$. From the last experiments using the new CTA we determined Q=0.27. In this case in order to obtain $L>0$ n=0.56 was chosen. As would be expected, factor Q does not depend on Reynolds number. The relation between these sensitivity factors is presented in fig.3.13. Ratio G/Q weakly depends on Reynolds number, which correlates with results of work of Smits et al.(1983).

The fluctuation mode diagrams of natural disturbances in wind tunnel test section at various Reynolds numbers are presented in fig.3.14. Since all dependencies $\theta(r)$ are linear functions, the fluctuation field corresponds to acoustic disturbances. The values of mass flux fluctuations and stagnation temperature fluctuations are presented in fig.3.15, 3.16 as total pressure and unit Reynolds number dependencies. From these data it follows that in the test section the level of stagnation temperature fluctuations is almost constant and does not exceed 0.01% at Mach number M=2 and unit Reynolds numbers range from 7.0×10^6 to 30×10^6 m^{-1}, while mass flux fluctuation level increases from 0.07% to 0.2%.

As mentioned above, the obtained fluctuation diagrams show the linear dependence, i.e.

$$\theta=<m>r+<T_0>.$$

According to Kovasznay, (1953) and Zinovject & Lebiga (1990) such form of the fluctuations diagram can correspond to either entropy or acoustic mode. As the relation $<T_0>$ and $<m>$ does not equal to

$$\alpha=\frac{1}{\left(1+\frac{\gamma-1}{2}M^2\right)},$$

we can conclude that the measured disturbances represent the acoustic fluctuations. If so, the equation for fluctuations can be rewritten in the form (Zinovjev & Lebiga 1990)

$$\theta=\beta<u>\left(1-\frac{<p>}{M^2<u>}\right)+\left(<p>-<u>\right)r,$$

where $\beta=\alpha(\gamma-1)M^2$; $<u>$ are velocity fluctuations; $<p>$ are pressure fluctuations;

$$\theta(0)=<T_0>;\quad \left.\frac{\partial\vartheta}{\partial r}\right|_{r\to\infty}=<m_o>\ .$$

To separate the fluctuations, the following system of equations was used:

$$\begin{cases} <p>-<u>=<m_0> \\ \dfrac{(\gamma-1)M^2}{1+\dfrac{\gamma-1}{2}M^2}<u>\left(1-\dfrac{<p>}{M^2<u>}\right)=<T_0>, \end{cases}$$

where M=2 and γ=1.4. The obtained numerical values of $<m>$, $<T_0>$, $<p>$, $<u>$ are presented in Table 3.1.

Table 3.1.

$Re_1 \times 10^6$ m^{-1}	P_0 atm	P_{st} kg/m^2	P_0 kg/m^2	$<\rho U>$ %	$<T_0>$ %	$<p>$ %	$<u>$ %
5.72	0.42	555.36	4278.3	0.0994	0.0169	0.158	0.059
9.83	0.72	955.17	7358.3	0.0715	0.0059	0.104	0.033
12.26	0.89	1188.04	9180.8	0.0769	0.0073	0.114	0.037
16.23	1.17	1575.19	12141.1	0.0864	0.0050	0.123	0.037
21.47	1.56	2061.05	16126.6	0.1134	0.0041	0.157	0.044
26.76	1.94	2566.80	20083.8	0.1693	0.0073	0.237	0.068
29.24	2.12	2799.72	21883.5	0.2028	0.0080	0.282	0.079

Mass flow pulsation spectra in free stream of test section are presented in fig.3.17, 3.18. The data were measured after polishing of nozzles. The spectra were determined on 4096 points from averaging of 16384 points of digital oscillogram obtained using 12 bit 750 kHz ADC. The ADC was made from parts sent by Dr. J.M.Kendall. Also the pulsations were measured using new CTA. We have been compared the data with pulsation spectra obtained by Dr. V.A.Lebiga in T-325 test section twenty years ago. In those measurements it was defined a maximum at f=8-9 kHz in the spectra. From our data follow that now the maximum corresponds to f=4-5 kHz. It maybe proposed that the changing of frequency spectra took place due to improvement of settling chamber and test section of T-325. Total level of mass flow pulsations corresponded to the data are shown in fig.3.16 (data for 3rd year).

3.3.2. Fluctuation level in T-325 test section at M=3.5

For given Mach number the detailed measurements of the fluctuation levels were carried out for the sole value of unit Reynolds number. Namely, the data presented below correspond to the fluctuation levels at $Re_1=7\times10^6$ m^{-1}. Calibration to mass flux was carried out at the wire ratio a_w=0.8, and calibration to overheat ratio at $Re_1=7\times10^6$ m^{-1}. The final fluctuation diagrams in the test section at M=3.5 are presented in fig.3.19. The diagrams show the linear character similar to the case M=2, which correspond to the fluctuations diagram of the acoustic mode. It was obtained, that the mass flux fluctuations are 0.15% and stagnation temperature fluctuations are 0.004% at $Re_1=7\times10^6$ m^{-1}.

3.3.3. Level of the controlled fluctuation field in T-325 test section at M=2

In these experiments, a certain value of initial amplitude of controlled disturbances from the local source was used. That value was kept constant through all further measurements of fluctuation field with accuracy not less than 5%. The experiments were made at $Re_1=9.9\times10^6$ m^{-1}. The measurements were carried out in free stream in the plane of the plate *2* at a distance $y_1=40$ mm from the surface of the plate *1*.

The amplitude-phase distributions of the controlled fluctuation field in x at constant frequency are presented in fig.3.20. The variation of G/Q with τ is presented in fig.3.21 and the controlled disturbance fluctuation diagrams in the free stream at frequency 20 kHz (dimensionless frequency parameter is $F=0.25\times10^{-4}$) is shown in fig.3.22. Notice, that measurements of fluctuation diagrams were carried out at $x=6.1$ mm, according to the data presented in fig.3.20. Coordinate x could be chosen arbitrary in this experiments. Value $x=0$ was chosen to provide the beginning of measurements before the region where the flow field was disturbed by controlled fluctuations. To convert this coordinate x to the distance from the leading edge of the plate *1*, it is necessary to add the value $x_2=79$ mm to x. This amplitude-phase distributions of fluctuations permit to distinguish four characteristic x-areas according to four maxima in these distributions. The analysis of similar amplitude and phase x-distributions was made in Kosinov et al. (1994). Notice that the first area at the left corresponds to the acoustic waves, propagated upstream, and the length of this area (2-3 mm) is similar to the value obtained in Kosinov et al. (1992) at boundary layer measurements close to the local source of disturbances at $M=2$. The complete analysis of these and other data are presented in subsequent chapters, where the leading edge receptivity is considered. Figs.3.23, 3.24 show amplitude and phase z-distributions for controlled fluctuations at frequency 20 kHz and $x=6.1$ mm.

The z-distributions of fluctuation amplitude and phase (real and imaginary parts) at $x=11$ mm are presented in Fig.3.25, 3.26. Related data for $x=17$ mm are shown in Fig.3.27, 3.28. The y-distributions of fluctuation amplitude and phase are presented in Fig.3.29. It is easy to observe that the obtained relations of the mass

flux fluctuations to the stagnation temperature fluctuations at x=6.1 mm; 11 mm and 17 mm are rather different. The obtained values are $A_o \approx 7.6$, 5, 9.5 and $A_{<m>} \approx 1.245$, 1.25, 1.35 correspondingly.

3.3.4. The level of controlled fluctuation field in T-325 test section, M=3.5

The study of the controlled disturbances field at M=3.5 was carried out in the same manner as for M=2.0. The main difference was that the distance between plates in normal direction decreased. The measurements were made at free stream unit Reynolds number $Re_1=7\times10^6$ м$^{-1}$ in the plane of the plate *2* at the distance y_1=26 mm from the plate *1* surface.

The amplitude and phase x-distribution for controlled fluctuations field for the same frequency 20 kHz (dimensionless frequency parameter $F=0.28\times10^{-4}$) is presented in fig.3.30. Variation of G/Q with τ is shown in fig.3.31, and fluctuation diagrams of the controlled disturbances in the free stream is shown in fig.3.32. To convert x-coordinate to the distance from the leading edge of the plate *1*, it is necessary to add $x_{3.5}$=90 mm to x value. Notice, that the measurement of the fluctuation diagrams was carried out at x=30.4 mm, according to the data presented in fig.3.30. Again, the value x=0 was chosen to provide the beginning of measurements before the region where the flow field in the test section was disturbed by controlled fluctuations. In this case, amplitude and phase distributions of fluctuations permit to distinguish three characteristic x-areas according to three maxima in these distributions. The first area corresponds to acoustic disturbances propagated upstream and its length in x (8-10 mm) is several times more as compared with the case M=2. The controlled disturbances field was measured in coordinate z and calibration measurements were made at three values of coordinate x: x=5 mm, x=16 mm, x=30.4 mm. These values were chosen in the areas of maxima in distributions .

Figs.3.33 and 3.34 show z-distributions of phase and amplitude of the controlled fluctuations at x=5 mm and frequency 20 kHz. The z-distribution of amplitude and phase of the mass flux fluctuations are presented in figs.3.35, 3.36 at

x=16 mm. The similar data for x=30.4 mm are shown in fig.3.37. It is seen that the obtained relations of the mass flux fluctuations to the stagnation temperature fluctuations at x=5 mm; 16 mm and 30.4 mm are different. It was obtained that $A_o \approx$11.064; 6.75; 6.4 and $A_{<m>}$=1.81; 1.82; 1.86 correspondingly.

3.4. Figures

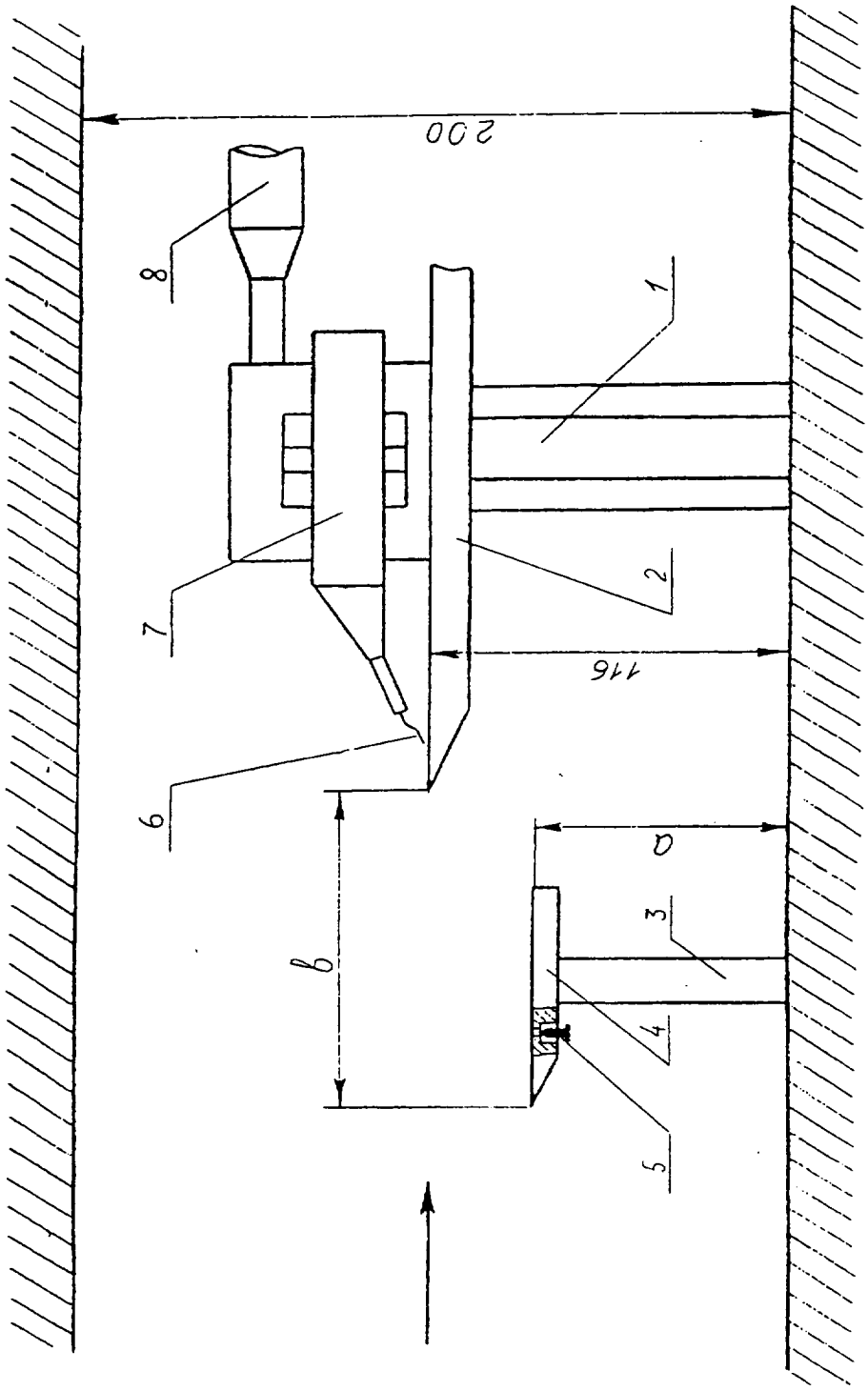

Fig.3.1. Experimental set-up: 1 - pylon; 2 - plate 2; 3 - traversing equipment bar of test section; 4 - plate *1*; 5 - localized source of disturbances; 6 - hot-wire probe; 7 - traversing equipment; 8 - traversing equipment bar of plate *1*.

Fig.3.2. Photo of models

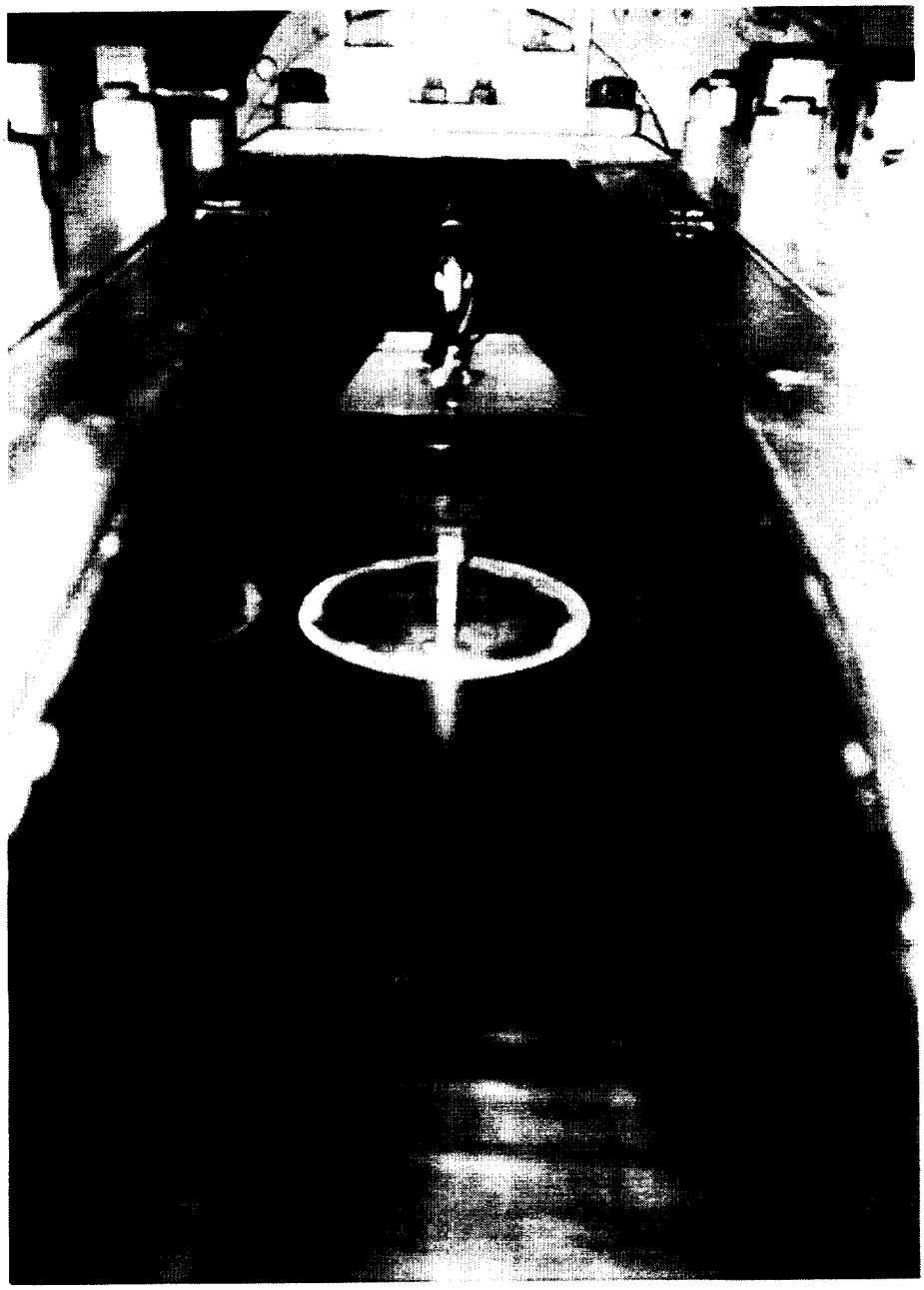

Fig.3.3. Photo of models

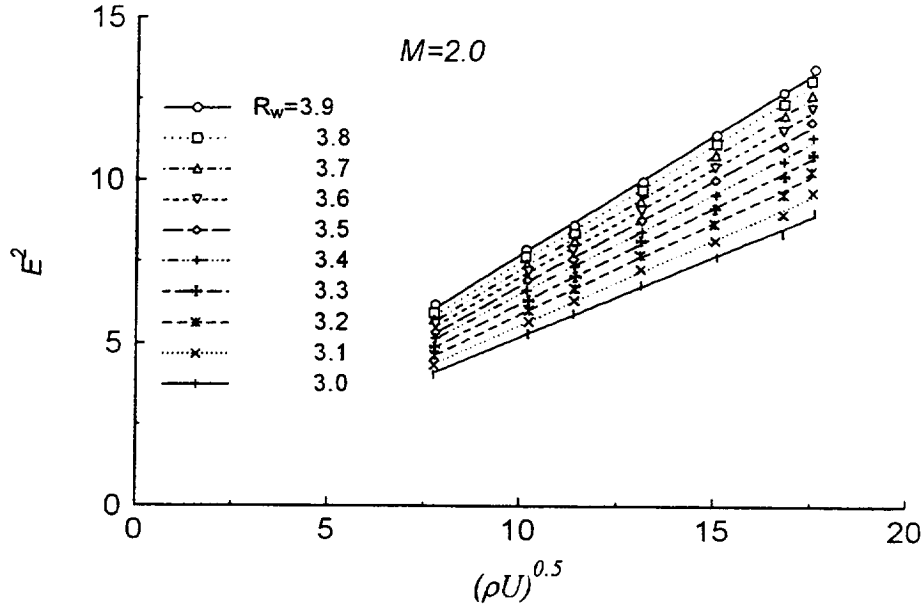

Fig.3.4. Dimensional calibration dependencies for various R_w.

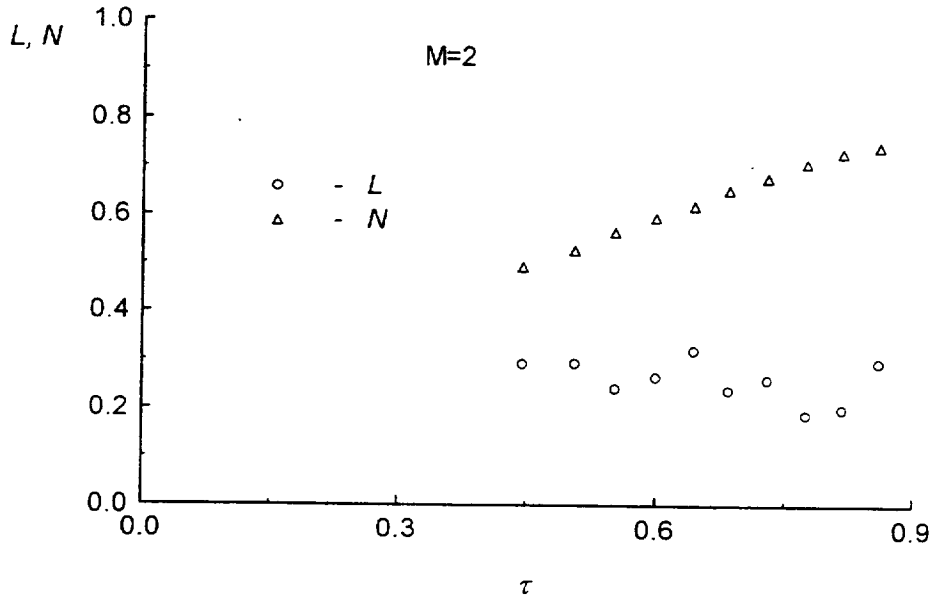

Fig.3.5. Dimensional calibration coefficients as a function of overheat ratio τ.

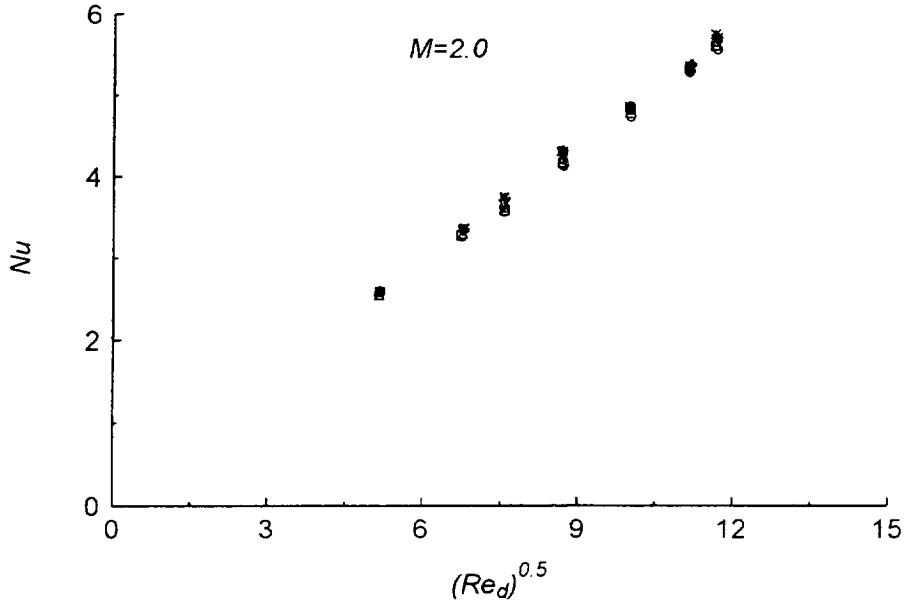

Fig.3.6. Dimensional calibration dependencies for various R_w.

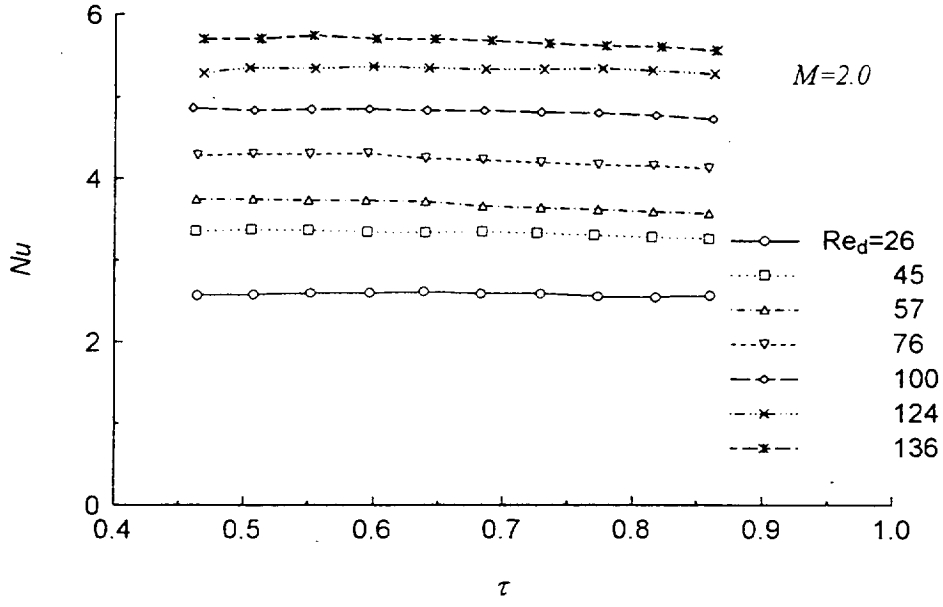

Fig.3.7. Nusselt number as a function of overheat ratio τ for various Re_d.

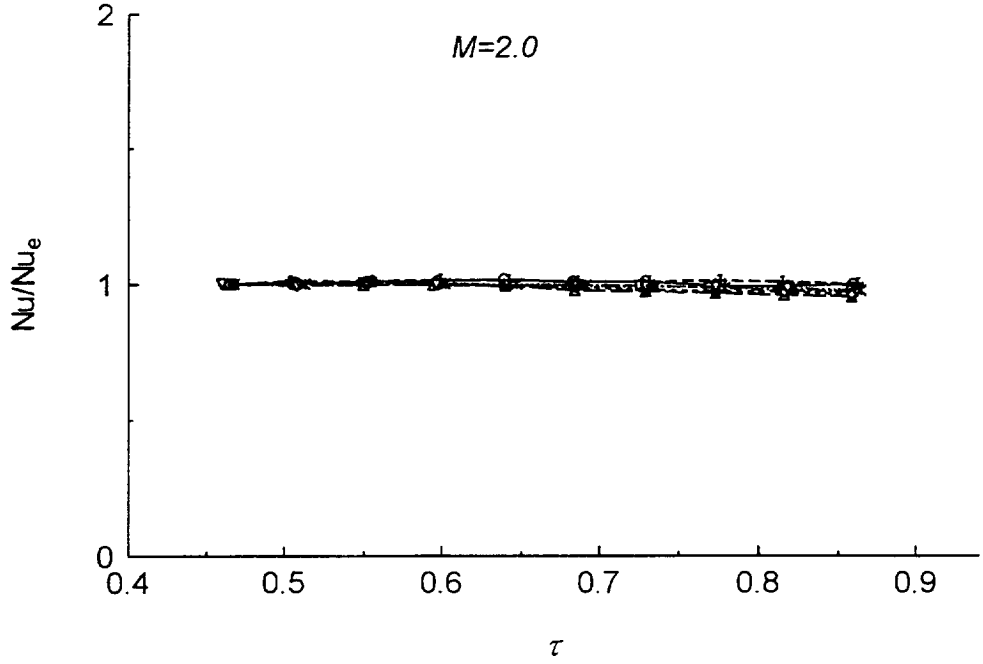

Fig.3.8. Normalized Nusselt number over τ for various Re_d.

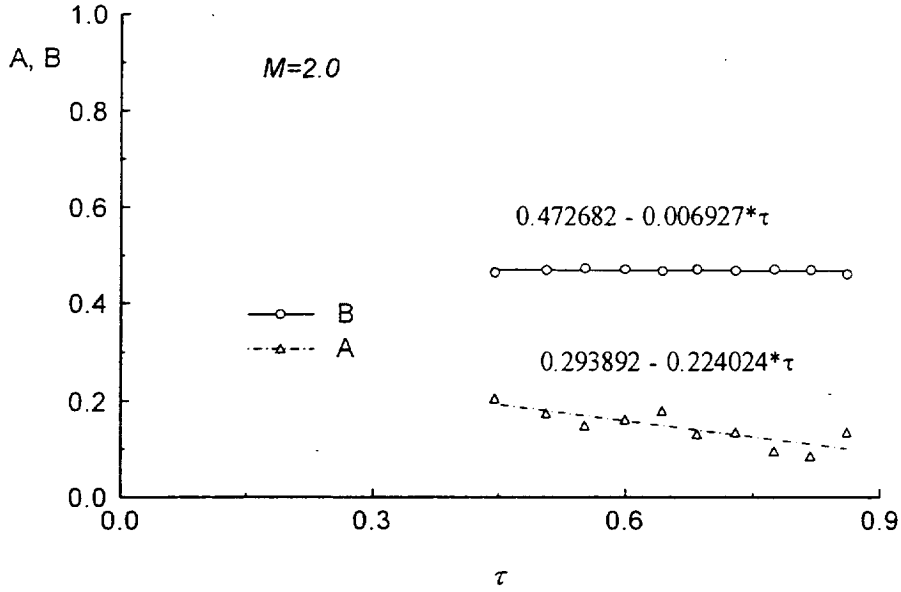

Fig.3.9. Dependence of dimensionless calibration coefficients versus τ.

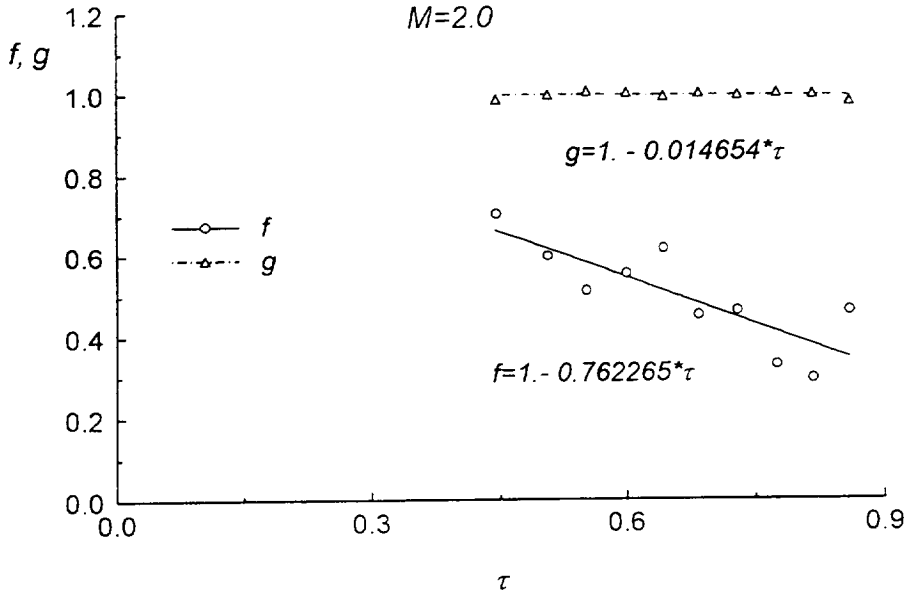

Fig.3.10. Dependence of functions f and g over τ.

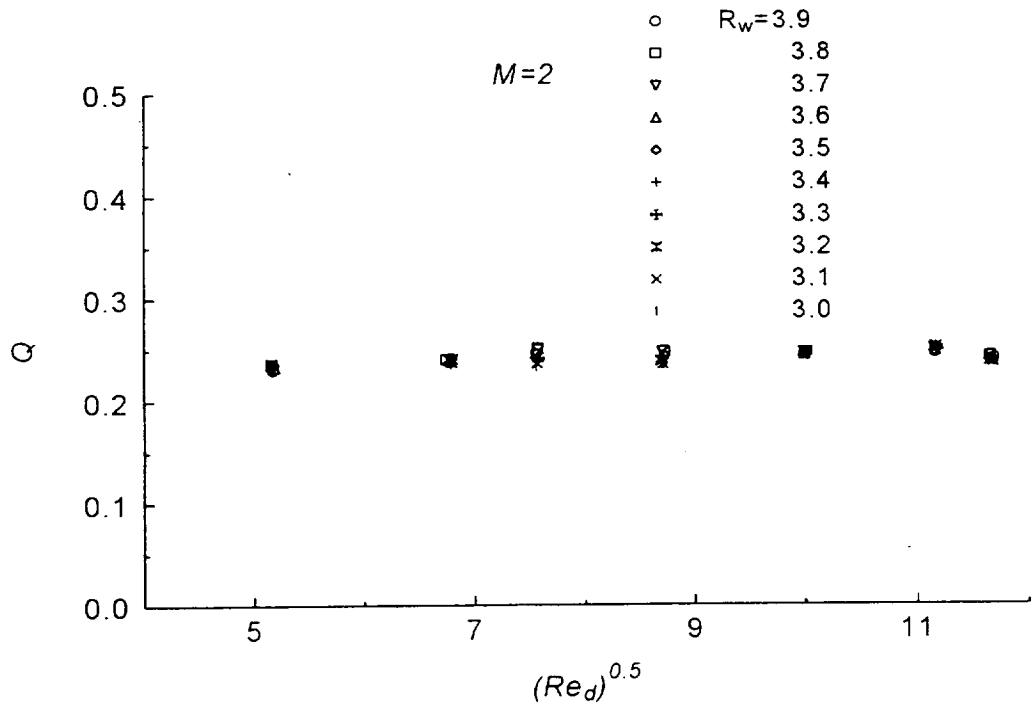

Fig.3.11. Dependence of dimensionless mass flow fluctuation sensitivity versus $(Re_d)^{0.5}$.

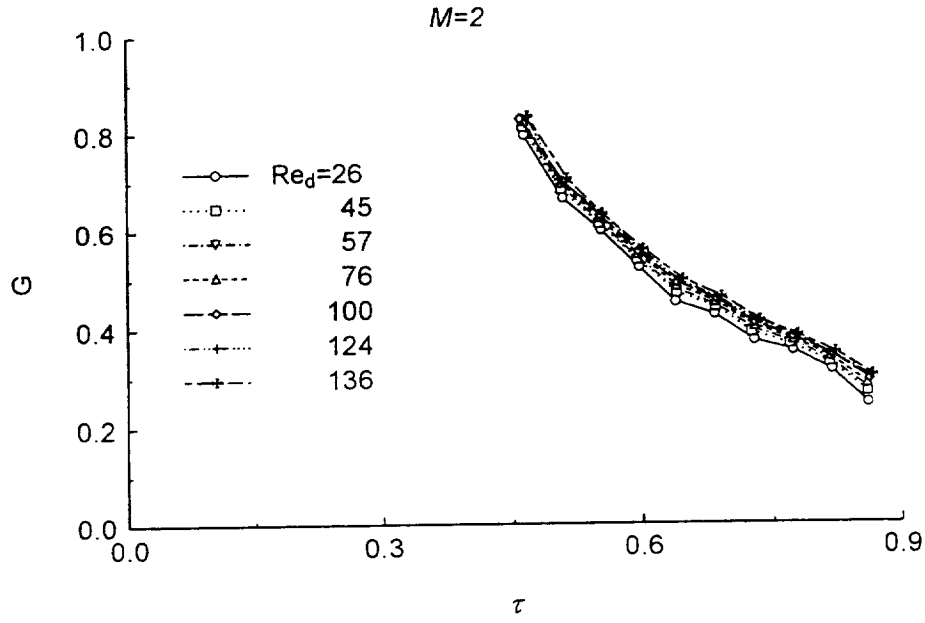

Fig.3.12. Dependence of dimensionless temperature fluctuation sensitivity versus τ.

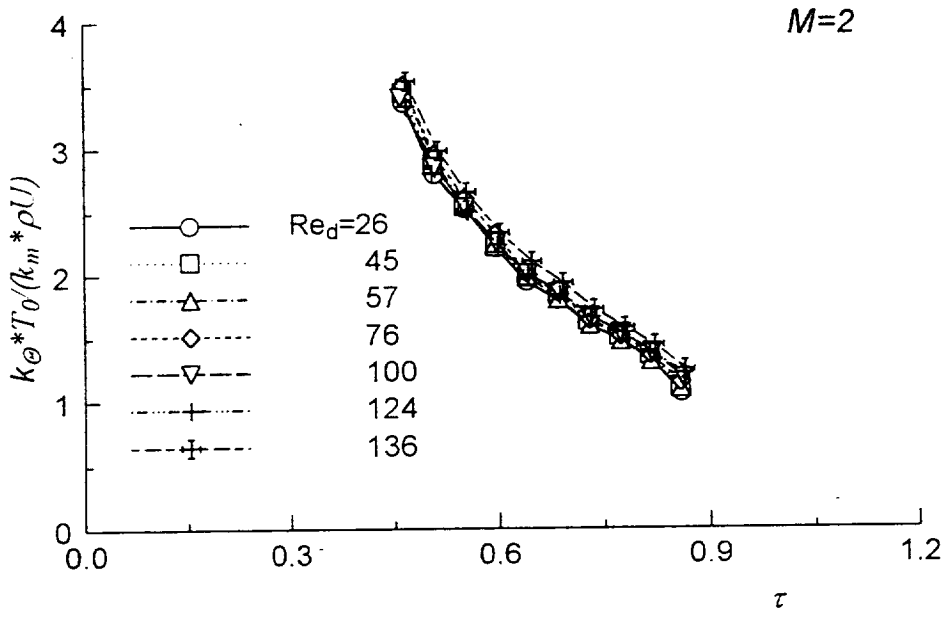

Fig.3.13. Relative sensitivities as a function of overheat ratio τ for various Re_d.

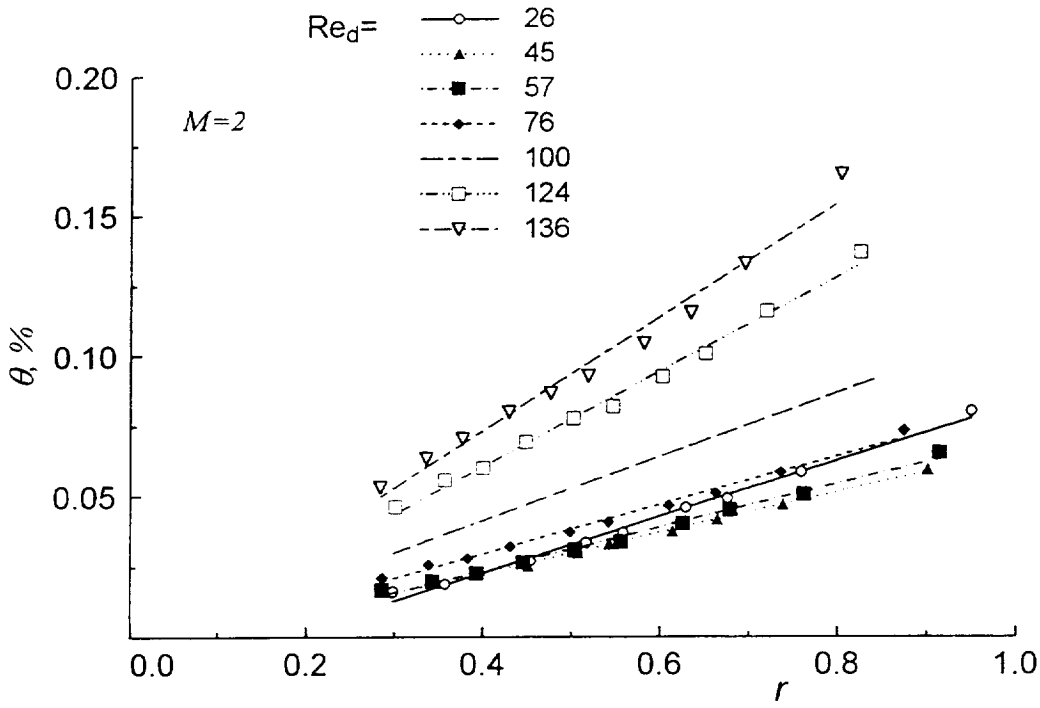

Fig.3.14. Fluctuation diagrams of natural disturbances.

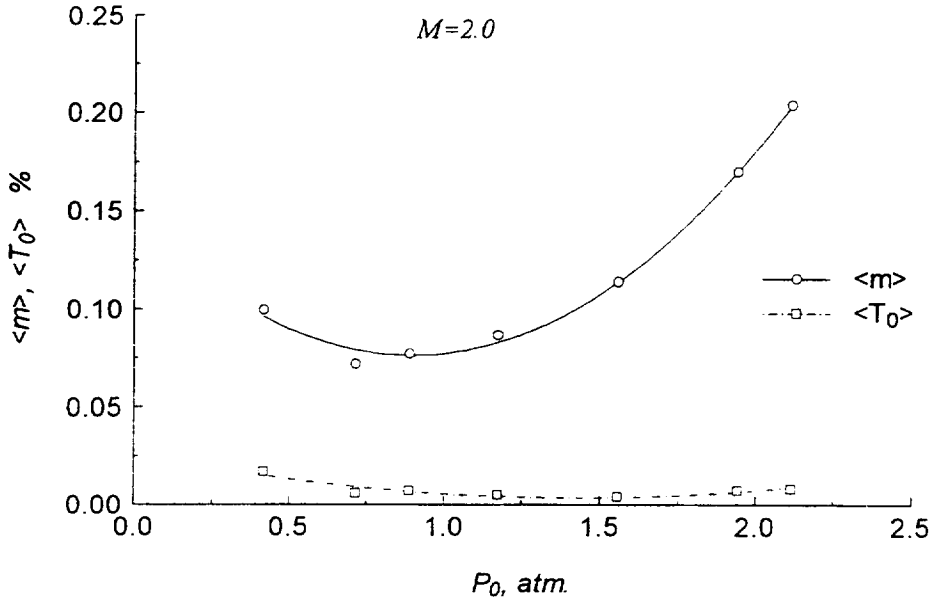

Fig.3.15. Dependence of mass flow fluctuation and stagnation temperature fluctuation versus of total pressure.

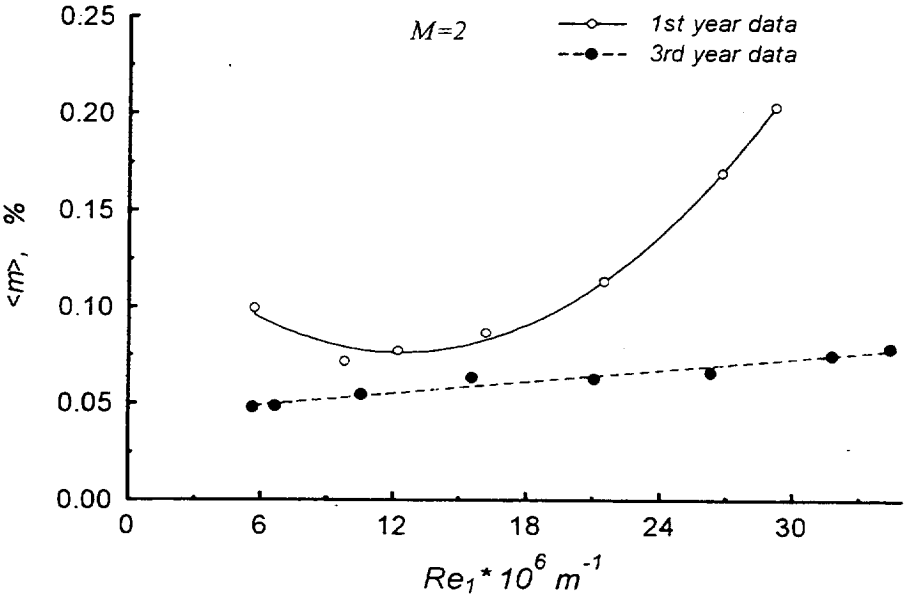

Fig.3.16. Dependence of mass flow fluctuation versus Re_1.

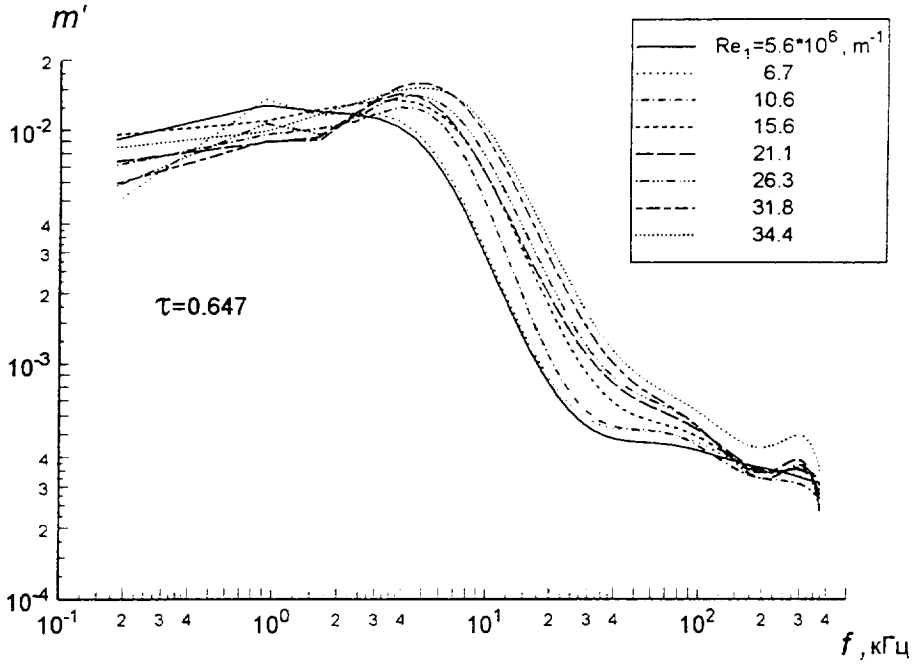

Fig.3.17.

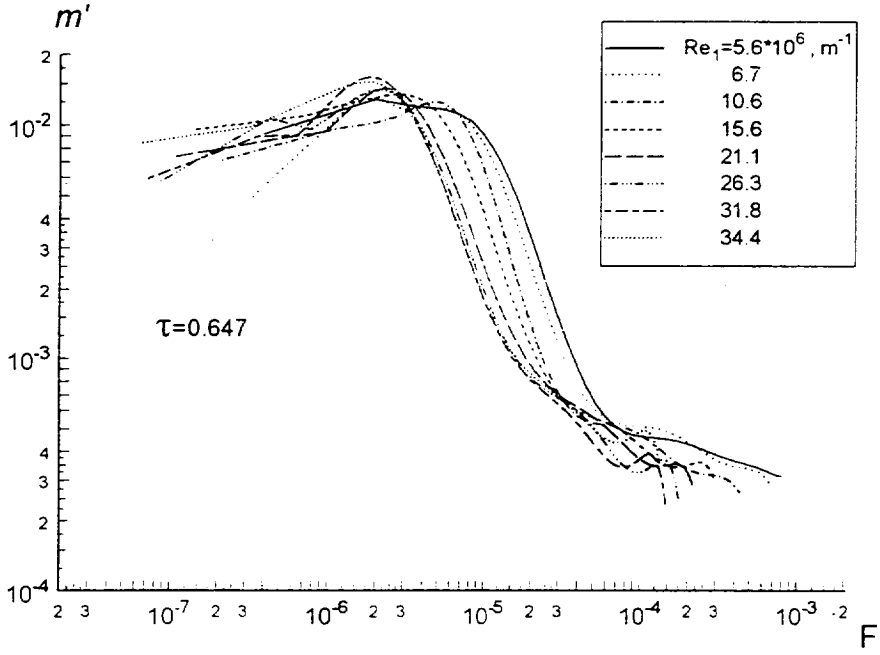

Fig.3.18.

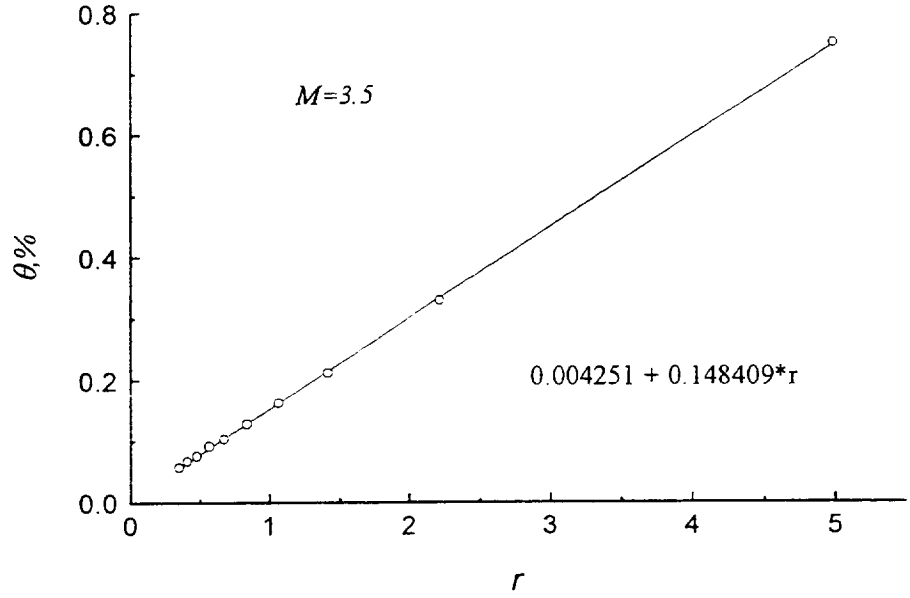

Fig.3.19. Fluctuation diagram of natural disturbances.

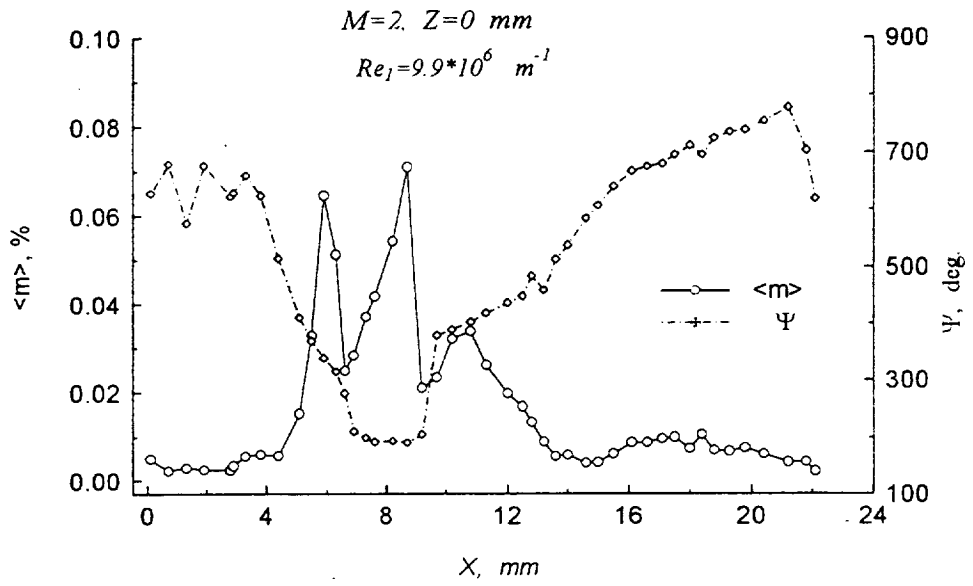

Fig.3.20. Distribution of amplitude and phase of mass flow fluctuation over *x* for controlled disturbances at frequency 20 kHz.

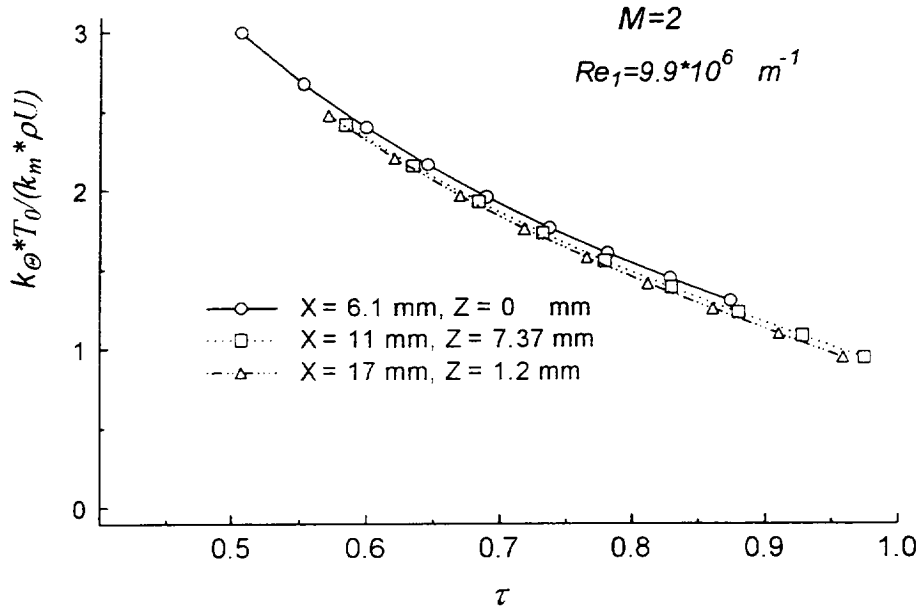

Fig.3.21. Dependence *G/Q* versus τ.

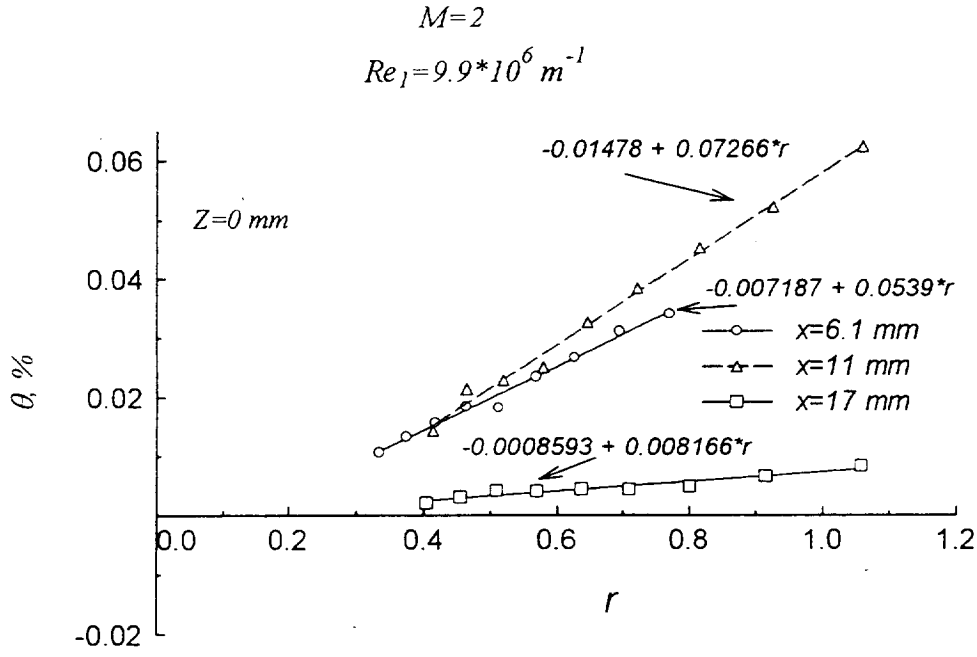

Fig.3.22. Fluctuation diagram of controlled disturbances.

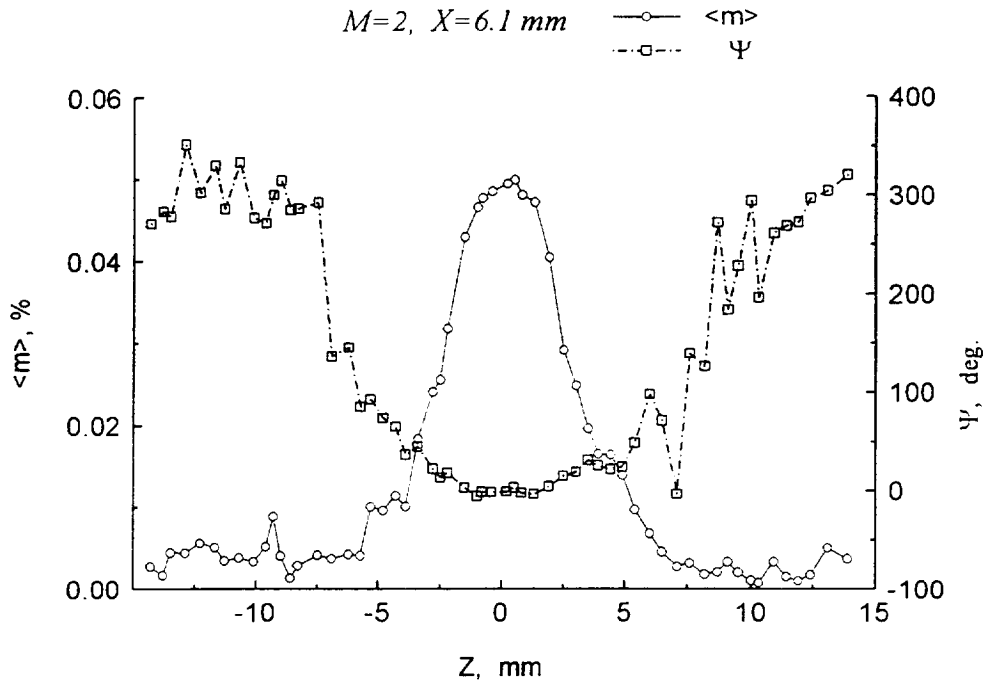

Fig.3.23, 3.24. Distribution of amplitude and phase of mass flow fluctuation over *z*.

Spanwise and normal distributions of controlled disturbances. To understand what sort of controlled disturbances should be used for testing the boundary layer response, let us consider a spatial distribution of pulsations in free stream.

The data for normal coordinate are shown in figs.4.2-4.5. Here amplitude of oscillograms is given in bits. For x=5mm (figs.4.2, 4.3) the border of controlled pulsation field is situated at y=2mm and disturbances have the same phases for y<1mm. More complicated data were obtained at x=16mm (figs.4.4, 4.5). It is possible to supply these data by complimentary information from figs.4.2, 4.3 in order to obtain the full structure of controlled disturbance field.

Instantaneous amplitude distributions are shown in figs.4.6, 4.8a, 4.9a (amplitudes in figs.4.6-4.9 are given in bits). These figures show an increased number of amplitude peaks in this distributions, namely, $2l+1$, where l is the number of zone. It looks to be a kind of «wakes» from the previous zones. This change leads to the changes in the phase distributions shown in figs.3.34, 3.36, 3.37. The main changes are observed at the central part of phase distributions, where the growth of phase for the first and the second zones and decrease of phase for the third zone can be seen. This might be a consequence of the different nature of radiation in these zones. Distributions $A(z)$ and $\Phi(z)$ measured in free stream at x=5, 16, 30.4 mm are presented in figs.3.34-3.37. Amplitude distributions presented in figs.3.33, 3.35, 3.37 correspond to the mass flux fluctuations.

Spanwise wave number spectra. β- spectra for the mentioned above zones were obtained using discrete Fourier-transformation. These spectra are shown in fig.4.10. One can see waves at *β-region* from -0.5 rad/mm to 0.5 rad/mm. For the first zone there is a maximum at $\beta=0$ in amplitude spectra. In other cases, three-dimensional waves increase. The total mass flux pulsations are 0.18% for the first zone, 0.28% for the second zone and 0.18% for the third zone.

4.3.2. Boundary layer response

Pulsation diagrams. To determine the mass flux pulsations from the hot-wire data we used the same method as have been used for the free flow measurements. Pulsation diagrams of the controlled disturbances in the boundary layer at z=0 are presented in fig.4.11. Since the diagrams are almost linear functions, it is possible to apply the described above relations in order to define the mass flux values. Values $A_o \approx 18.3$, 16.9, 4.9, and $A_{<m>}$=1.96, 1.99, 1.8 were obtained for different zones and each x, correspondingly. These values were used to define the mass flux pulsation amplitude. As $A_{<m>}$ takes the close values in free stream and boundary layer as well(see 4.3.1), it was proposed to use $A_{<m>} \approx 1.9$ for both cases. More important conclusion from these data is that it is possible to define transfer factors directly from amplitude β -spectra without using the diagram technique. This approach was used by Semionov et al. (1996).

Spanwise distributions of controlled disturbances in boundary layer. To study disturbance field, excited by external controlled pulsations, in the boundary layer, the plate 2 was placed in such a way that the leading edge was consistently in those sections, where external disturbances were measured (that means that coordinates of the leading edge were x=5, 16 and 30 mm). The distributions $A_f(z)$ and $\Phi_f(z)$ were measured for two x^* positions of the plate 2 in the boundary layer, with exception for the first position (x^*=40 and 50 mm, where x^* is a distance from the leading edge of the plate 2). The data are presented in figs.4.12-4.15. Instantaneous amplitude distributions are shown in figs.4.12b, 4.13c,d, 4.15. For these data the amplitude is given in bits. Amplitude distributions presented in figs.4.12-4.14 correspond to the mass flux fluctuations. It may be seen that regular wave structures observed in the free stream are destroyed in the boundary layer in all zones.

β-spectra. Amplitude and phase β-spectra of excited disturbances for the leading edge position x=5 mm are presented in fig.4.16. It can be seen that the oscillation amplitudes in the boundary layer are not equal to zero, contrary to the case M=2 (Semionov et al. 1996). For the case M=2 it was obtained that the external

disturbances propagated upstream do not practically cause any response in supersonic boundary layer.

Amplitude and phase β-spectra of excited oscillations in the boundary layer at x=16 and 30 mm are presented in figs.4.17 and 4.18. The amplitude of the excited oscillations in the boundary layer are some times higher than the forced disturbances. The waves with $\chi \approx 0°$ are excited in the boundary layer more readily than oblique waves. The obtained data correspond to the theoretical conclusions (Fedorov & Khohlov 1992; Gaponov 1995).

Among the shown data, only the phase spectra at x=16mm are similar to the phase spectra of wave trains in the boundary layer (Kosinov et al. 1990[2]; 1994[2]).

Presented data allow to obtain the mean values of the mass flux pulsations excited in the boundary layer by external controlled disturbances. Total mass flux pulsations are: 0.25% for excitation in the first zone and for x^*=40mm, 0.58% for the second zone and 0.47% for the third zone.

4.3.3. Transfer factors

Let us to estimate the transfer factors for each described above case. The relevant data are shown in fig.4.19. Only for the first zone there is a smooth β-dependence of the transfer factors. For the second and the third zones there are some peaks in these dependencies. Obtained experimental data correlate with data described by Gaponov (1995).

A possible reason of such behavior of transfer factors for the second and the third zones is an incorrect definition of these factors without definition of α_r - spectra of the forced disturbances. For the linear case of the transformation of external pulsations into unstable boundary layer disturbances it is necessary to consider the disturbances which have the same wave characteristics (Gaponenko et al. 1996).

Using mean total values of mass flux pulsations obtained in free flow and in boundary layer, respectively, we can define mean transfer factors for each case. The relevant data are presented in table 4.1.

Table 4.1.

	x=5 mm			x=16 mm			x=30.4 mm		
	$\langle m \rangle_{fs}$ %	$\langle m \rangle_{bl}$ %	K_1	$\langle m \rangle_{fs}$ %	$\langle m \rangle_{bl}$	K_2	$\langle m \rangle_{fs}$ %	$\langle m \rangle_{bl}$ %	K_3
x*=40	0.185	0.251	1.357	0.285	0.583	2.042	0.183	0.47	2.564
x*=50	0.185	none	none	0.285	0.59	2.070	0.183	0.47	2.573

To illustrate what kind of disturbances is excited in the boundary layer by external controlled pulsations, we consider phase velocity of the waves. The data are shown in fig.4.20. Here the solid line separates the waves of discrete and continuous spectra. This line corresponds to the critical phase velocity $C^{\cdot}=1-1/(M\cos\chi)$. Experimental data are compared with linear stability calculations performed by I. I. Maslennikova for $F=0.28\times10^{-4}$ and $Re=560$. From these data follows that the excited waves are first mode instability waves.

4.4. *Leading edge receptivity at Mach 2*

The experiments were carried out at Mach number $M=2$ and unit Reynolds number $Re_1=9.9\times10^6$ m^{-1}. The controlled disturbances with frequency $f=20$ kHz ($F=0.26\times10^{-4}$) were generated by electric discharge in chamber. Measurements of controlled disturbances ware accompanied by the calibration tests in order to estimate the mass flux pulsation magnitude just like it was made at $M=3.5$.

4.4.1. Initial data

Here we consider streamwise distributions of amplitudes and phases of the harmonic controlled pulsations in the free flow.

The initial field of the controlled fluctuations was measured in the free stream in the plane of the plate *2* at distance $y_1=40$ mm from the surface of the plate *1* (the plate *2* was mounted further downstream). In this case the plate *2* was used as a

support for traversing mechanism. The measurements were carried out along coordinates x, y, z at fixed power of the local source.

Distributions of the amplitudes and phases $A(x)$, $\Phi(x)$ at z=0 are shown in fig.4.21. Here x-coordinate was measured from the upstream border of the forced radiation zone. To analyze the obtained data we used the same simplified physical model of disturbance source as for the discussed earlier case M=3.5. Using the physical model of the source, three characteristic zones may be distinguished in $A(x)$ and $\Phi(x)$ distributions. These zones were tested for boundary layer response and resulting regions can be classified as follows. The first zone (4 mm<x< 8 mm) corresponds to acoustic waves, radiated by upstream propagated disturbances from the source in the boundary layer of the plate *1*. The second zone corresponds to radiation from a vortex behind of the aperture (9mm<x<13 mm), and the third zone is observed for x>13 mm as radiation from TS waves.

Notice that in the experiments at M=2 the initial amplitudes of the forced waves is less than corresponding values at M=3.5. To illustrate this method we consider below an example of the pulsation diagram for the second zone.

Pulsation diagrams. Using data obtained in the first year experiments and presented in previous report, the calibration measurements were performed. The measurements were made at z=0 and x=11 mm. The fluctuation diagrams shown in fig.4.22 look like linear functions, which indicates an acoustic nature of the radiation. Values of the mass flux and the stagnation temperature pulsations are given in this figure. The diagrams for the first and the third radiation zones were not measured because for the second zone practically the same values of $A_{<m>}$ were obtained, so previous values of $A_{<m>}$ were used for other zones. The following values of A_o and $A_{<m>}$ were defined at x=11 mm: $A_o \approx 7.9$ and $A_{<m>}$=1.22. Some examples of the pulsation diagrams were demonstrated in fig.3.22.

Spanwise distributions of controlled disturbances. To understand what kind of controlled disturbances have been used for testing the boundary layer response, let us consider the spanwise distributions of pulsations in the free stream.

Distributions $A(z)$ and $\Phi(z)$ measured in the free stream at x=7, 11 mm are presented in figs.4.23, 4.24. The measurements at x=18 mm have shown that the

initial amplitude of the forced waves for this zone is too small to perform these experiments. For data shown in figs.4.23a,b-4.24a,b the amplitude is given in bits. Instantaneous amplitude distributions are shown in figs. 4.23a-4.24a, amplitude isolines are presented in figs. 4.23b-4.24b. These data along with the phase distributions shown in figs.4.23c-4.24c allow us to consider the presented data to be related to the mixed zones. First data are typical for the mixture of the first and the second zone while the data at x=11 mm are typical for the mixture of the second and the third zone. The amplitude distributions Presented in figs.4.23c-4.24c correspond to the mass flux fluctuations.

β-spectra. Using discrete Fourier-transformation, the wave β-spectra were obtained for the mentioned above zones. These spectra are shown in figs.4.25-4.26. One can see waves at β-regions (-1 rad/mm; 1 rad/mm) for x=7 mm and about (-1.5 rad/mm; 1.5 rad/mm) for x=11 mm. For the first zone there is a sole maximum at $\beta=0$ in amplitude spectra while in other cases three-dimensional waves increased. The total mass flux pulsation levels are 0.087% for x=7 mm and 0.093% for x=11 mm.

4.4.2. Boundary layer response

Pulsation diagrams. Pulsation diagrams of the controlled disturbances in the boundary layer at z=0 are presented in fig.4.27. As the diagrams are almost linear functions, it is possible to apply the described above relations in order to define the mass flux values. It was obtained that $A_0 \approx 5.6$, 42 and $A_{<m>}$=1.35, 1.58 accordingly for every x *values*. The factors $A_{<m>}$ have the close values both in free stream and in the boundary layer as it was at M=3.5.

Spanwise distributions of controlled disturbances in the boundary layer. To study the disturbance field in the boundary layer, excited by external controlled pulsations, the plate *2* was placed so that the leading edge was consistently in those sections, where external disturbances were measured (namely, coordinate of a leading edge was x=7 and 11 mm). The distributions $A_f(z)$ and $\Phi_f(z)$ were measured for two x^*-positions in the boundary layer of the plate 2 (x^*=40 and 50 mm, where x^* is a distance from the leading edge of the plate *2*). The data are presented in

figs.4.28-4.33. Instantaneous amplitude distributions and amplitude isolines are shown in figs.4.29, 4.30, 4.32, 4.33. For these data the amplitude is given in bits. Presented in figs.4.28, 4.31 the amplitude distributions represent the mass flux fluctuations.

β-spectra. Amplitude and phase β-spectra of excited disturbances at the leading edge position x=7 mm are presented in fig.4.34. It can be seen, that the oscillation amplitude in the boundary layer is not equal to zero.

Amplitude and phase β-spectra for excited oscillations in the boundary layer at x=11 mm are presented in fig.4.35. The waves with $\chi \approx 0°$ are easier excited in the boundary layer than oblique waves. The obtained data correlate to the theoretical conclusions (Fedorov & Khohlov 1992; Gaponov 1995).

The mean values of the mass flux pulsations in the boundary layer, excited by external controlled disturbances, can be obtained from presented data. Total mass flux pulsations are 0.04% for the x=7 mm and 0.09% for x=11 mm.

4.4.3. Transfer factors

The obtained data allow to estimate the transfer factors for each described above case. The data are shown in fig.4.36. Only for the first zone there is a smooth β-dependence of the transfer factors. There is a number of peaks in these dependencies for the second zones as for the case M=3.5.

Using mean total values of the mass flux pulsations obtained in free flow and in the boundary layer, the mean transfer factors can be defined for each case. These data are presented in table 4.2.

Table 4.2.

	x=7 mm			x=11 mm		
	$\langle m \rangle_{fs}$ %	$\langle m \rangle_{bl}$%	K_1	$\langle m \rangle_{fs}$ %	$\langle m \rangle_{bl}$ %	K_2
x^*=40	0.087	0.04	0.46	0.093	0.092	0.99
x^*=50	0.087	0.043	0.49	0.093	0.095	1.02

To illustrate what kind of disturbances is excited in the boundary layer by external controlled pulsations, we consider phase velocity of the waves. The data are shown in fig.4.37. From these data it follows that the excited waves are first mode instability waves for x=11 mm, and phase velocity of the excited waves starting from x=7 mm coincides with phase velocity of acoustic waves up to 45 degrees and with the vortex waves for χ>45°. Experimental data are compared with linear stability calculations performed by I. I. Maslennikova for $F=0.26\times10^{-4}$ and Re=670.

4.5. Figures

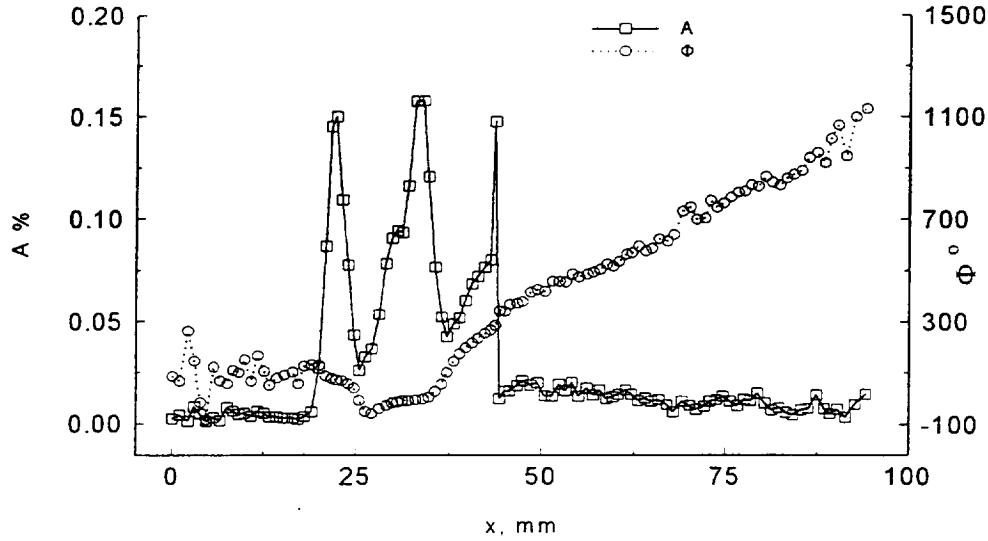

Fig.4.1. Dependence of amplitude $A(x)$ and phase $\Phi(x)$ over streamwise coordinate x at distance y=5.25 mm above the plane of plate 2 at z=0

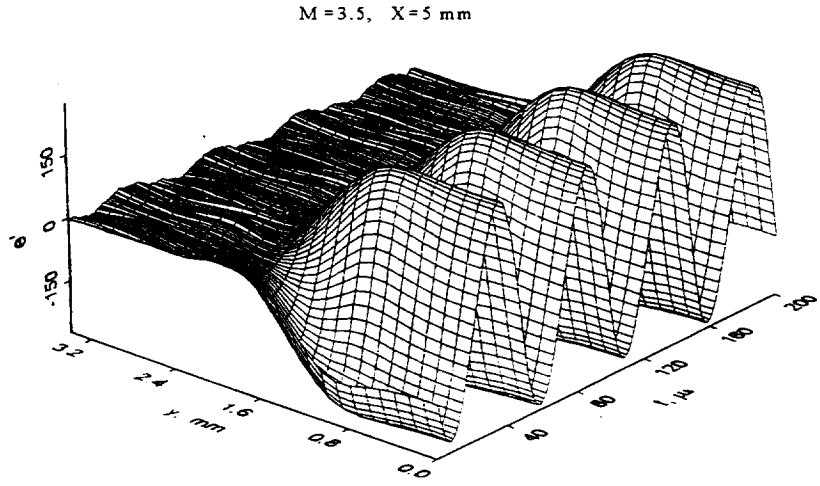

Fig.4.2. Dependence of amplitude of oscillograms of controlled disturbances over normal coordinate y at x=5 mm. 3-D plot.

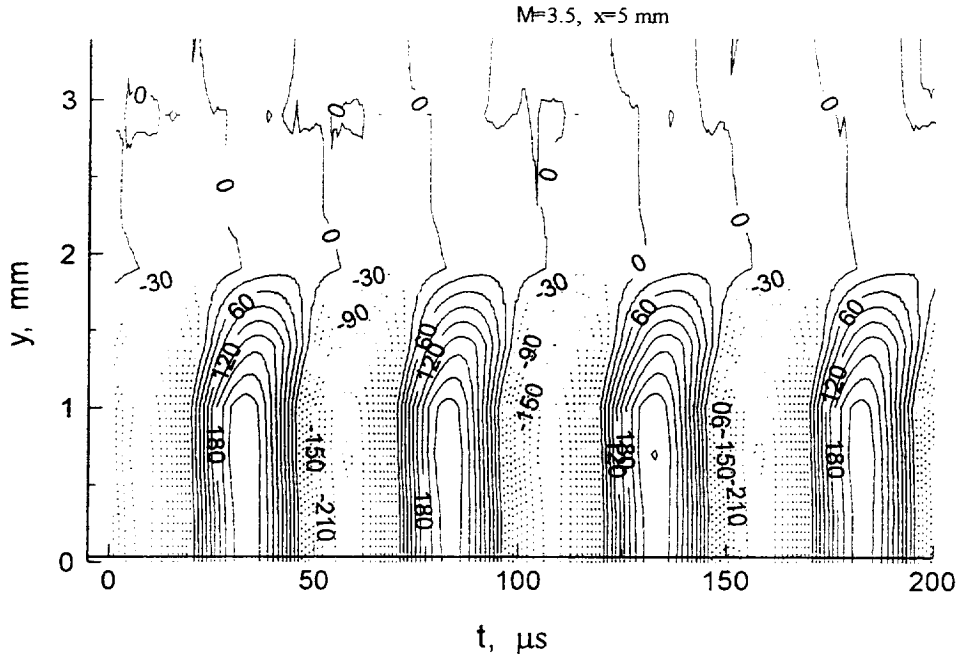

Fig.4.3. Dependence of amplitude of oscillograms of controlled disturbances over normal coordinate *y* at *x*=5 mm. Contour-grid line plot.

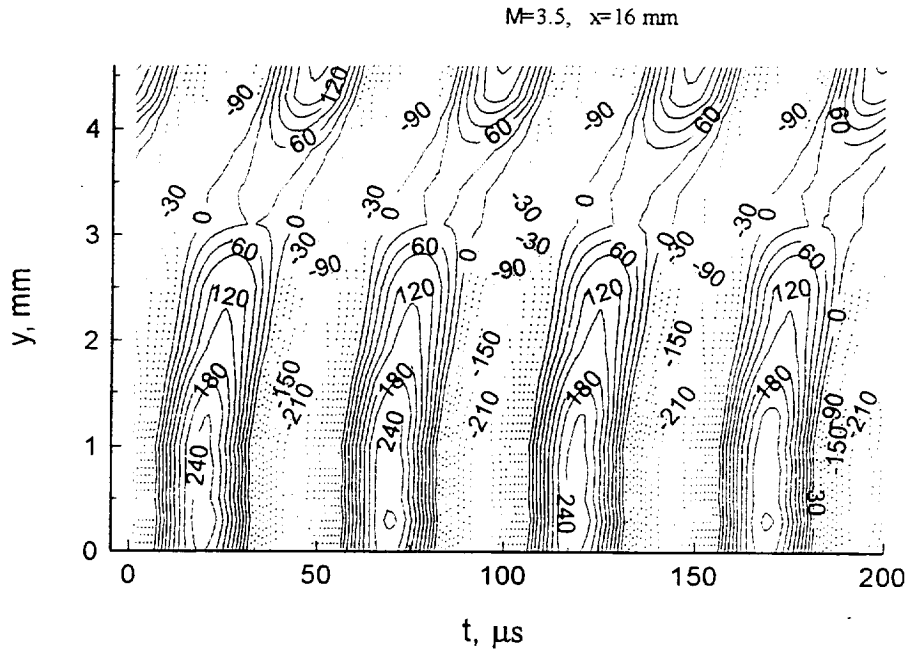

Fig.4.4. Dependence of amplitude of oscillograms of controlled disturbances over normal coordinate *y* at *x*=5 mm. Contour-grid line plot.

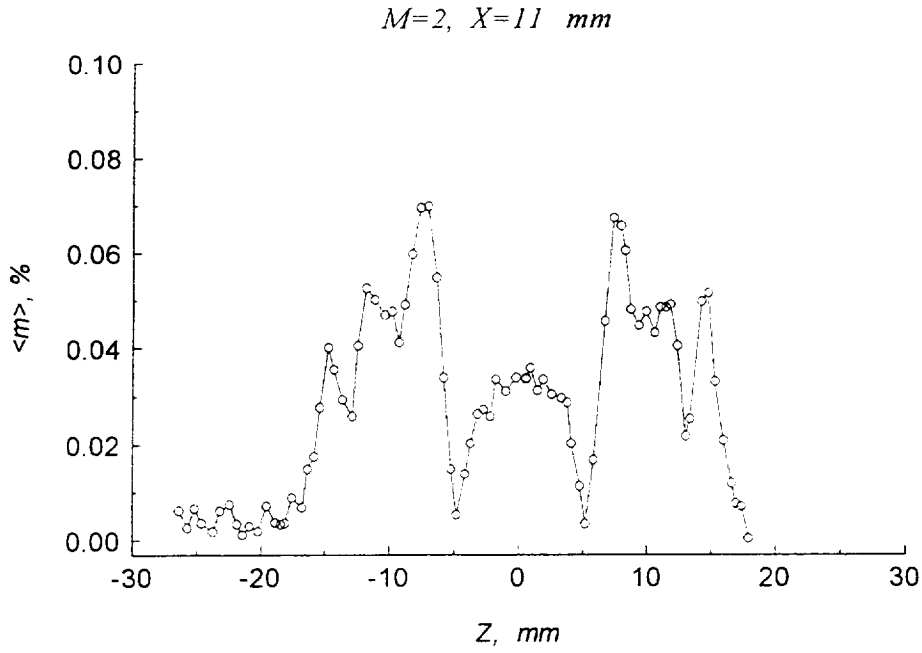

Fig.3.25. Distribution of amplitude of mass flow fluctuation over transversal coordinate *z*.

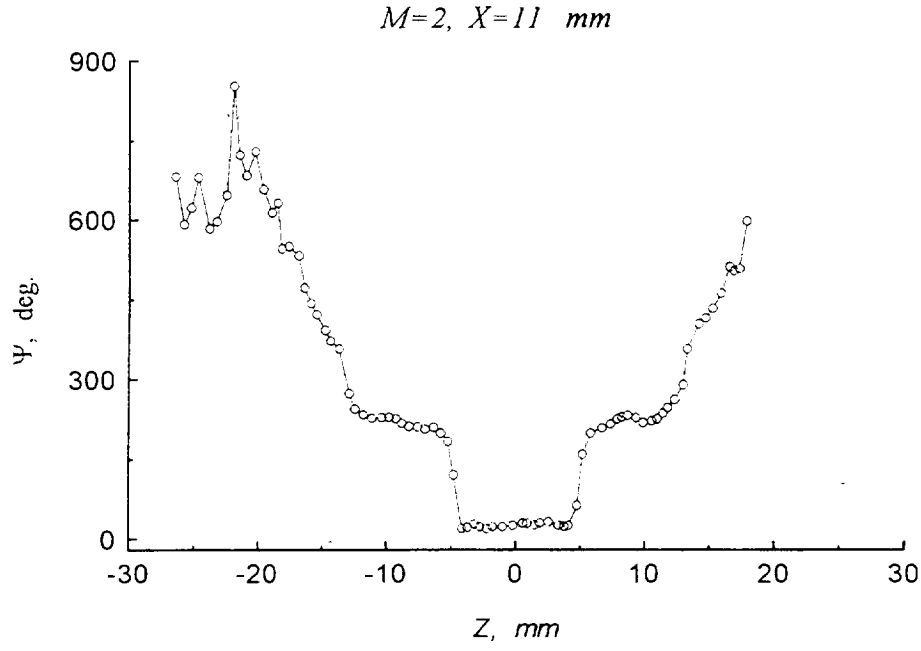

Fig.3.26. Distribution of phase of mass flow fluctuation over transversal coordinate *z*.

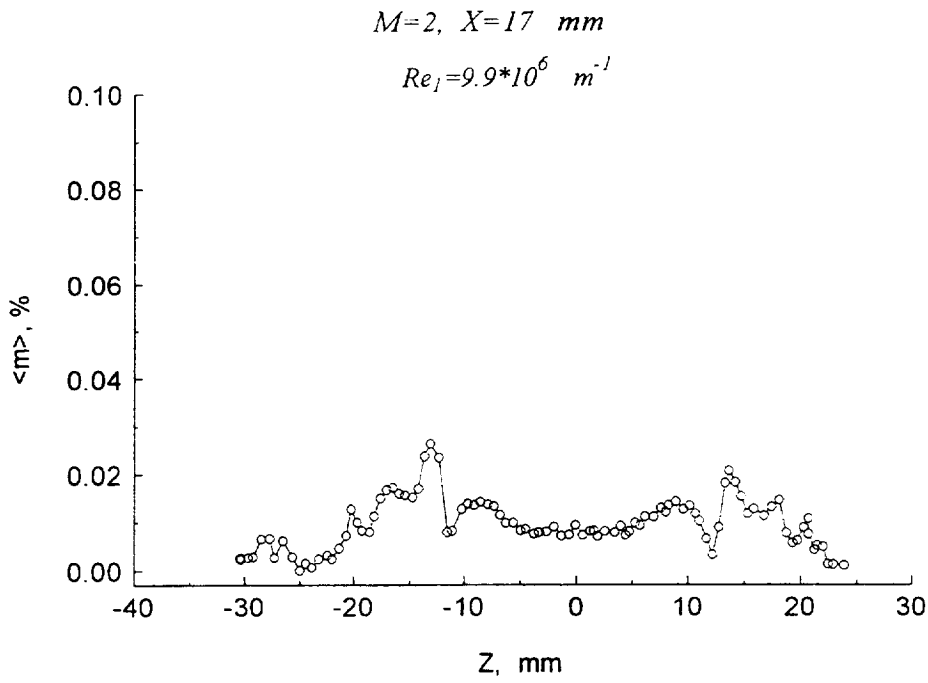

Fig.3.27. Distribution of amplitude of mass flow fluctuation over z.

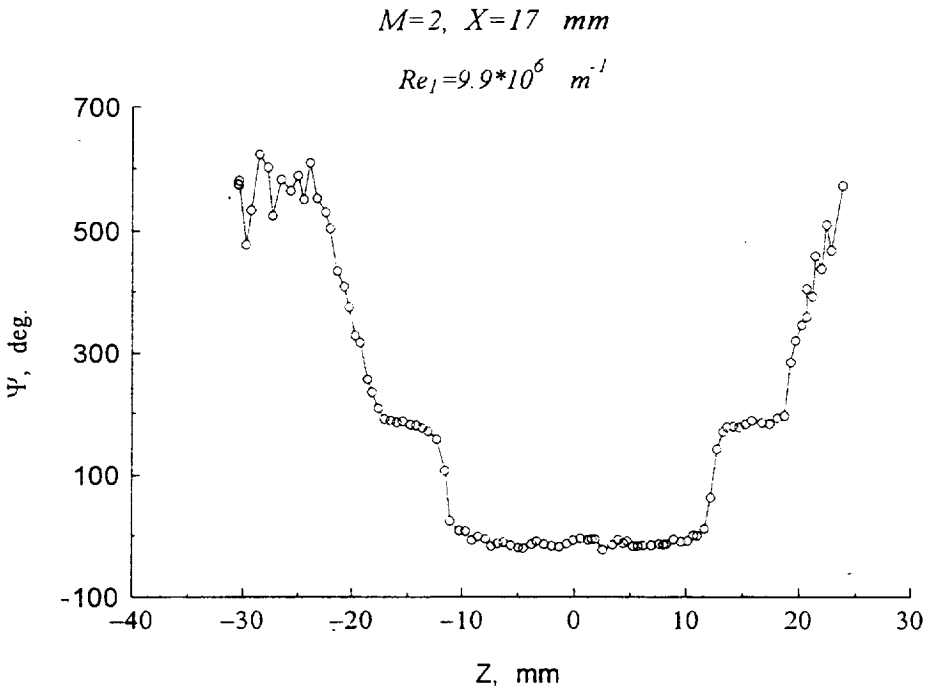

Fig.3.28. Distribution of phase of mass flow fluctuation over z.

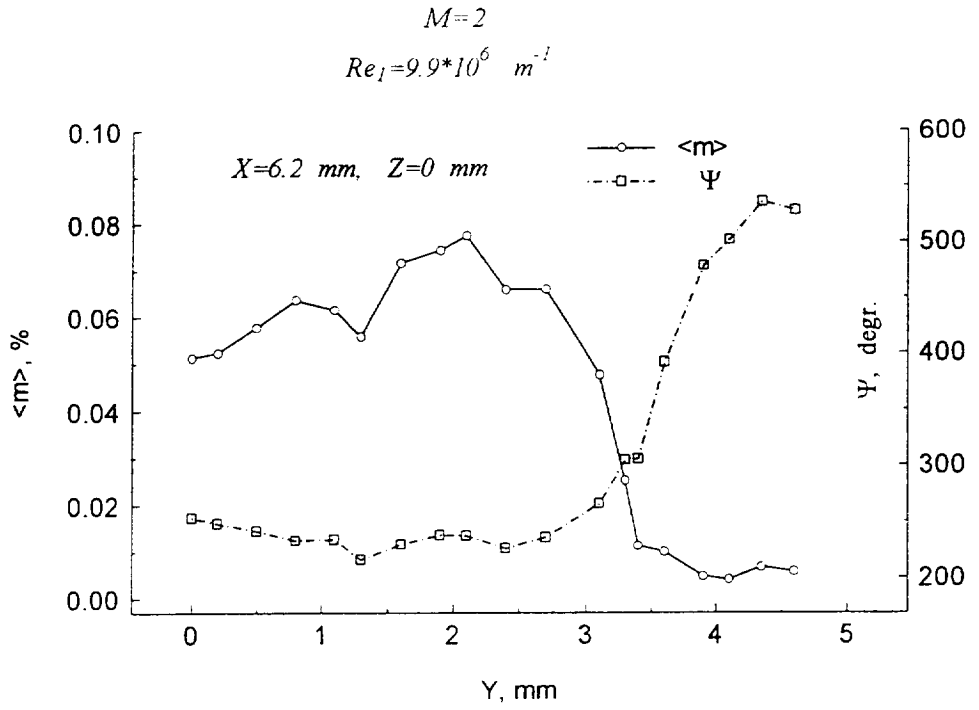

Fig.3.29. Distribution of amplitude and phase of mass flow fluctuation over *y*.

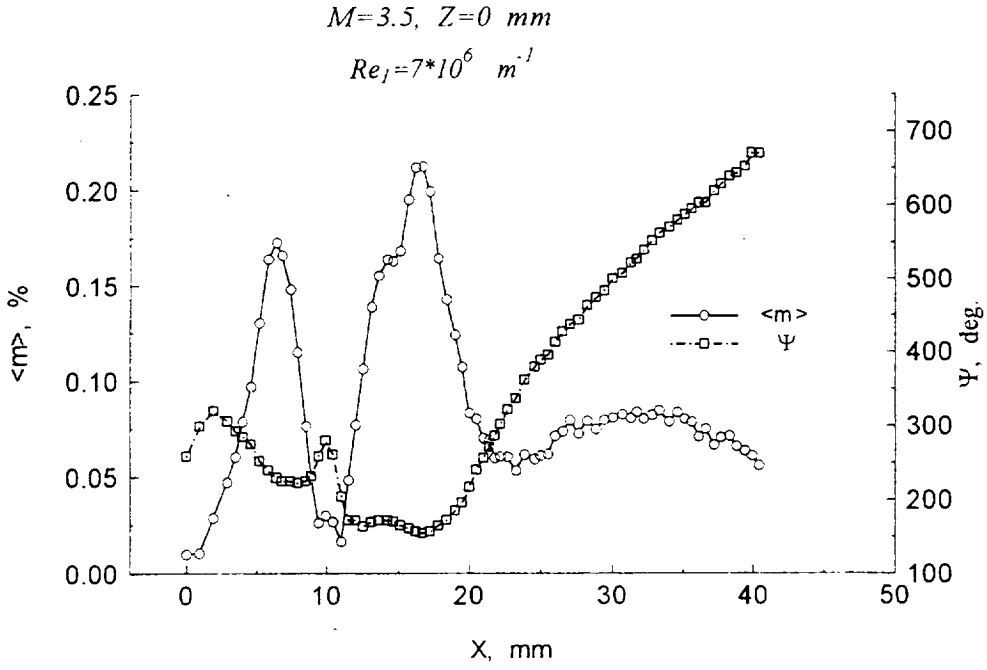

Fig.3.30. Distribution of amplitude and phase of mass flow fluctuation over *x* for controlled disturbances at frequency 20 kHz.

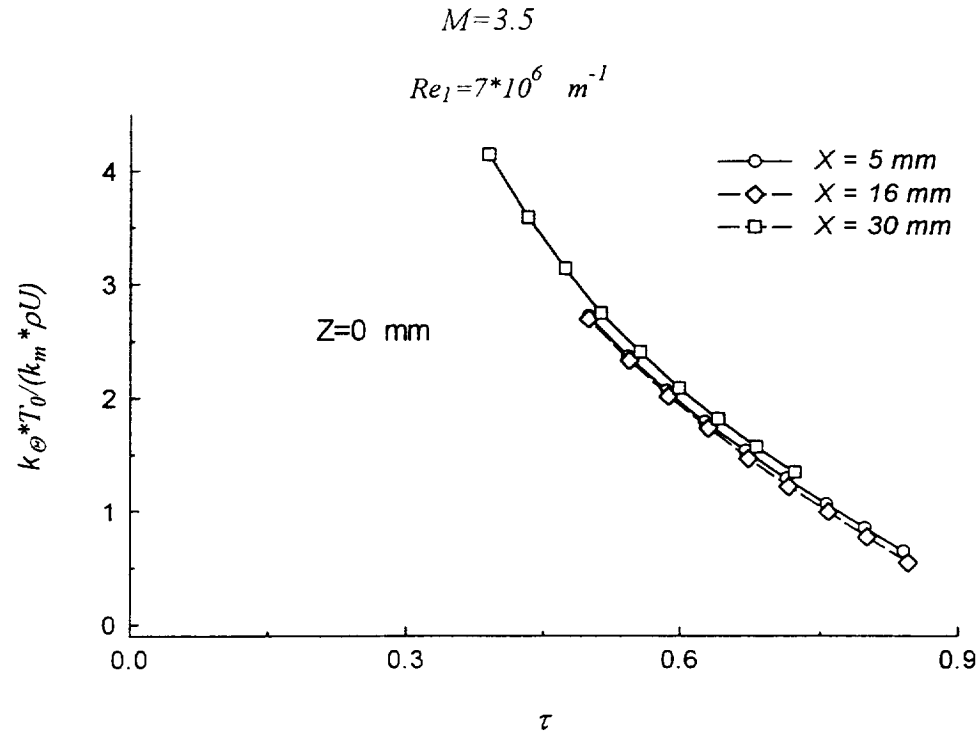

Fig.3.31. Dependence G/Q versus τ.

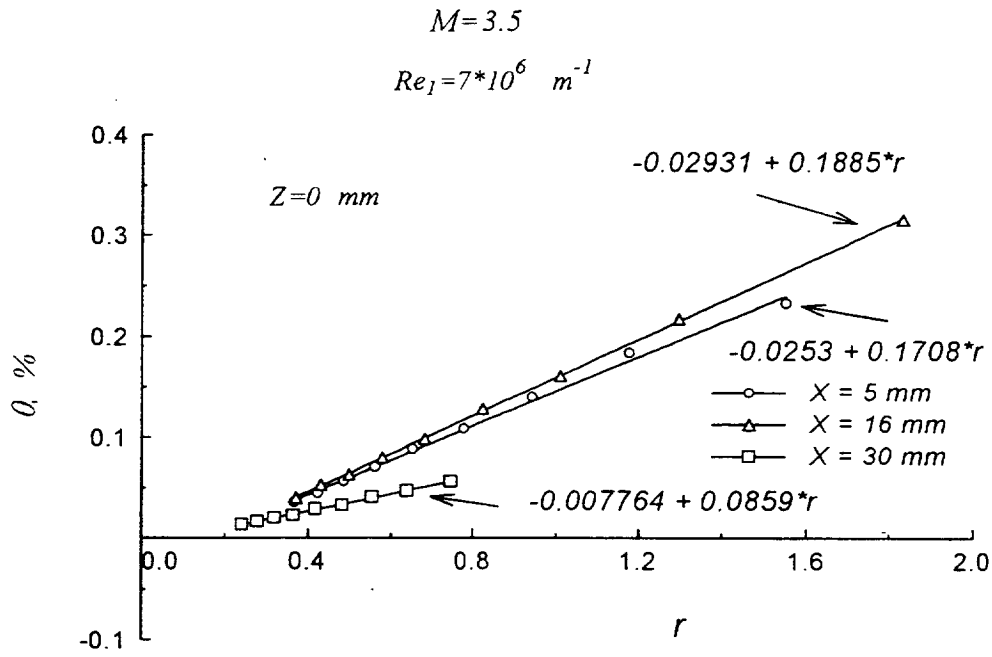

Fig.3.32. Fluctuation diagram of controlled disturbances.

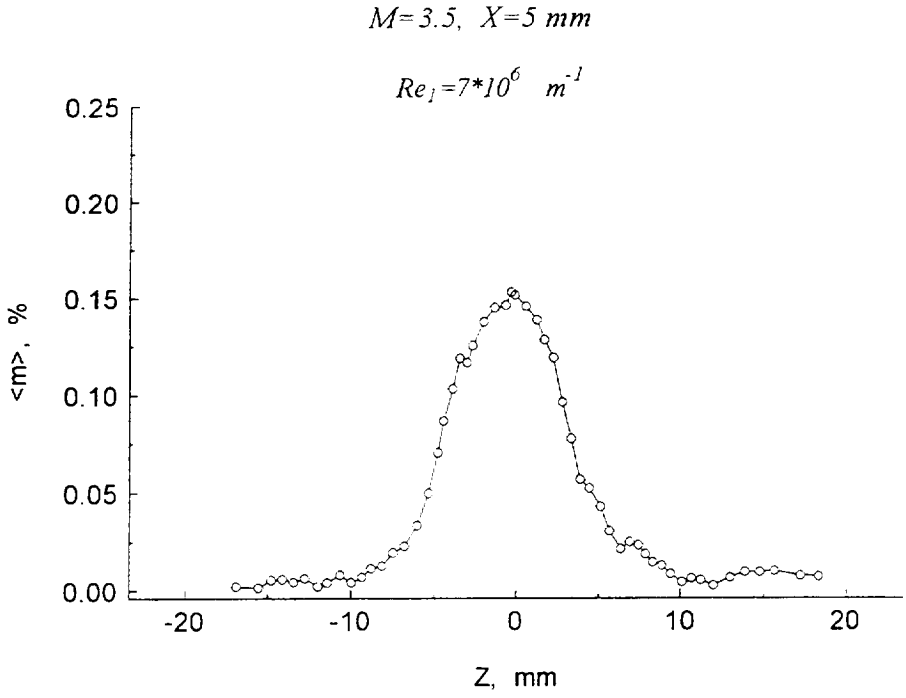

Fig.3.33. Distribution of amplitude of mass flow fluctuation over coordinate *z*.

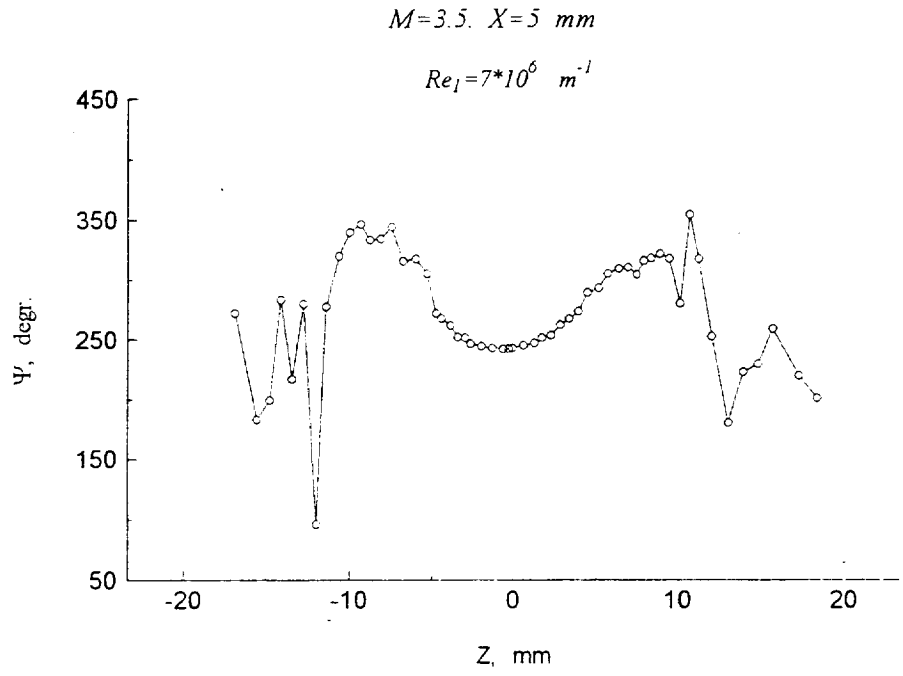

Fig.3.34. Distribution of phase of mass flow fluctuation over transversal coordinate *z*.

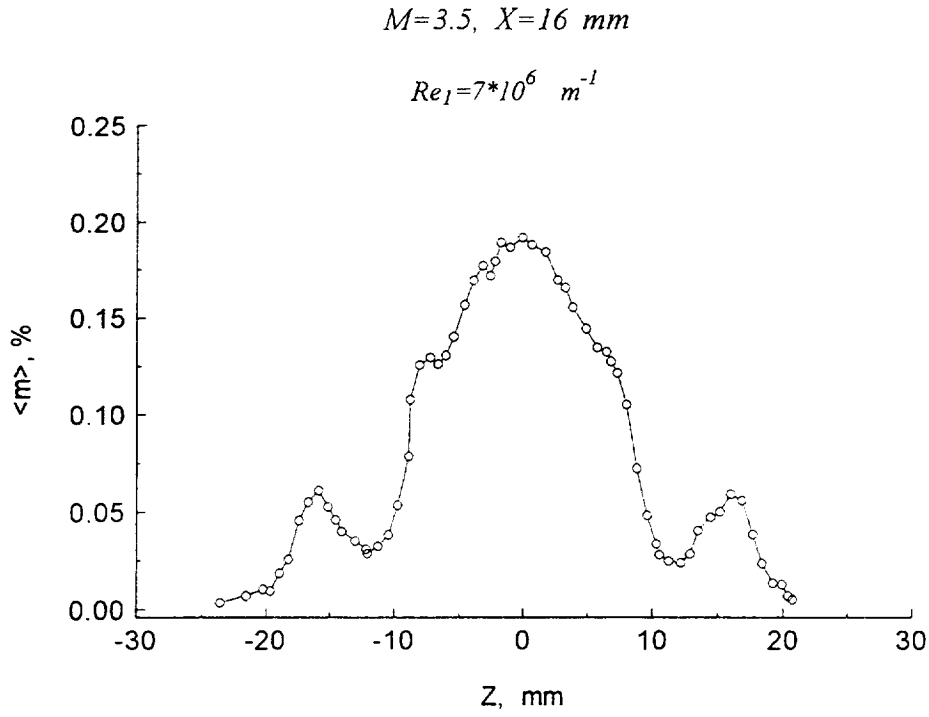

Fig.3.35. Distribution of amplitude of mass flow fluctuation over coordinate z.

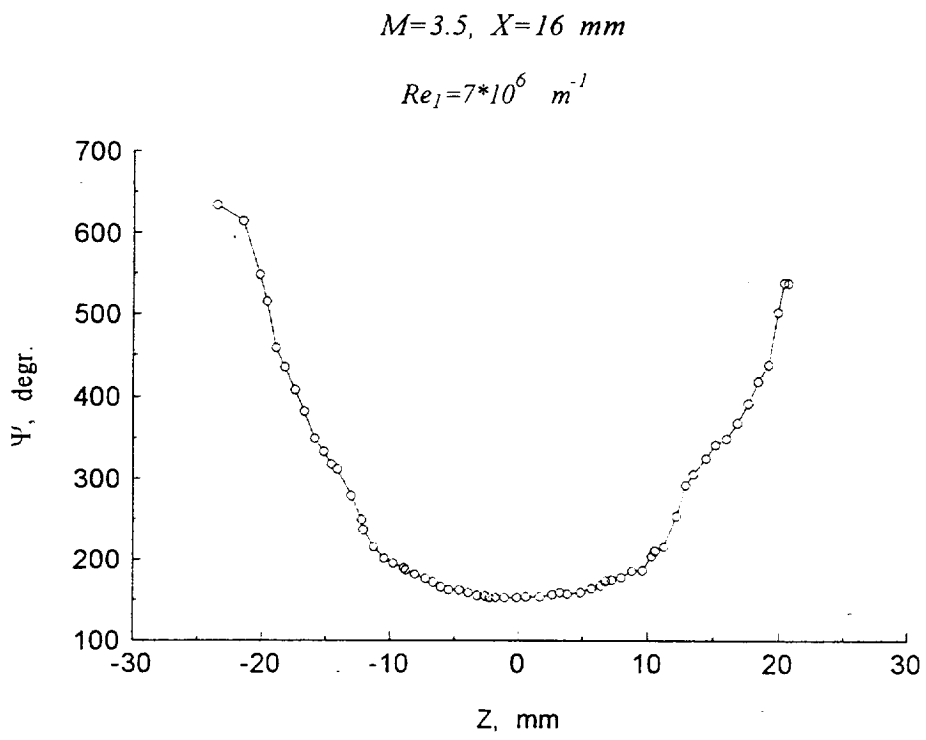

Fig.3.36. Distribution of phase of mass flow fluctuation over transversal coordinate z.

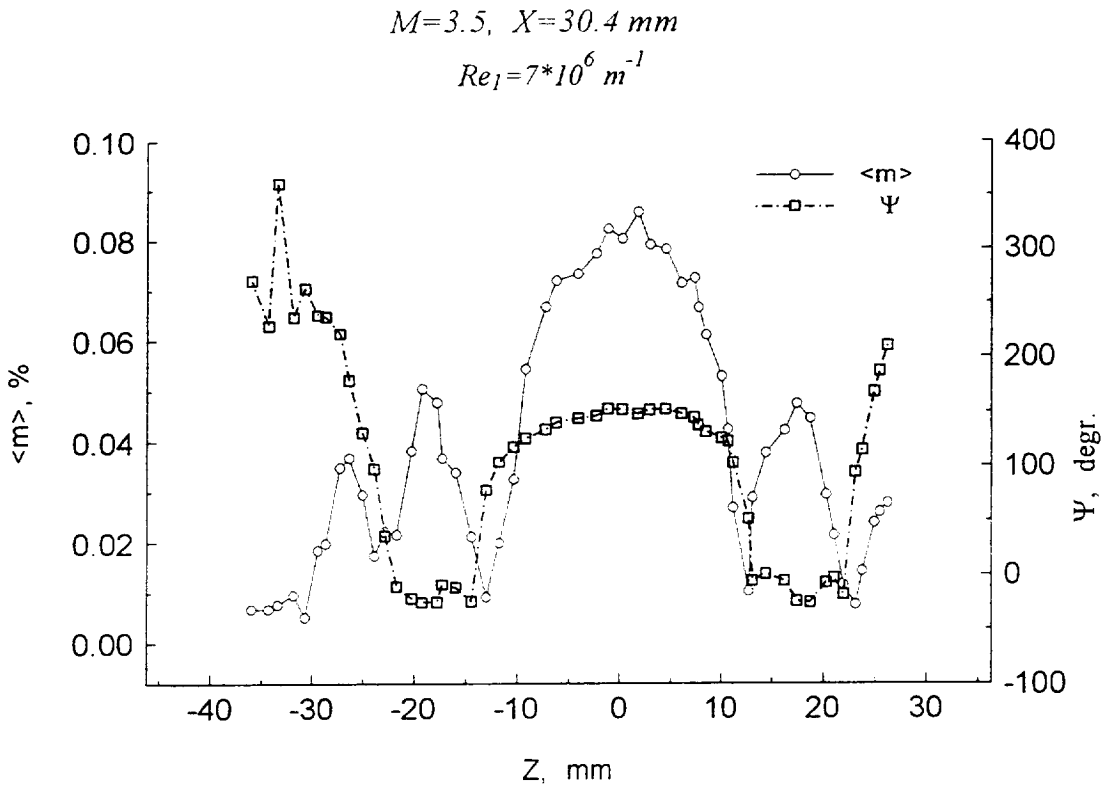

Fig.3.37. Distribution of amplitude and phase of mass flow fluctuation over coordinate *z*.

4. Sharp leading edge receptivity

4.1. Organization of experiments

The experiments were carried out at Mach number M=3.5 and unit Reynolds number Re_1=7×10^6 m^{-1}. The controlled disturbances of frequency f=20 kHz (F=0.28×10^{-4}) were generated by electric discharge in chamber. The initial amplitude of controlled disturbances from the local source were fixed during these experiments. Measurements of controlled disturbances were accompanied by calibration tests in order to estimate the pulsation magnitude.

4.2. Flat plates

The test set-up is shown in figs.3.1, 3.3. To make the experiments we used two trapezoidal plates, mounted under zero angle of attack. The plate *1* with generator of periodic disturbances was mounted on traversing equipment bar and could be moved during experiment on various distances from the wall of the test section of wind tunnel. The plate *1* is 80 mm length, 80 mm width at top and 60 mm at bottom, 5 mm thick. Slope angles of leading edge and lateral sides are 14°30′. Distance from the plate *1* to the wall of the test section depended on Mach numbers. Namely, this distance was a=76 mm for M=2 (see fig.3.1), and a=90 mm for M=3.5. The design of the generator of periodic disturbances is based on electric discharge in chamber and is similar to the source described in Kosinov et al. (1990[2]). The artificial disturbances were entered into supersonic flow through an aperture with diameter 0.5 mm in working surface of the flat plate. Coordinates of the source were: x=18±0.25 mm, z=0, where x is a streamwise coordinate from the leading edge of the plate *1*, z is a spanwize coordinate in a symmetry plane of the plate *1*. Being rather intensive to radiate acoustic waves in free stream (Maslov & Semionov 1987[2]), disturbances at frequency 20 kHz were generated with the help of the high-frequency electric discharge.

The plate *2* was fastened to pylon at the distance 116 mm from the wall of the test section of T-325 wind tunnel. The plate *2* was 280 mm length, 160 mm width at top and 80 mm at bottom, 7 mm thick. Slope angles of sharp leading edge and lateral sides were 14°30′. A possibility was provided for remounting of the plate *2* in streamwise direction at various distances *b* (see fig.3.1) between leading edges of plates. The leading edge radius was less than 0.03 mm.

4.3. Leading edge receptivity at Mach 3.5

4.3.1. Initial data

First of all we should consider streamwise amplitude and phase distributions for controlled pulsations in free stream flow.

An initial field of controlled fluctuations was measured in free stream in the plane of the plate *2* at the distance y_1=26 mm from the surface of the plate *1* (plate *2* was mounted further downstream). In this case the plate *2* was used as a support for traversing mechanism. The initial amplitude of controlled disturbances was measured along coordinates *x, y, z* at fixed power level of the local source of disturbances. Distributions of the amplitude and phase $A(x)$, $\Phi(x)$ at z=0 are shown in fig.3.30. Coordinate *x* was measured from the upstream border of the forced radiation zone.

To analyze the obtained data, it is useful to present a simplified physical model of the source of disturbances. The artificial disturbances entered the boundary layer through the aperture in the plate *1*. Hence, it is obvious that vortices with different directions of rotation in *yx*-plane were formed as the result of deceleration of the flow in the near upstream and downstream fields of discharge. Further downstream, the generated disturbances became themselves the origin of Tollmien-Schlichting (TS) waves in the boundary layer of the plate *1*. This process was accompanied by a radiation of various types of controlled disturbances into the free stream. The radiation propagated inside the Mach cone from the discharge.

On the basis of this model, three characteristic zones can be distinguished corresponding to the various types of functions $A_0(x)$ and $\Phi_0(x)$. Now we shall classify these regions. The first zone (1 mm<x< 9 mm) corresponds to acoustic waves, radiated by the source and propagated upstream in the boundary layer of the plate *1*. The region of propagated upstream disturbances in the boundary layer from the controlled source was also observed by Kosinov et al. (1992). The second zone corresponds to the sound waves radiated from a vortex behind of aperture (11 mm < x < 20 mm), and the third zone is observed for x>22 mm as the sound wave radiation from TS waves. The maximum at $x\approx$10 mm corresponds to the disturbance directly radiated from the source aperture on the surface of the plate *1*. These zones have been tested for the boundary layer response.

Amplitude and phase distributions $A(x)$ and $\Phi(x)$ for the controlled disturbances in the free stream flow, measured in the plane of the plate *2* at y=5 mm, when the leading edge of the plate 2 was placed at x=30 mm, are shown in fig.4.1. The maximum *1* in distribution $A(x)$ at y=5 corresponds to the Mach line from the leading edge of the plate *2*. The distributions $A(x)$ and $\Phi(x)$ up to this maximum are similar to ones presented in fig.3.30. Note that the amplitude of disturbances over the plate *2* is very small, however the phase growth is rather pronounced. These data confirm that the unstable disturbance generation by acoustic waves occurs only near the leading edge of the plate *2*.

Pulsation diagrams. The measurements were made at z=0; x=5, 16, 30.4 mm for each above mentioned zone. Fluctuation diagrams shown in fig.3.32 are linear functions and the value $<T_0>$ is small, that indicates an acoustic nature of radiated waves (Kovasznay 1950). Values of the mass flux and stagnation temperature pulsations are given in plots. The obtained values of ratio of the mass flux fluctuations to the stagnation temperature fluctuations at x=5 mm; 16 mm and 30.4 mm appeared to be different. Namely, the obtained values were: $A_o\approx$11.1, 6.8, 6.4 and $A_{<m>}$=1.81, 1.82, 1.86 correspondingly to each x. Actually the values $A_{<m>}$ were used to define the mass flux pulsation amplitude.

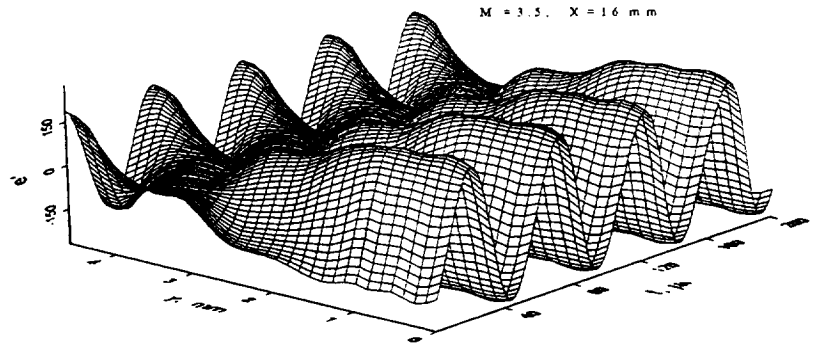

Fig.4.5. Dependence of amplitude of oscillograms of controlled disturbances over normal coordinate *y* at *x*=16 mm. 3-D plot.

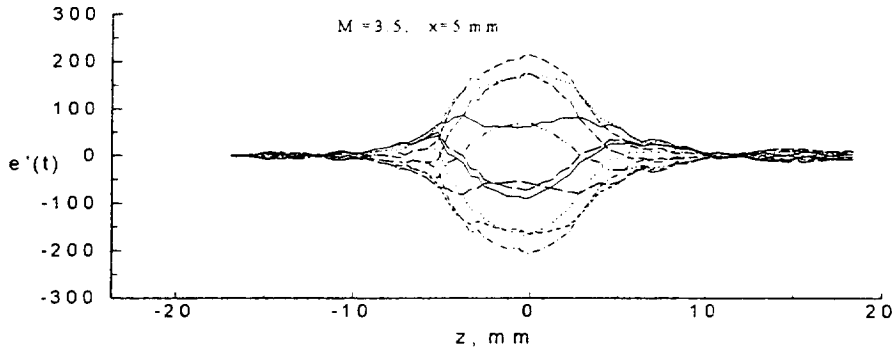

Fig.4.6. Dependence of controlled disturbances over spanwise coordinate *z* at *x*=5 mm. Instantaneous distributions of oscillograms amplitude.

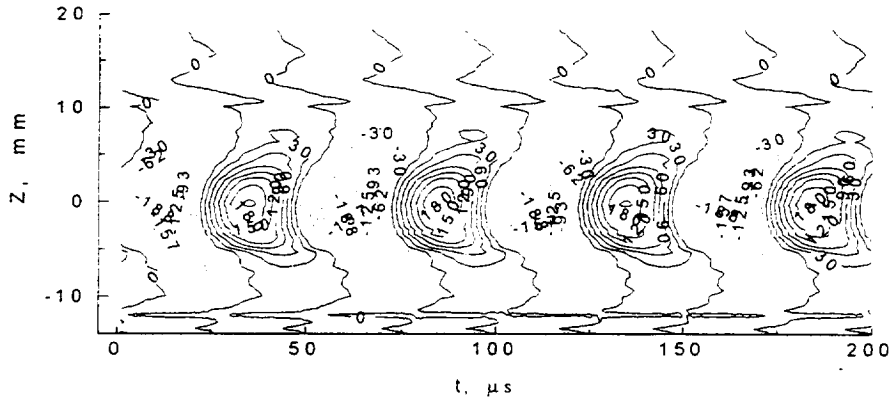

Fig.4.7. Dependence of controlled disturbances over spanwise coordinate *z* at *x*=5 mm. Isolines of oscillograms amplitude.

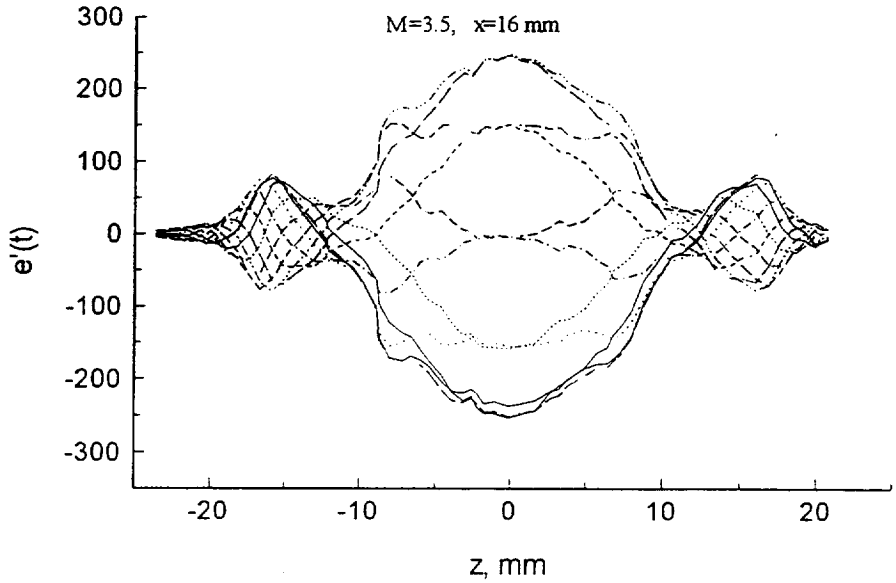

Fig.4.8.a. Dependence of controlled disturbances over spanwise coordinate *z* at *x*=16 mm. Instantaneous distributions of oscillograms amplitude.

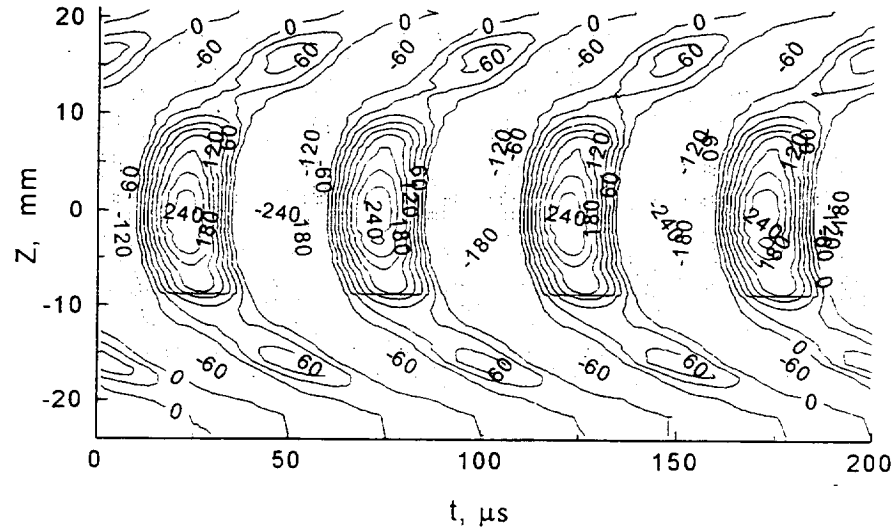

Fig.4.8.b. Dependence of controlled disturbances over spanwise coordinate *z* at *x*=16 mm. Isolines of oscillograms amplitude.

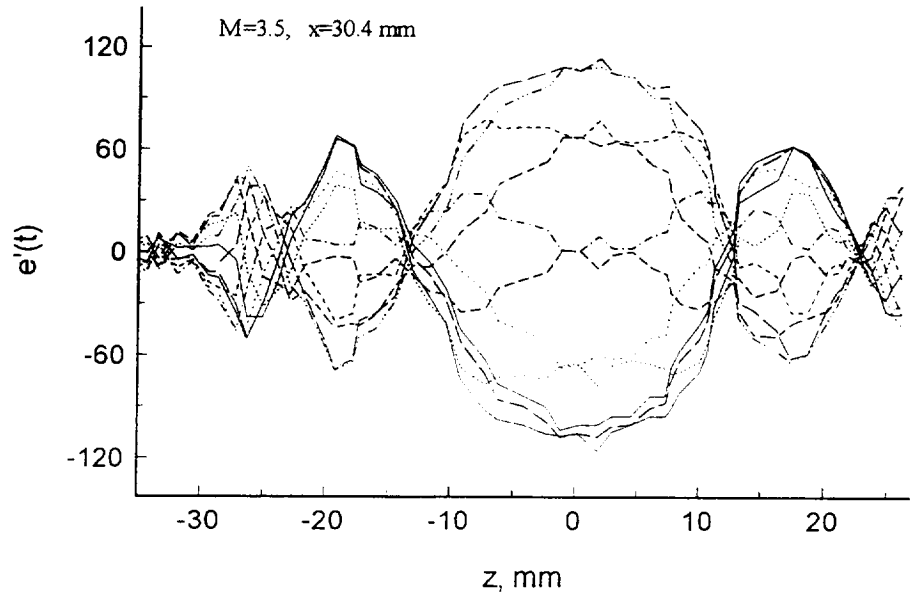

Fig.4.9.a. Dependence of controlled disturbances over spanwise coordinate *z* at *x*=30.4 mm. Instantaneous distributions of oscillograms amplitude.

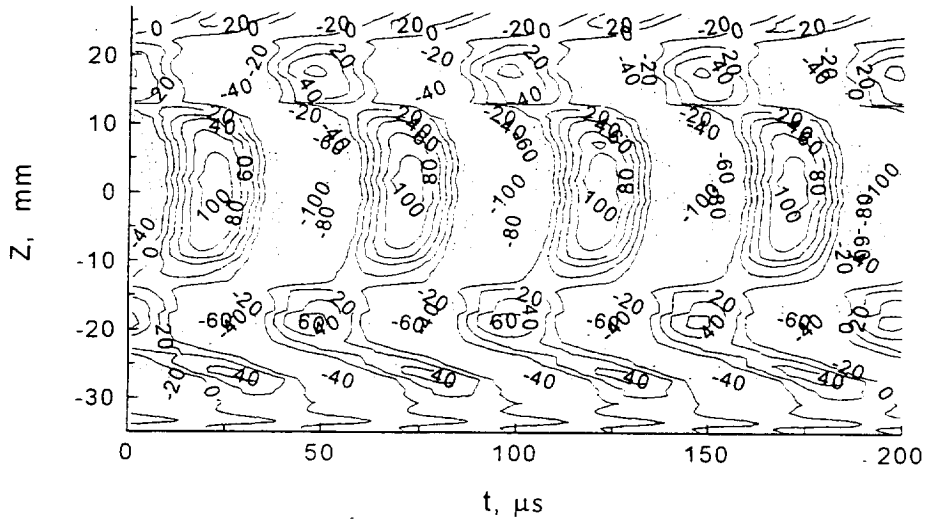

Fig.4.9.b. Dependence of controlled disturbances over spanwise coordinate *z* at *x*=30.4 mm. Isolines of oscillograms amplitude.

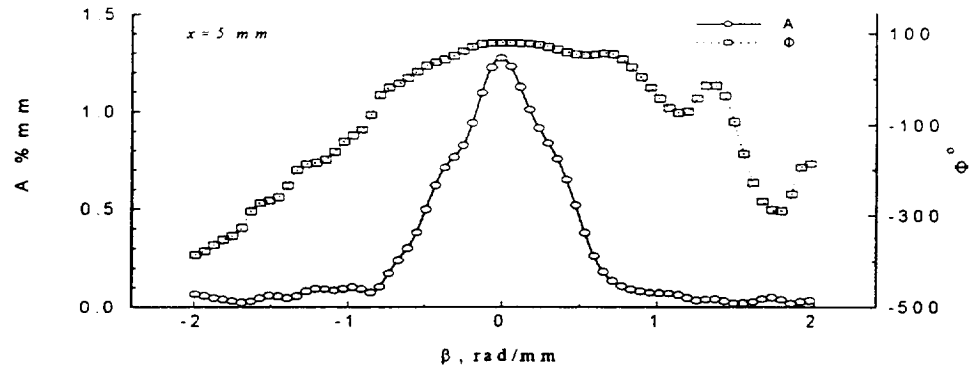

Fig.4.10.a. Distributions of $A_f(\beta)$ and $\Phi_f(\beta)$ of external acoustic disturbances for different radiation zones. x=5 mm.

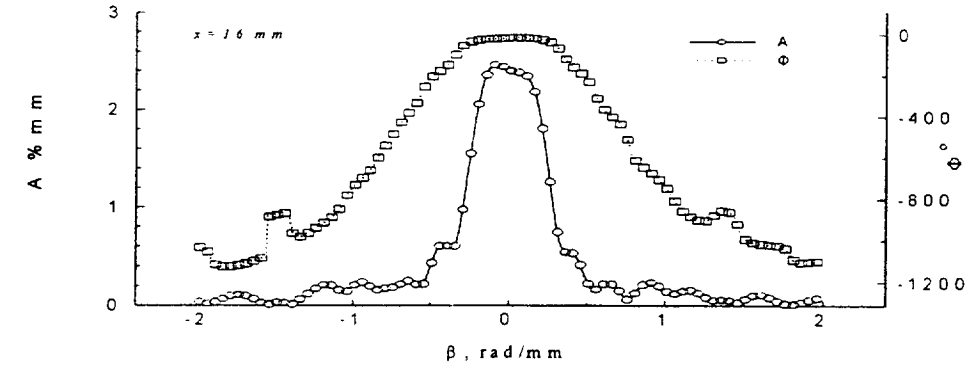

Fig.4.10.b. Distributions of $A_f(\beta)$ and $\Phi_f(\beta)$ of external acoustic disturbances for different radiation zones. x=16 mm.

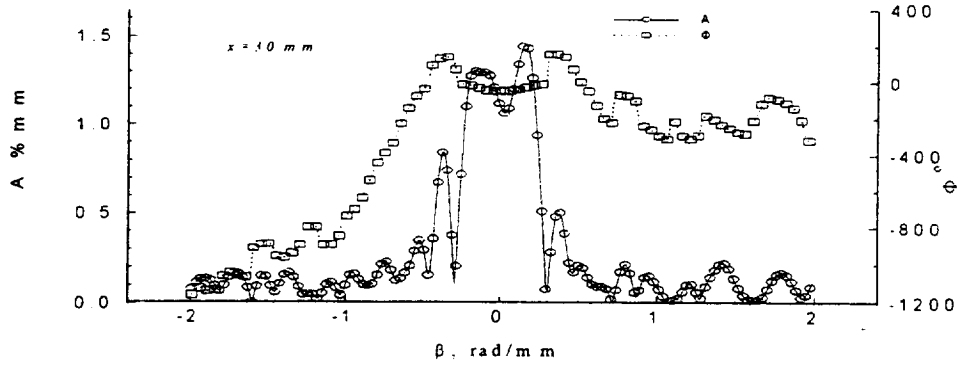

Fig.4.10.c. Distributions of $A_f(\beta)$ and $\Phi_f(\beta)$ of external acoustic disturbances for different radiation zones. x=30.4 mm.

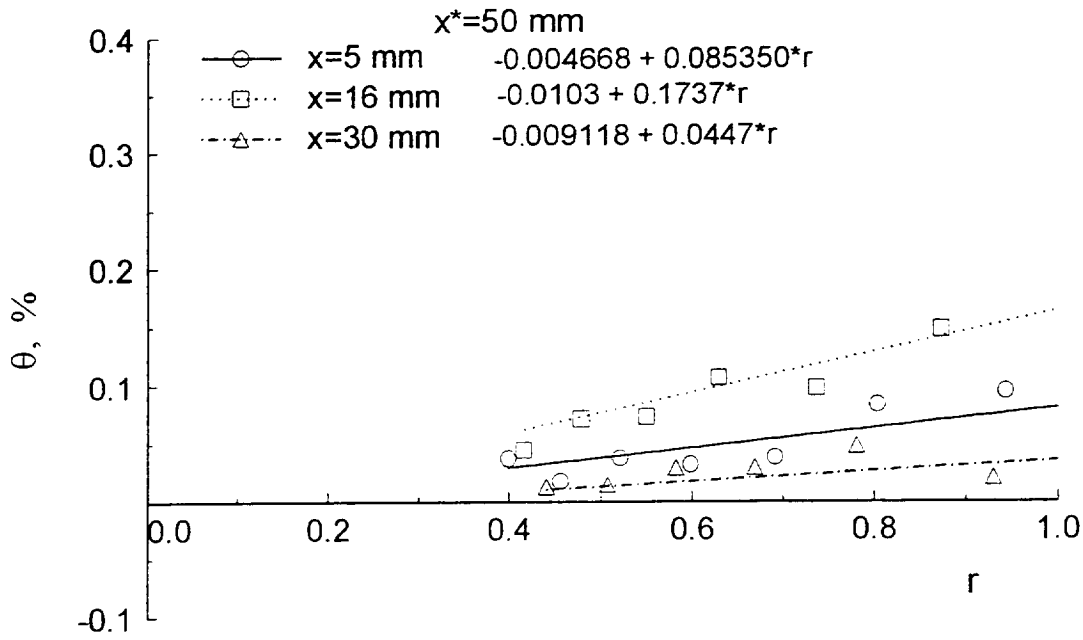

Fig.4.11. Fluctuation diagrams of disturbances in boundary layer.

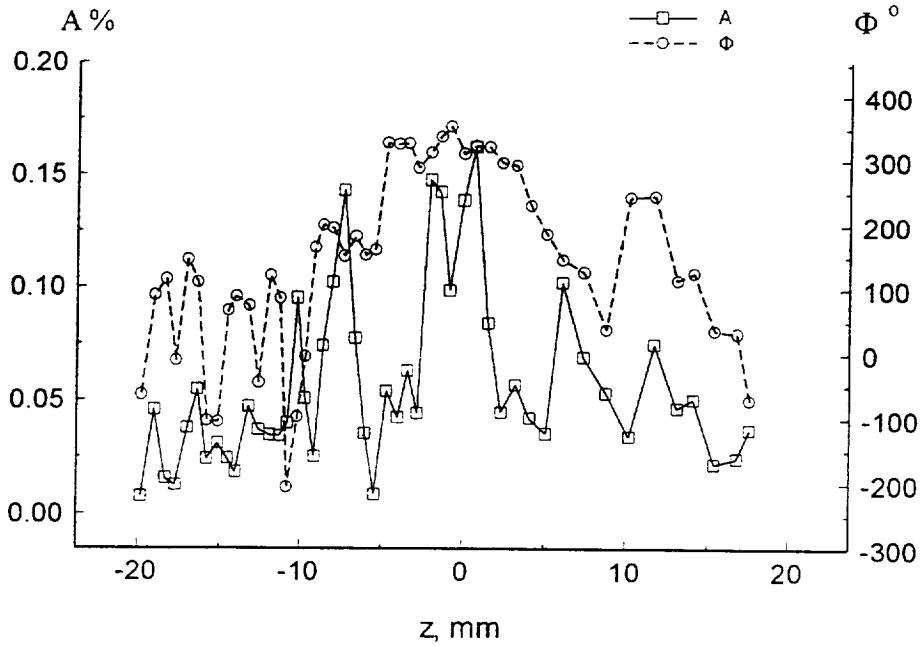

Fig.4.12.a. Amplitude and phase spectra of excited disturbances in boundary layer depending upon spanwise coordinate *z* at *x*=5 mm.

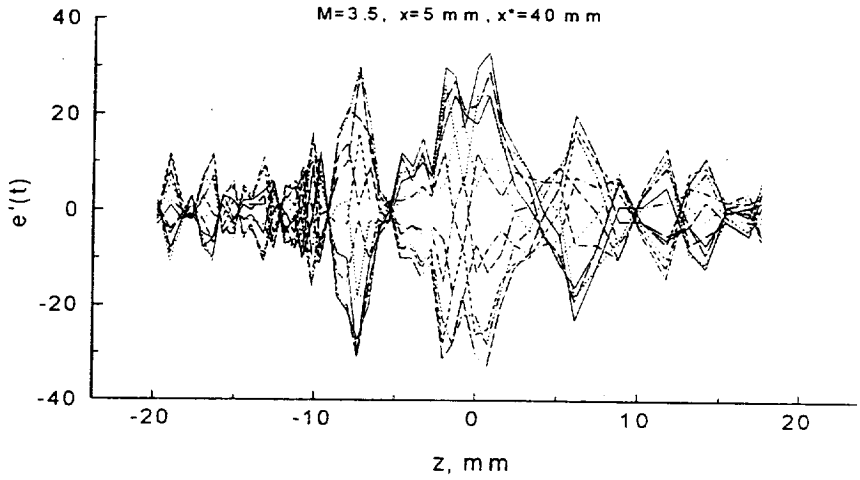

Fig.4.12.b. Instantaneous distributions of oscillograms amplitude over spanwise coordinate *z* at *x*=5 mm.

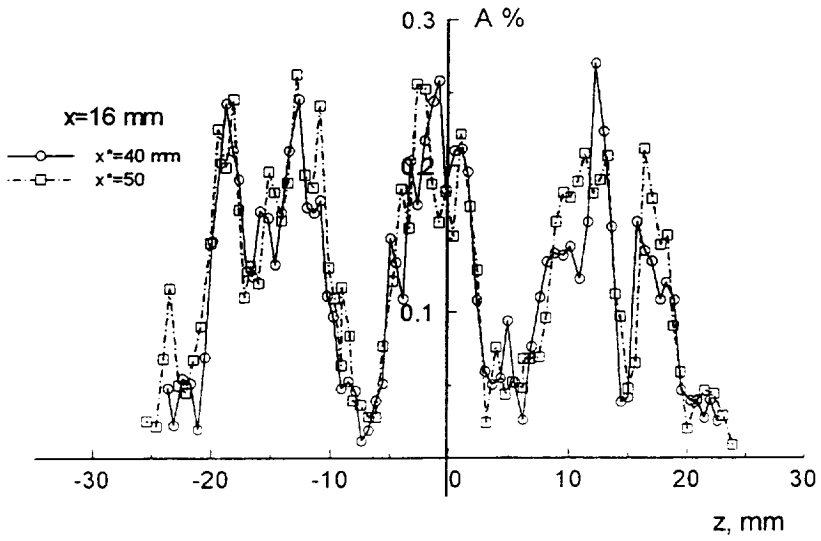

Fig.4.13.a. Amplitude spectra of excited disturbances in boundary layer depending upon spanwise coordinate z at x=16 mm.

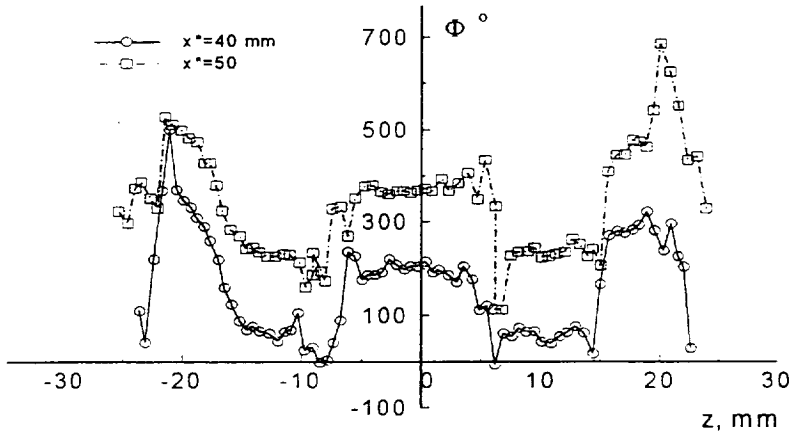

Fig.4.13.b. Phase spectra of excited disturbances in boundary layer depending upon spanwise coordinate z at x=16 mm.

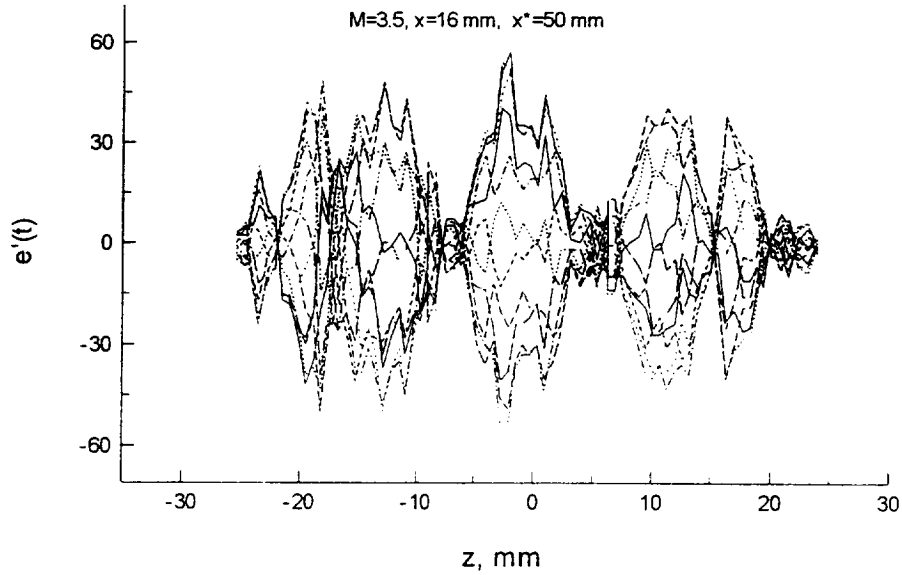

Fig.4.13.c. Instantaneous distributions of oscillograms amplitude over spanwise coordinate z at x=16 mm.

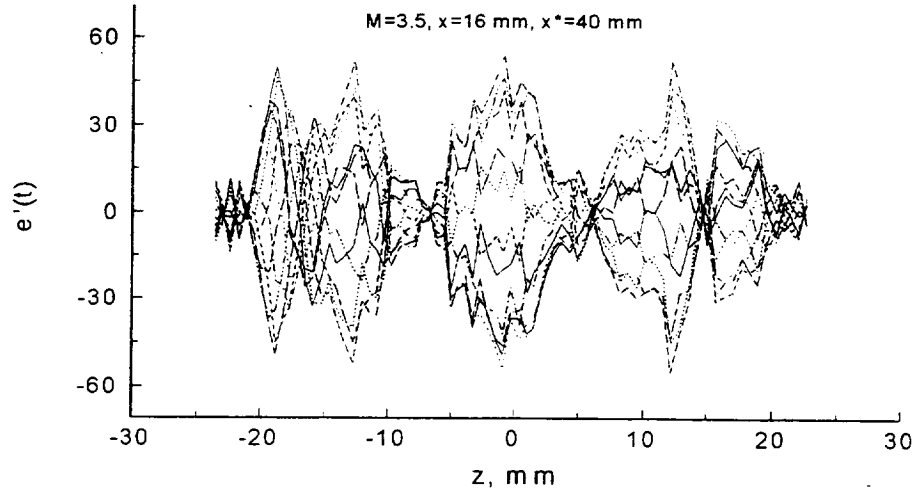

Fig.4.13.d. Instantaneous distributions of oscillograms amplitude over spanwise coordinate z at x=16 mm.

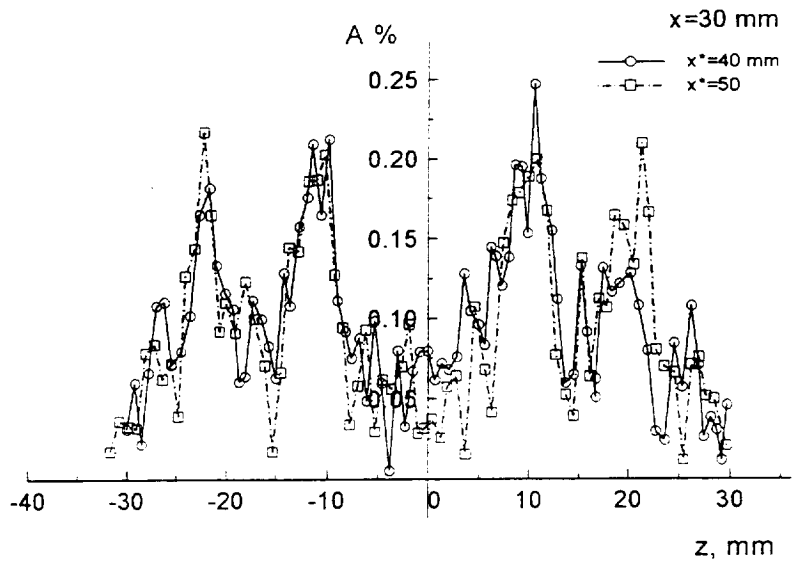

Fig.4.14.a. Amplitude spectra of excited disturbances in boundary layer depending upon spanwise coordinate *z* at *x*=30 mm.

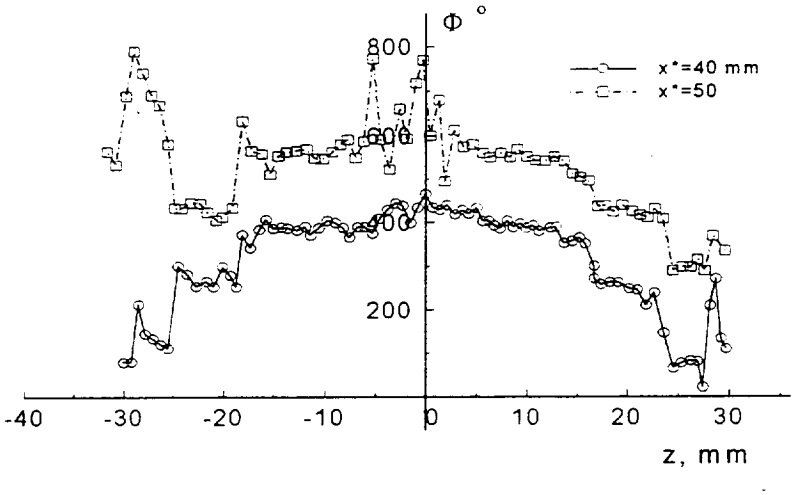

Fig.4.14.b. Phase spectra of excited disturbances in boundary layer depending upon spanwise coordinate *z* at *x*=30 mm.

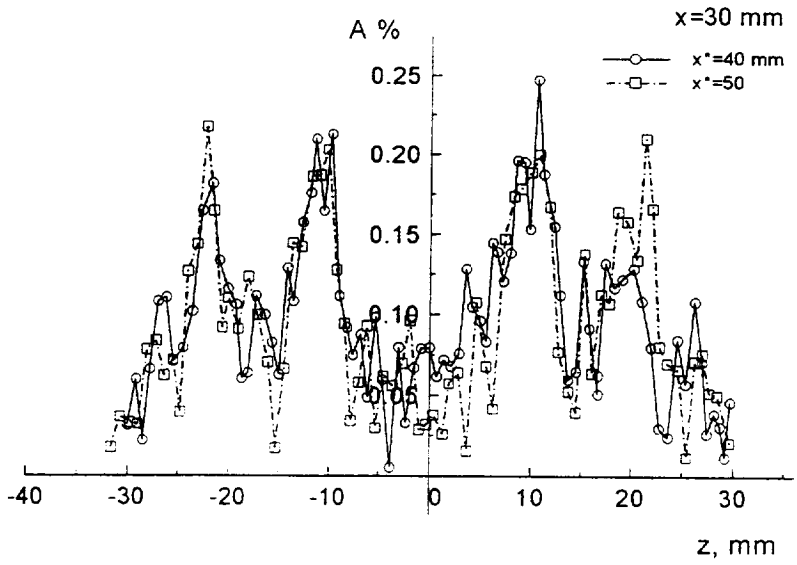

Fig.4.14.a. Amplitude spectra of excited disturbances in boundary layer depending upon spanwise coordinate *z* at *x*=30 mm.

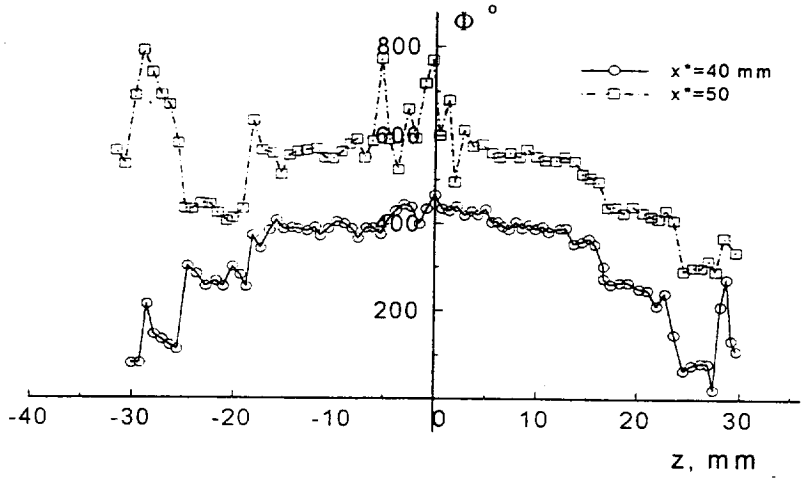

Fig.4.14.b. Phase spectra of excited disturbances in boundary layer depending upon spanwise coordinate *z* at *x*=30 mm.

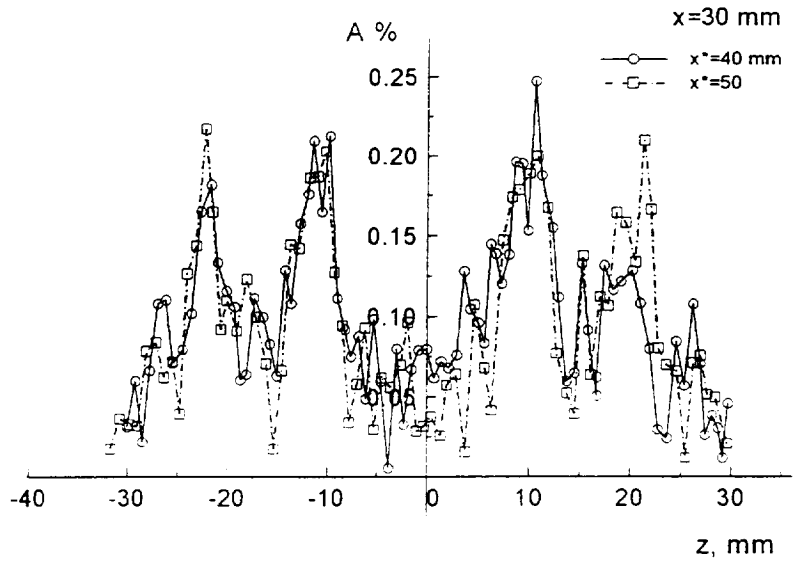

Fig.4.14.c. Amplitude spectra of excited disturbances in boundary layer depending upon spanwise coordinate *z* at *x*=30 mm.

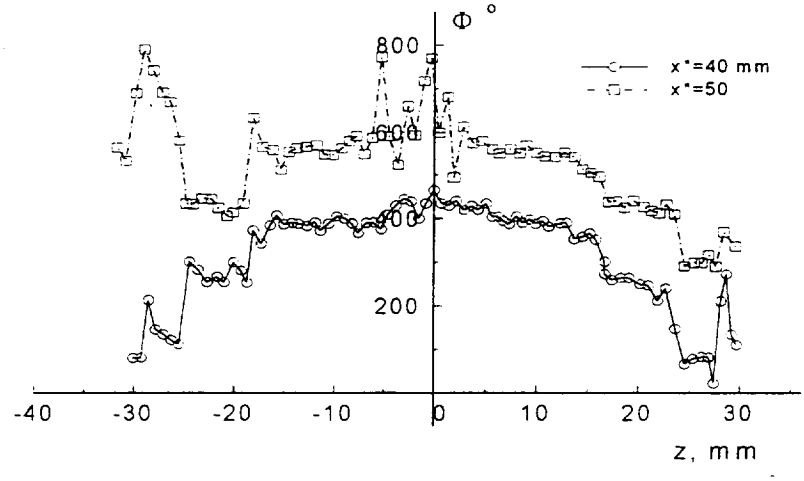

Fig.4.14.d. Phase spectra of excited disturbances in boundary layer depending upon spanwise coordinate *z* at *x*=30 mm.

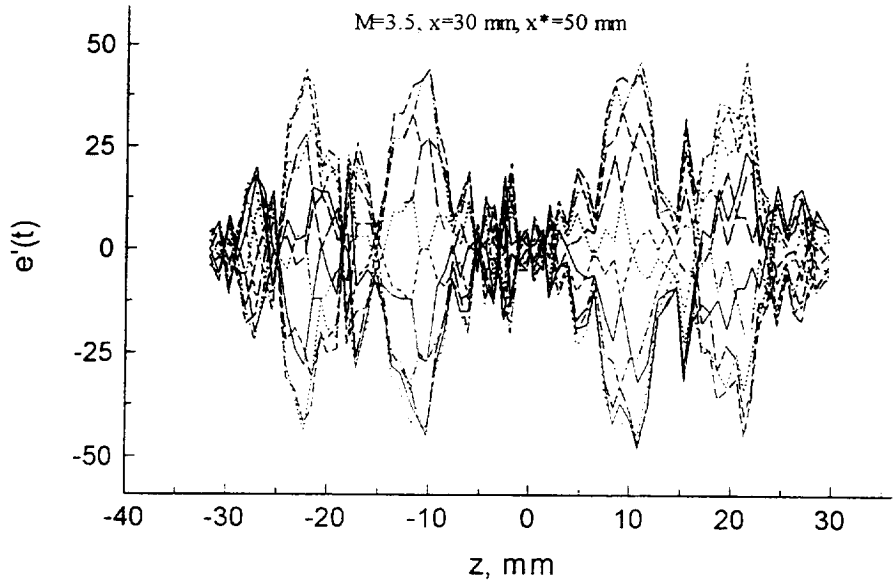

Fig.4.15.a. Instantaneous distributions of oscillograms amplitude over spanwise coordinate *z* at x=30.4 mm.

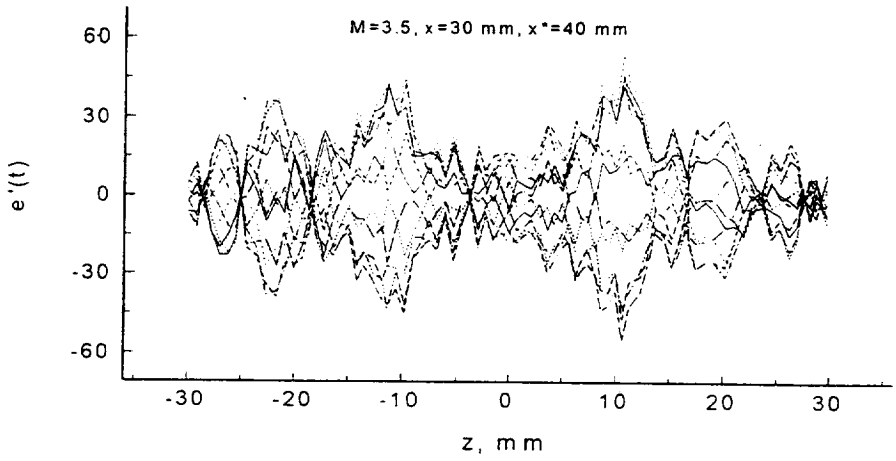

Fig.4.15.b. Instantaneous distributions of oscillograms amplitude over spanwise coordinate *z* at x=30.4 mm.

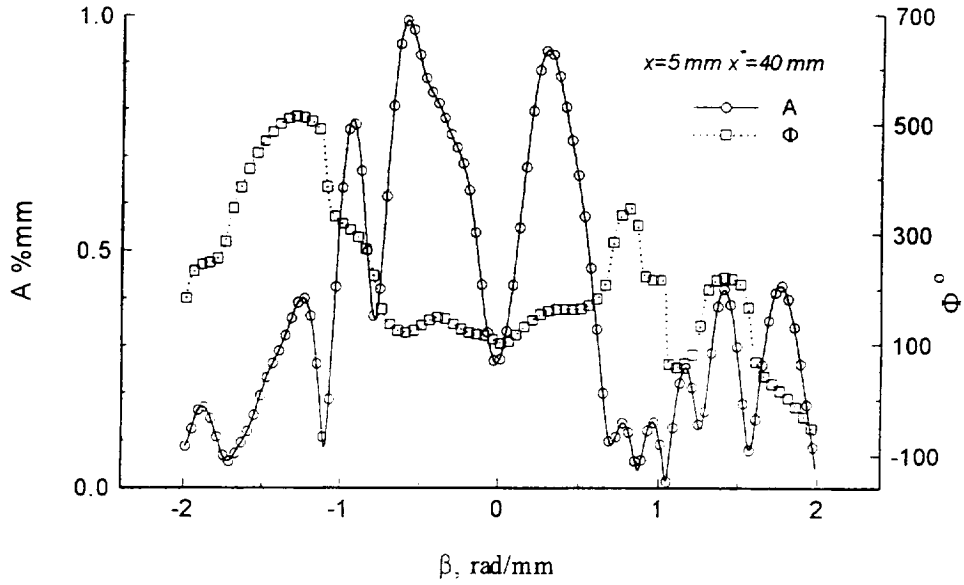

Fig.4.16. Distributions of $A(\beta)$ and $\Phi(\beta)$ of excited eigen oscillations at x=5 mm.

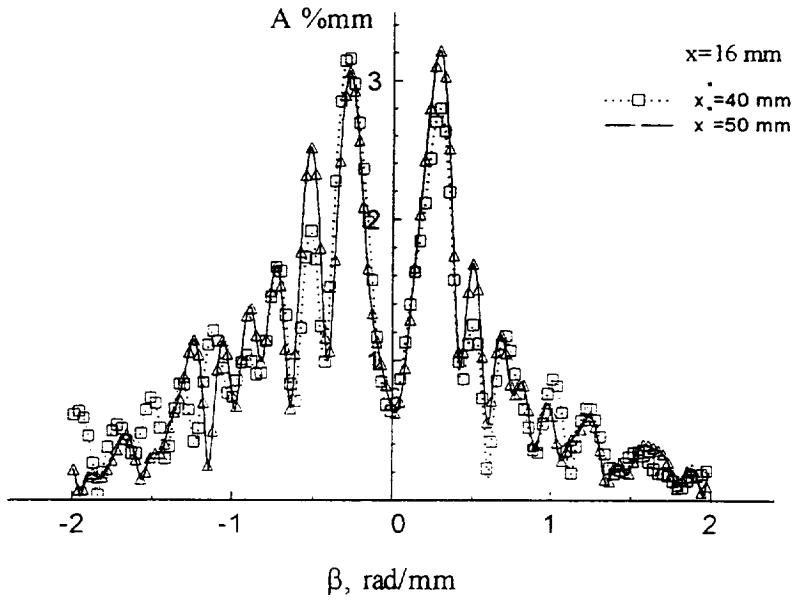

Fig.4.17.a. Distributions of $A(\beta)$of excited eigen oscillations at x=16 mm.

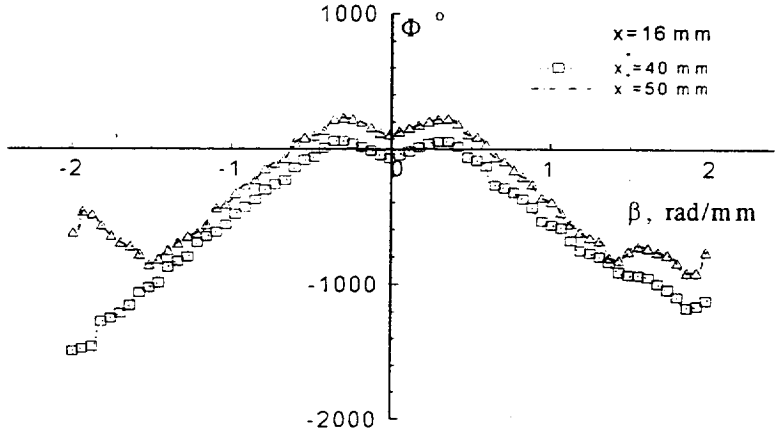

Fig.4.17.b. Distributions of $\Phi(\beta)$ of excited eigen oscillations at x=16 mm.

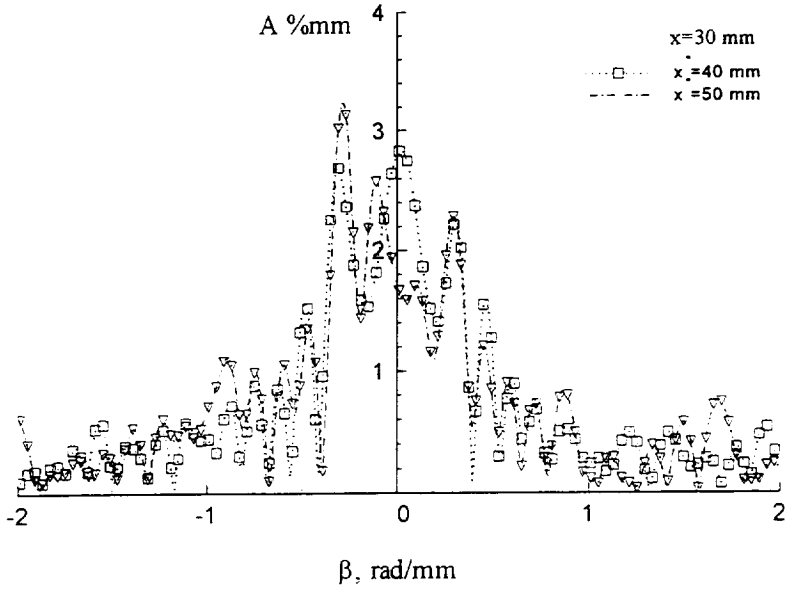

Fig.4.18.a. Distributions of $A(\beta)$of excited eigen oscillations at x=30 mm.

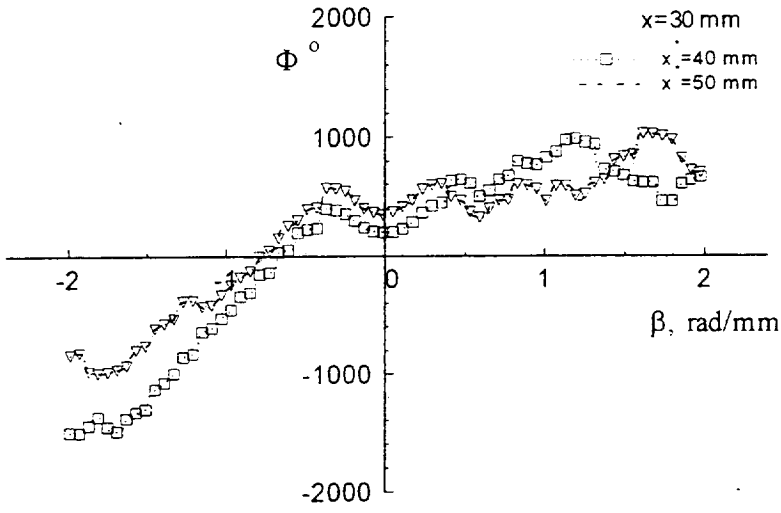

Fig.4.18.b. Distributions of $\Phi(\beta)$ of excited eigen oscillations at x=30 mm.

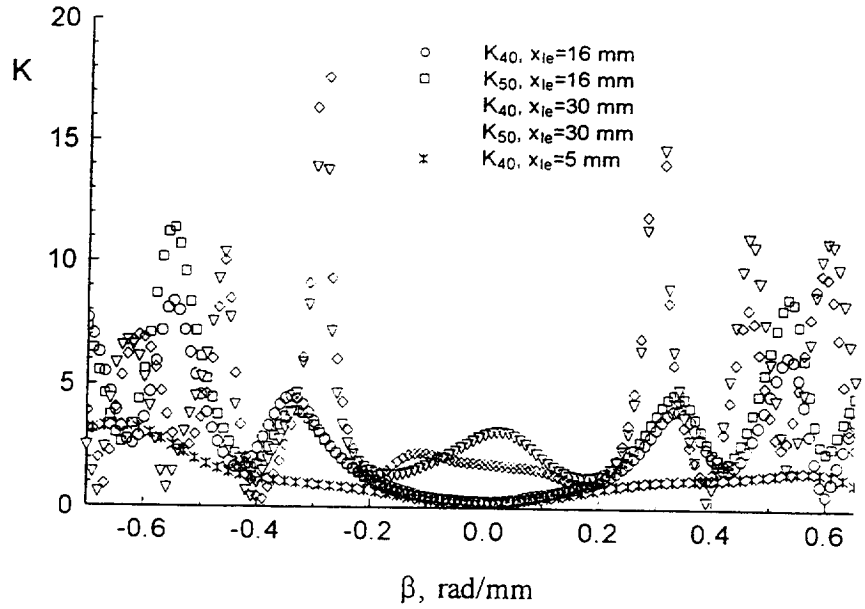

Fig.4.19. Transformation coefficients of disturbances $K(\beta)$ excited by different radiation zones at M=3.5.

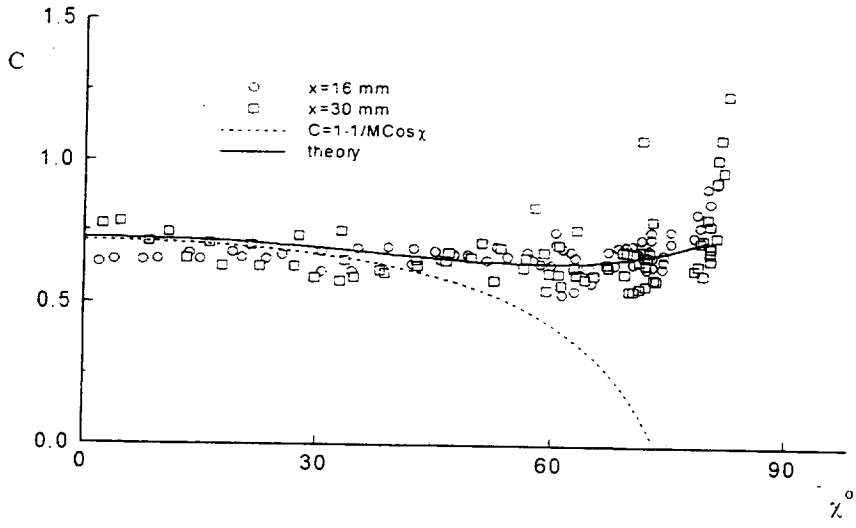

Fig.4.20. Phase velocities of boundary layer disturbances excited by acoustic waves.

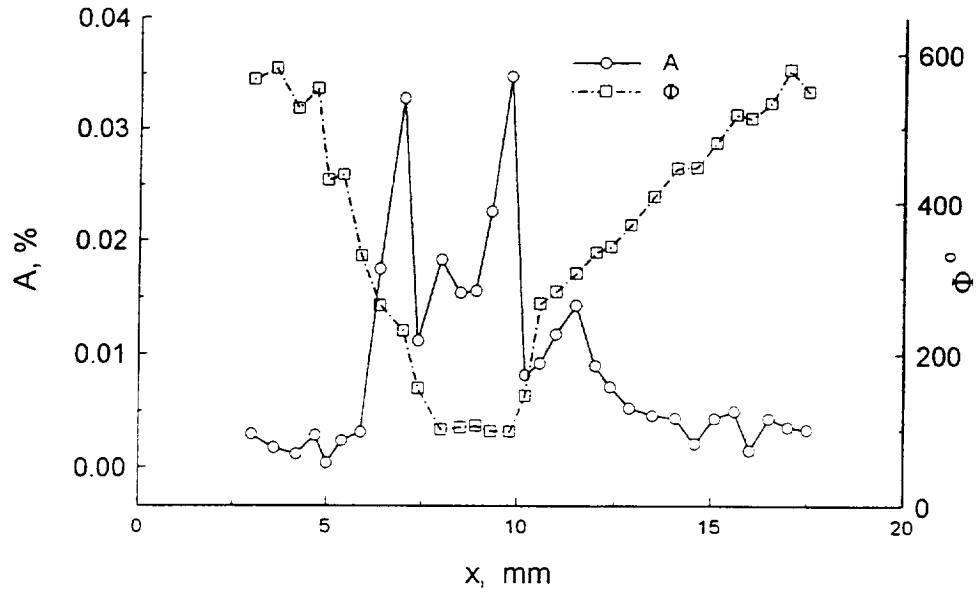

Fig.4.21. Dependence of amplitude *A(x)* and phase *Φ(x)* over streamwise coordinate *x* in plane of plate *2* at *z*=0

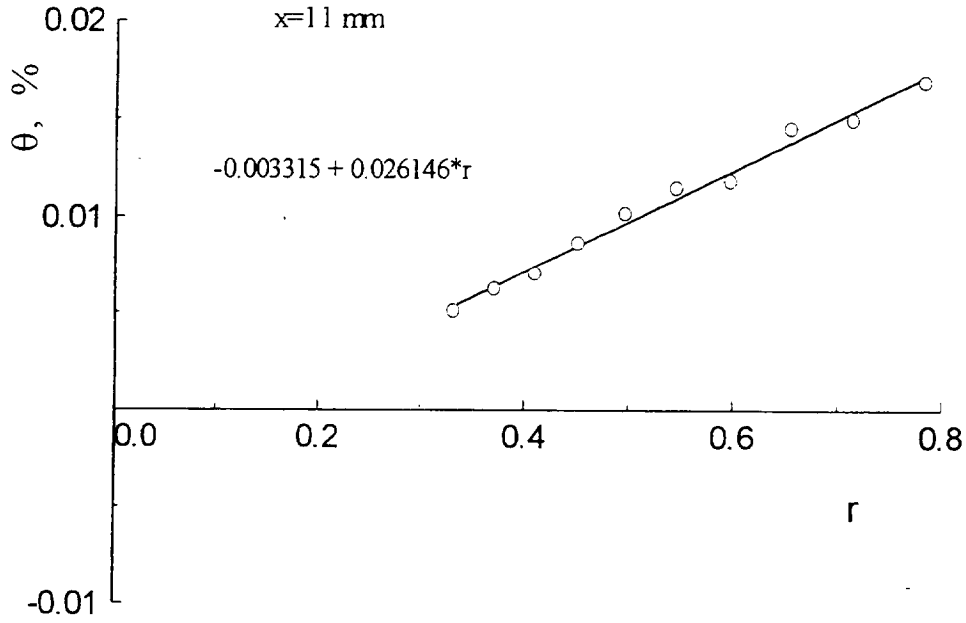

Fig.4.22. Fluctuation diagrams of external controlled disturbances in plane of plate *2* at *x*=11 mm.

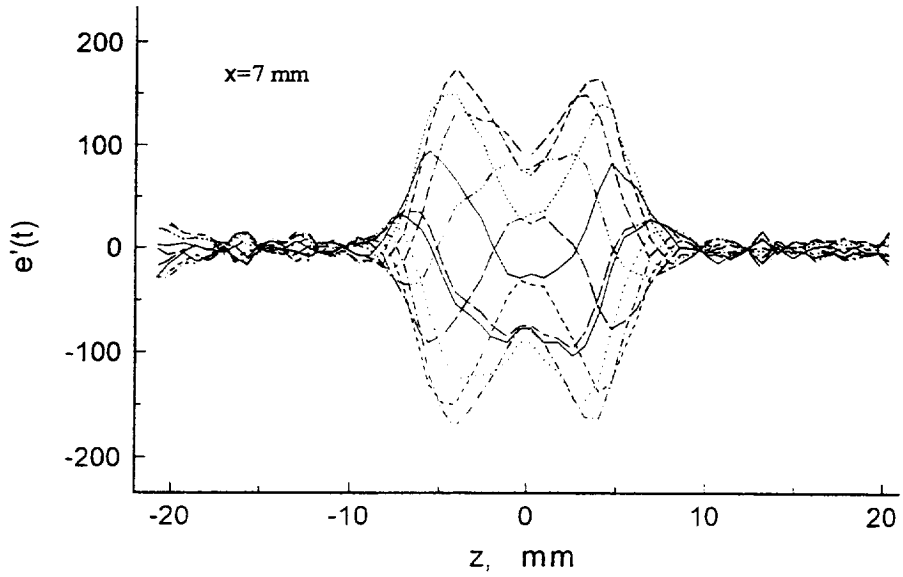

Fig.4.23.a. Instantaneous distributions of oscillograms amplitude over spanwise coordinate *z* at *x*=7 mm.

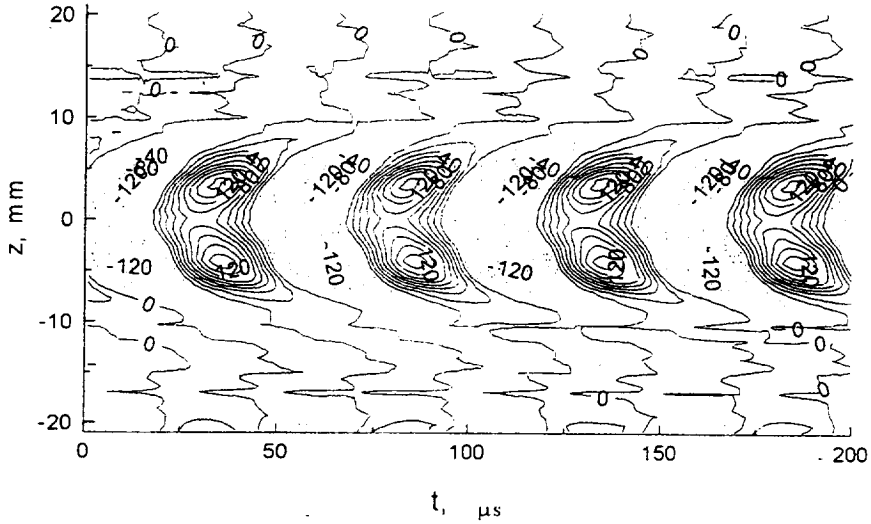

Fig.4.23.b. Isolines of oscillograms amplitude over spanwise coordinate *z* at *x*=7 mm.

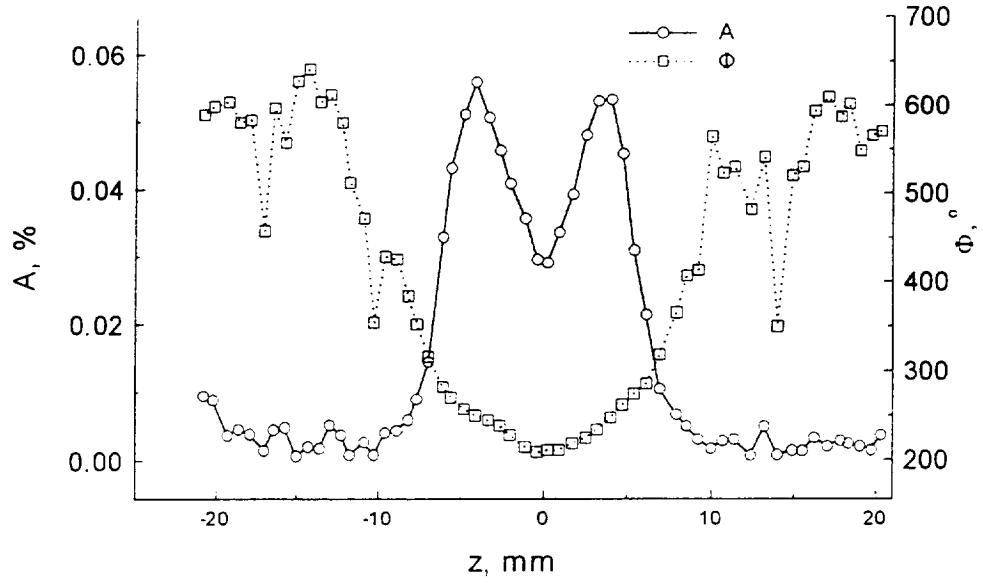

Fig.4.23.c. Distributions of $A_f(z)$ and $\Phi_f(z)$ of controlled disturbances over spanwise coordinate z at x=7 mm.

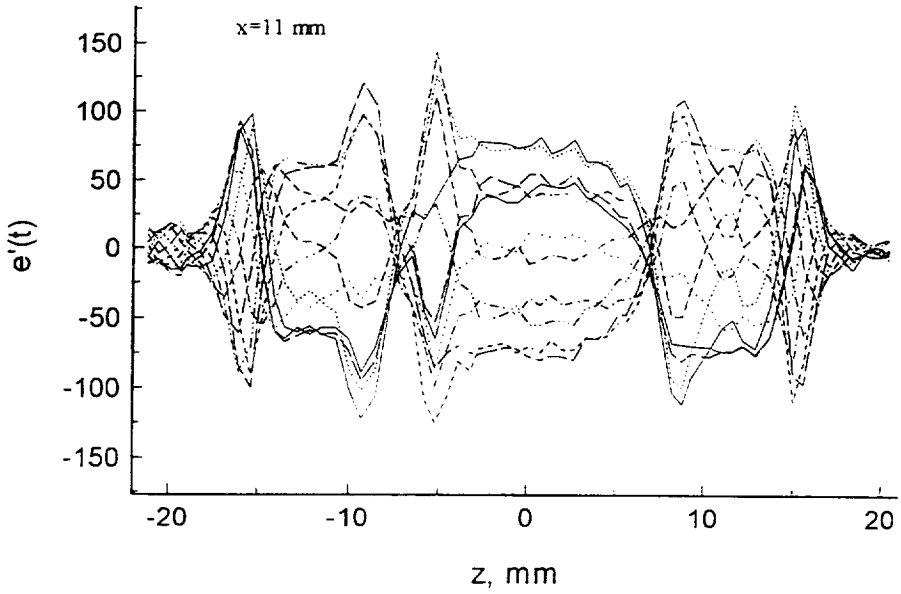

Fig.4.24.a. Instantaneous distributions of oscillograms amplitude over spanwise coordinate *z* at *x*=11 mm.

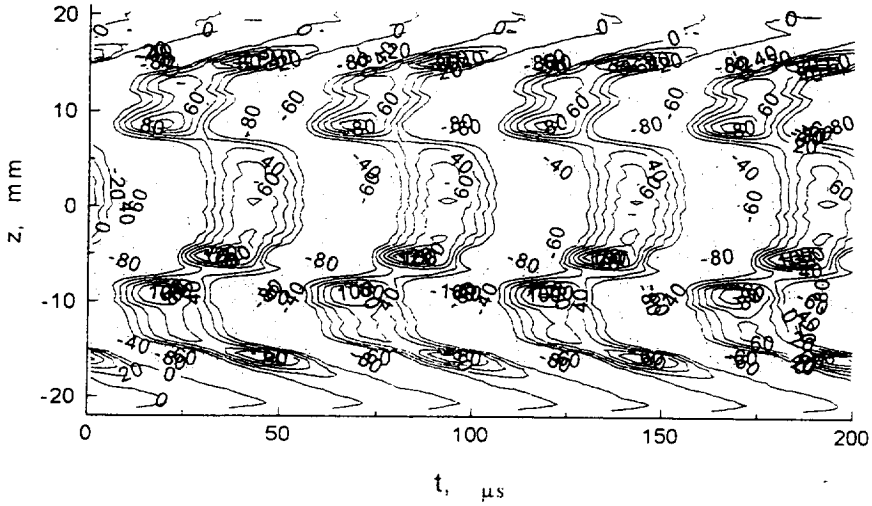

Fig.4.24.b. Isolines of oscillograms amplitude over spanwise coordinate *z* at *x*=11 mm.

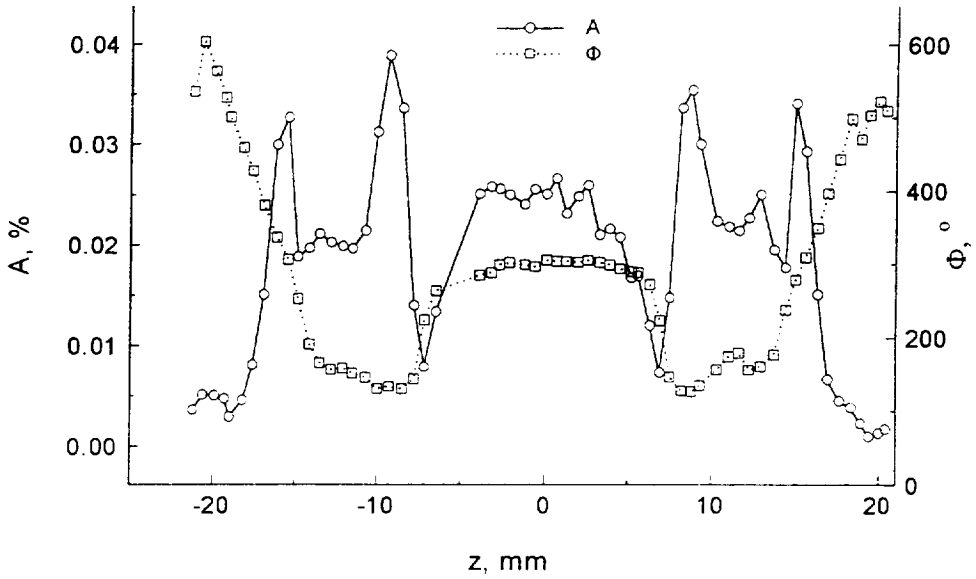

Fig.4.24.c. Distributions of $A_f(z)$ and $\Phi_f(z)$ of controlled disturbances over spanwise coordinate z at x=11 mm.

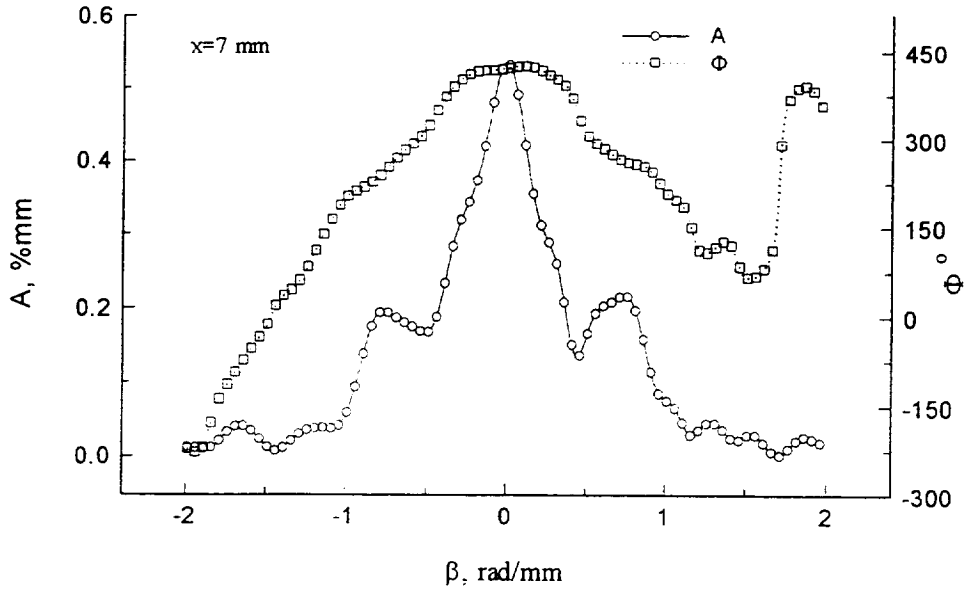

Fig.4.25. Distributions of $A_f(\beta)$ and $\Phi_f(\beta)$ of external acoustic disturbances at x=7 mm.

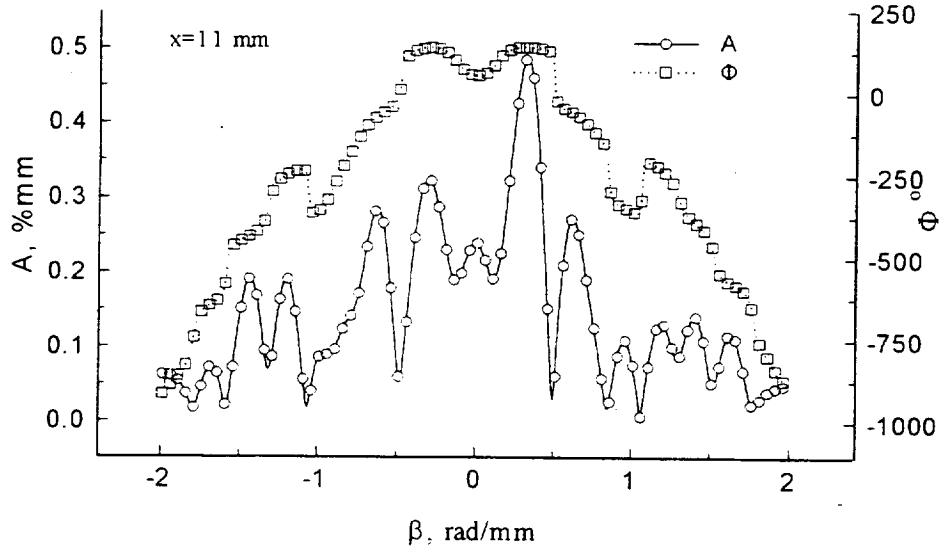

Fig.4.26. Distributions of $A_f(\beta)$ and $\Phi_f(\beta)$ of external acoustic disturbances at x=11 mm.

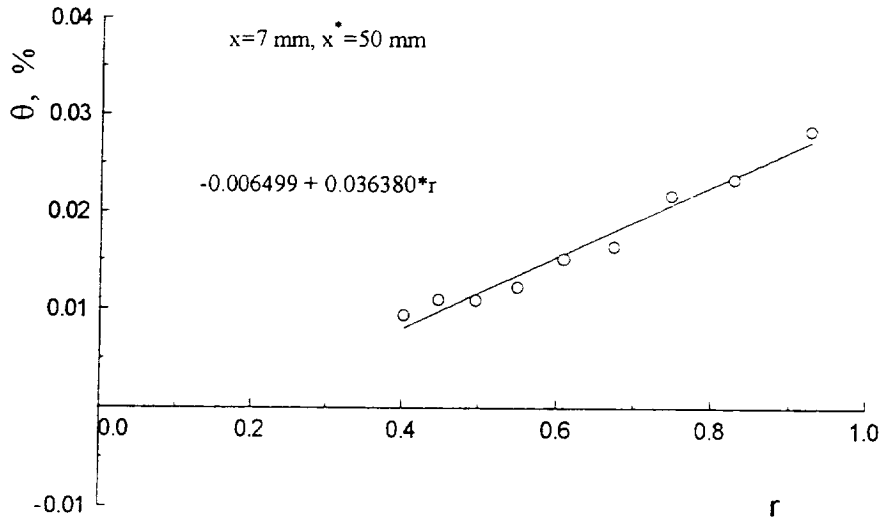

Fig.4.27.a. Fluctuation diagrams of boundary layer disturbances at x=7 mm.

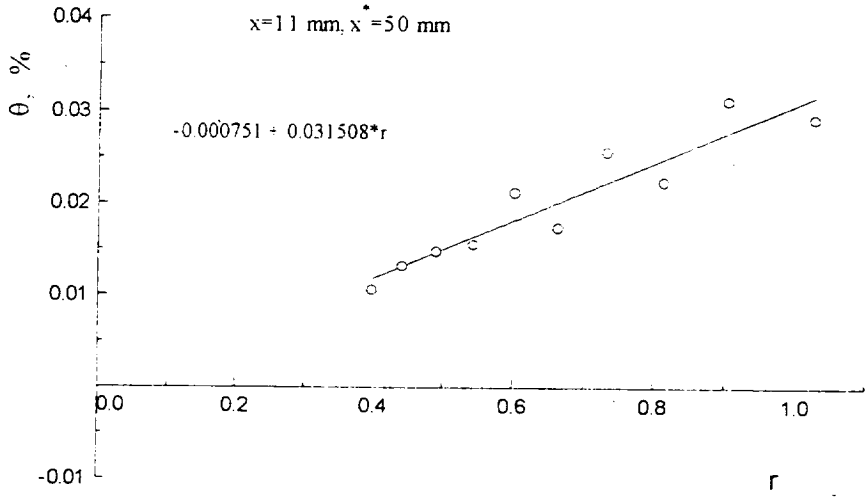

Fig.4.27.b. Fluctuation diagrams of boundary layer disturbances at x=11 mm.

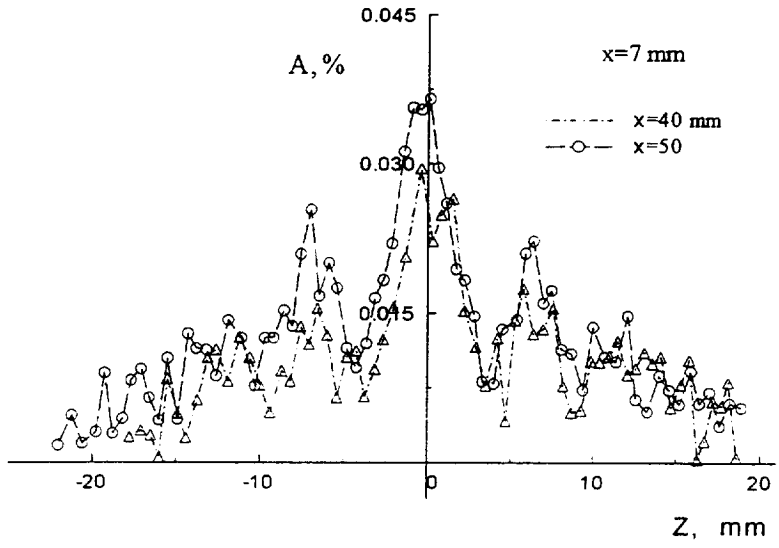

Fig.4.28.a. Distributions of amplitude excited disturbances in boundary layer over *z*. Leading edge at *x*=7 mm.

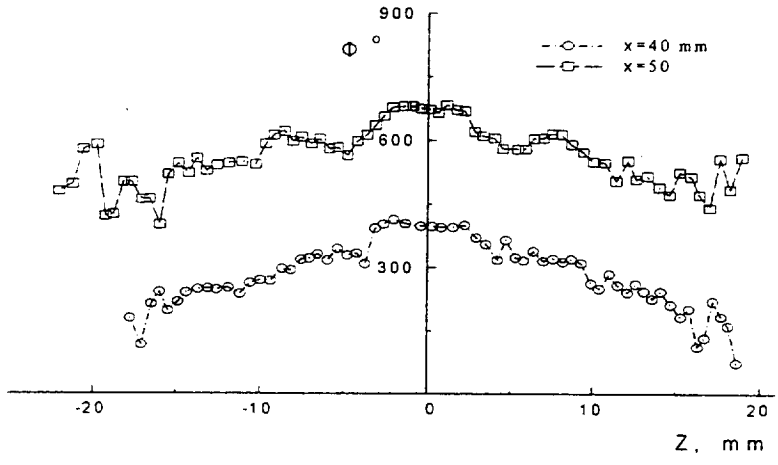

Fig.4.28.b. Distributions of phase excited disturbances in boundary layer over *z*. Leading edge at *x*=7 mm.

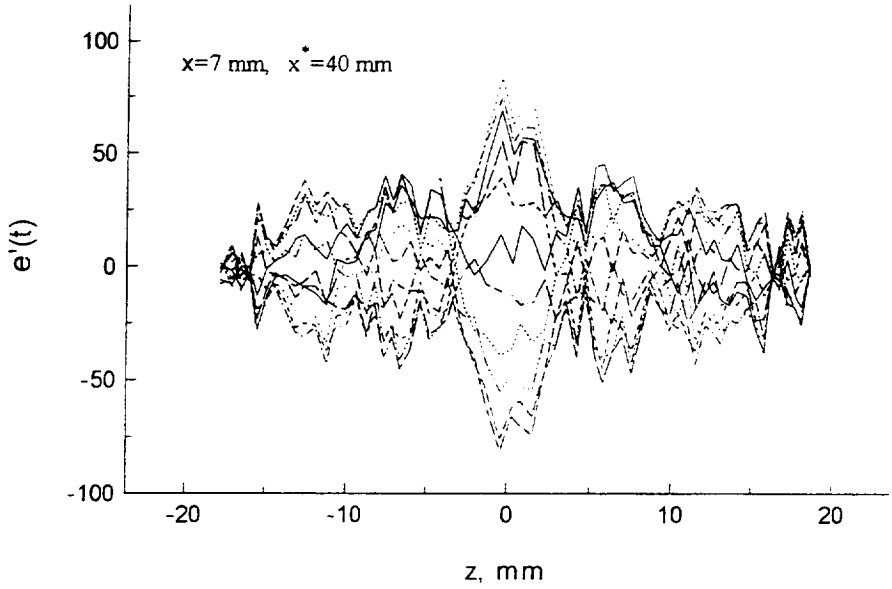

Fig.4.29.a. Instantaneous distributions of oscillograms amplitude over spanwise coordinate *z* at x=7 mm and *x**=40 mm.

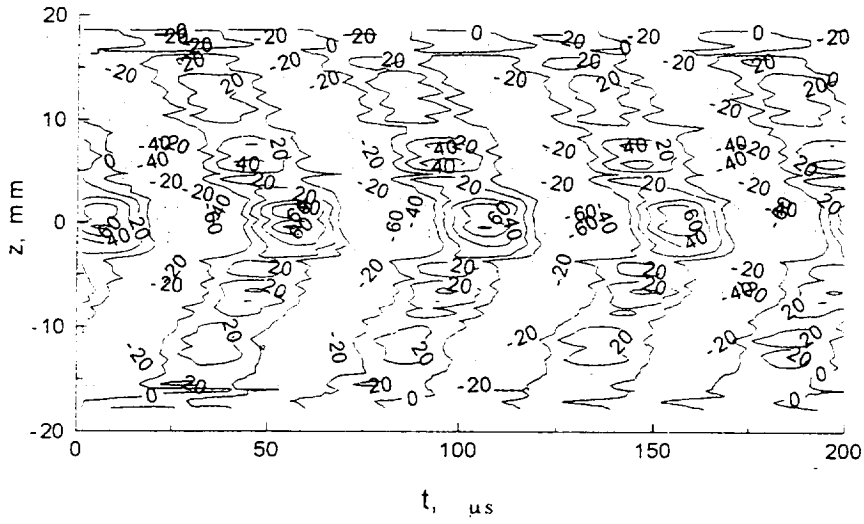

Fig.4.29.b. Isolines of oscillograms amplitude over spanwise coordinate *z* at x=7 mm and *x**=40 mm.

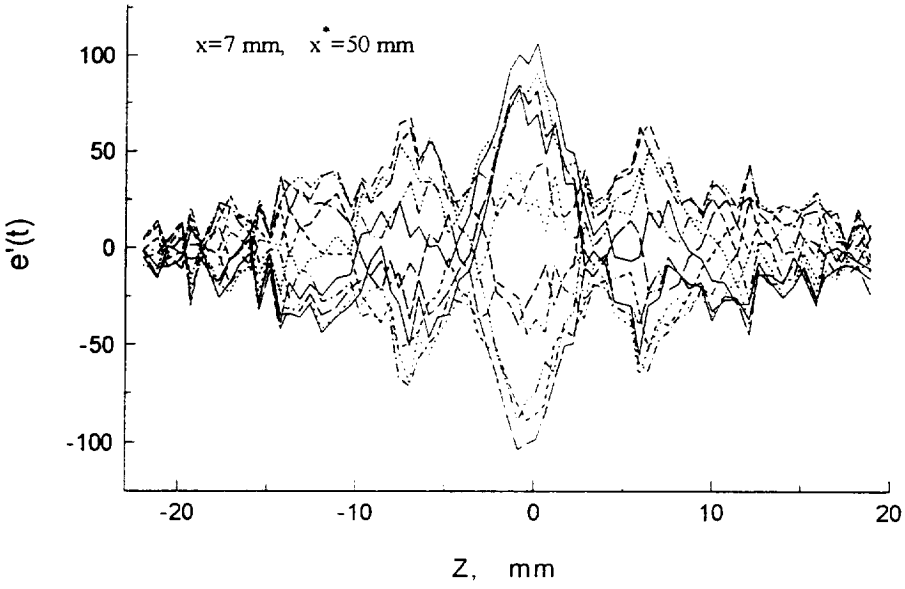

Fig.4.30.a. Instantaneous distributions of oscillograms amplitude over spanwise coordinate *z* at x=7 mm and *x**=50 mm.

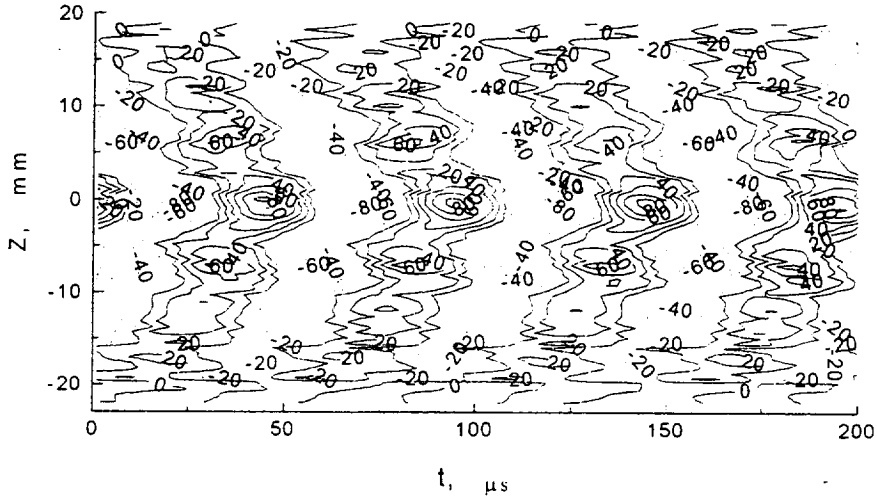

Fig.4.30.b. Isolines of oscillograms amplitude over spanwise coordinate *z* at x=7 mm and *x**=50 mm.

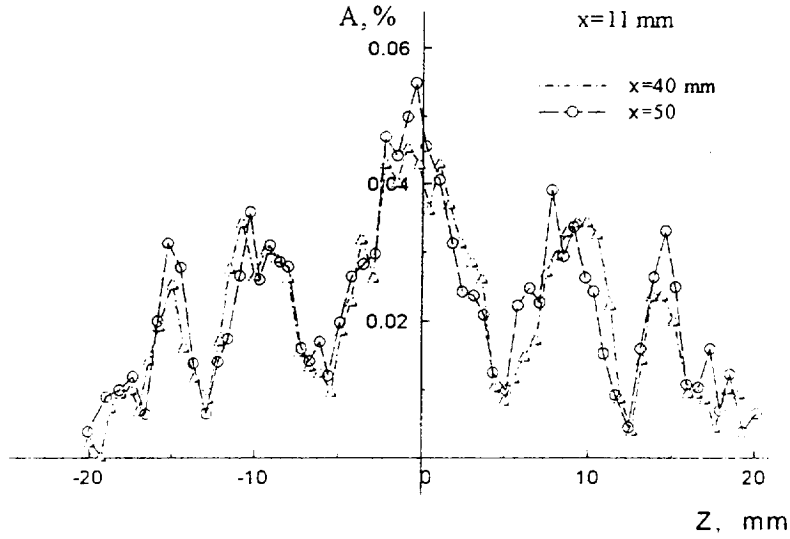

Fig.4.31.a. Distributions of amplitude excited disturbances in boundary layer over *z*. Leading edge at *x*=11 mm.

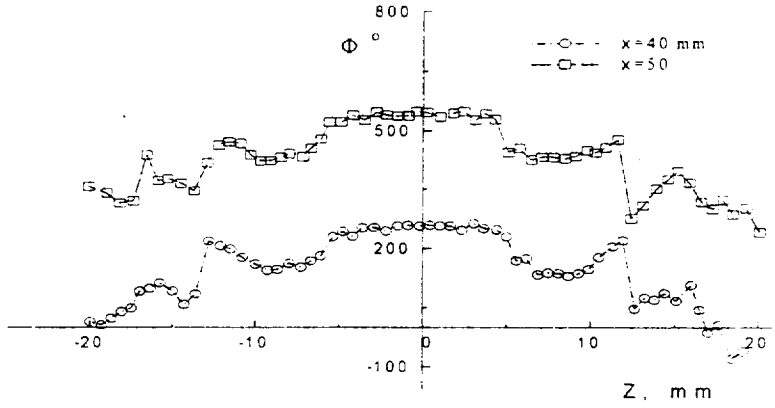

Fig.4.31.b. Distributions of phase excited disturbances in boundary layer over *z*. Leading edge at *x*=11 mm.

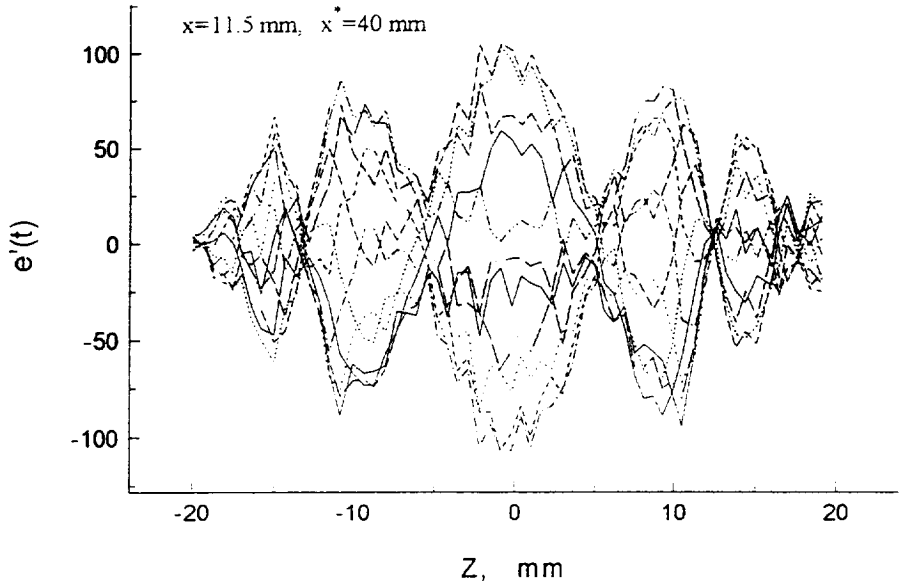

Fig.4.32.a. Instantaneous distributions of oscillograms amplitude over spanwise coordinate *z* at x=11 mm and *x**=40 mm.

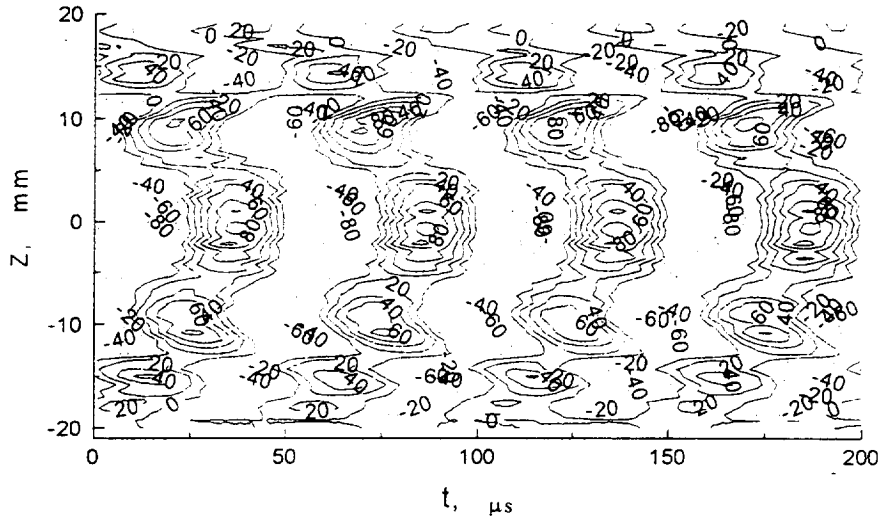

Fig.4.32.b. Isolines of oscillograms amplitude over spanwise coordinate *z* at x=11 mm and *x**=40 mm.

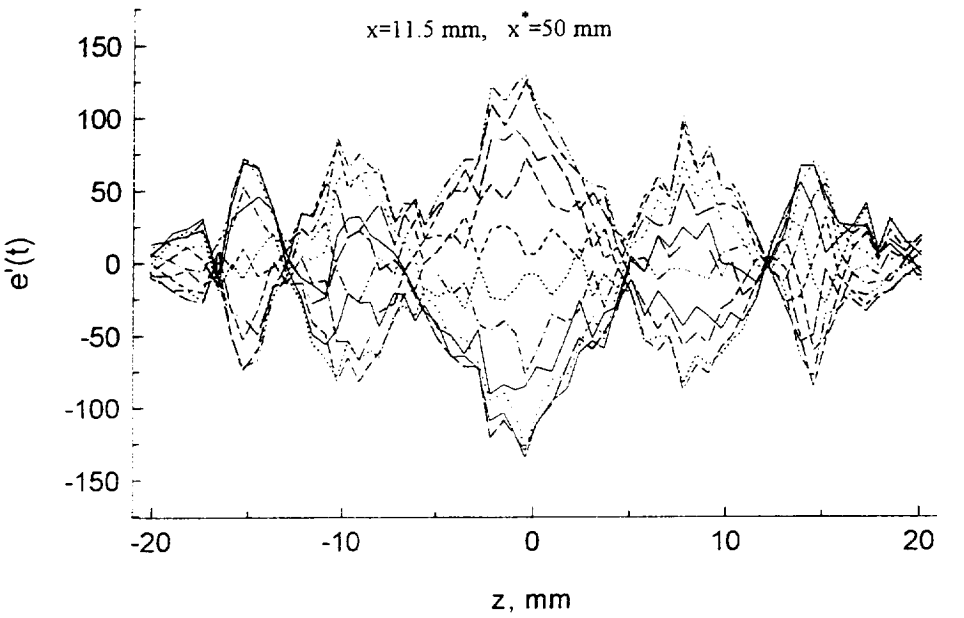

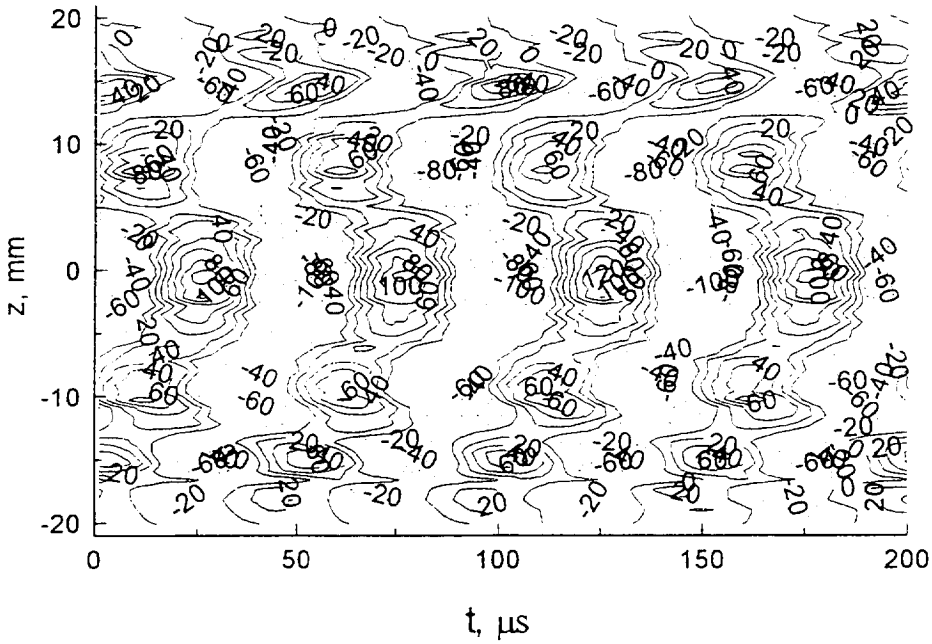

Fig.4.33. Instantaneous amplitude distributions and isolines of oscillograms over spanwise coordinate z at x=11 mm and x^*=50 mm

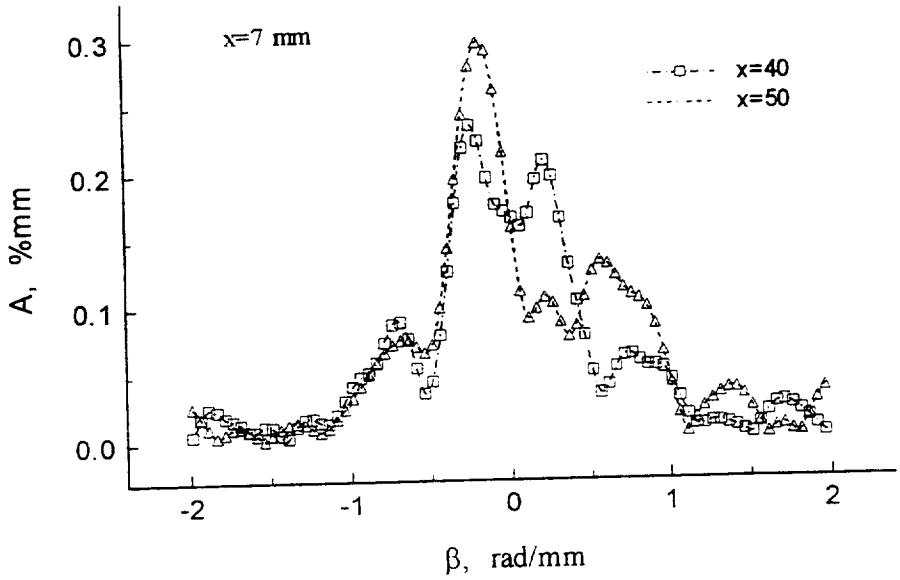

Fig.4.34.a. Distributions of $A_f(\beta)$ of excited oscillations at x=7 mm.

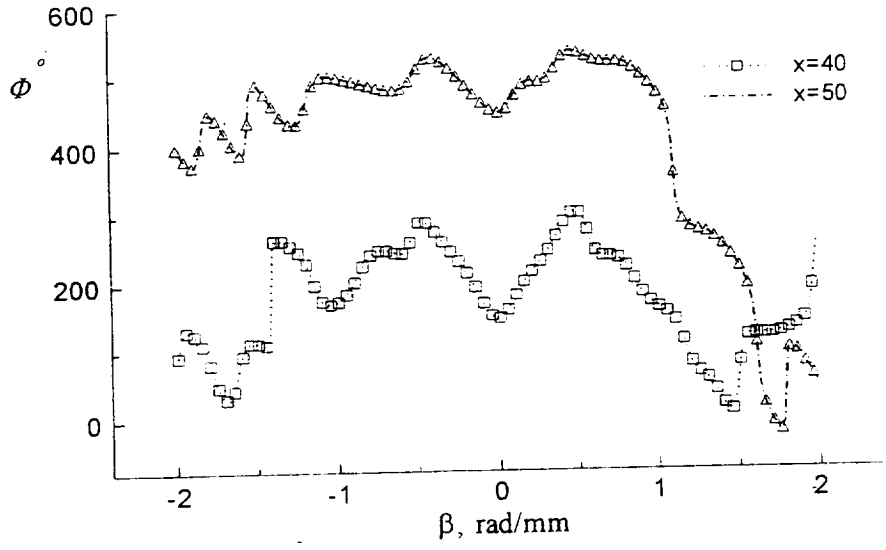

Fig.4.34.b. Distributions of $\Phi_f(\beta)$ of excited oscillations at x=7 mm.

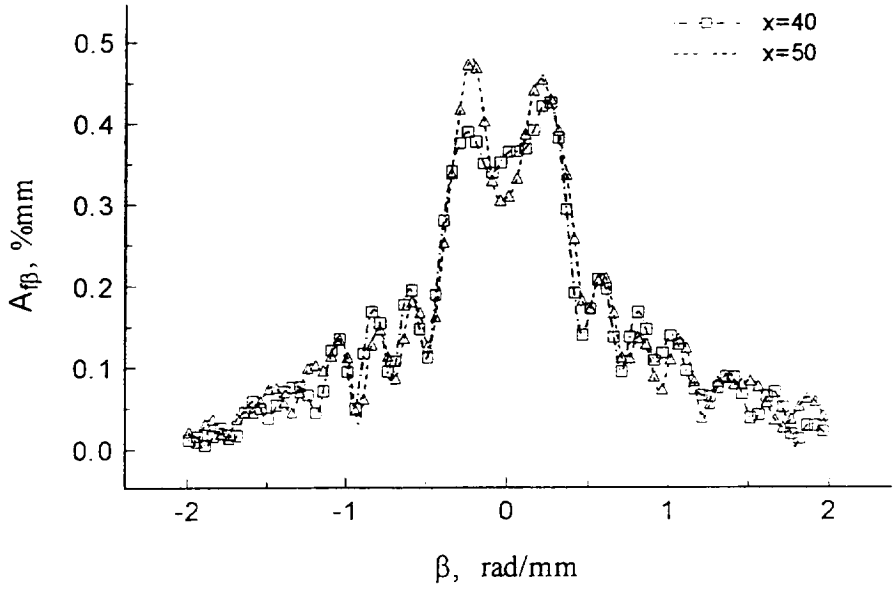

Fig.4.35.a. Distributions of $A_f(\beta)$of excited oscillations at x=11 mm.

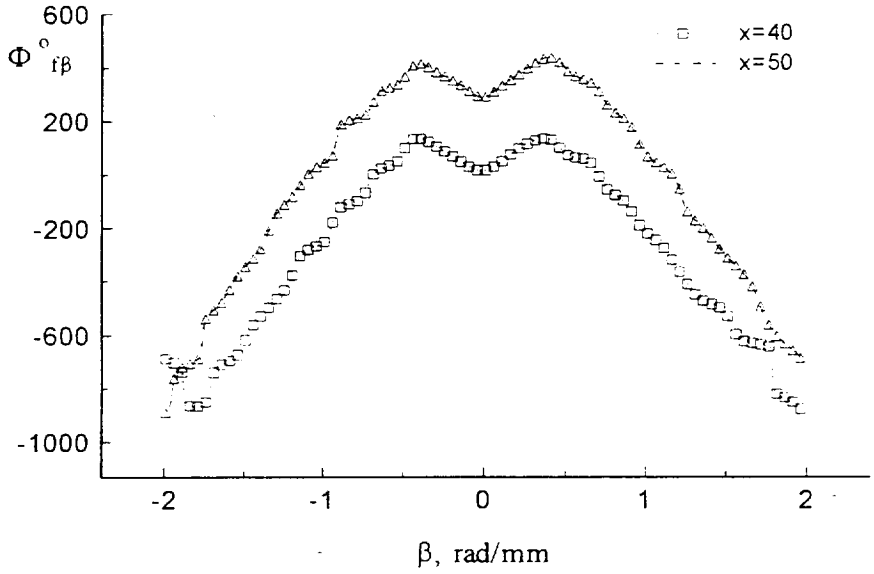

Fig.4.35.b. Distributions of $\Phi_f(\beta)$ of excited oscillations at x=11 mm.

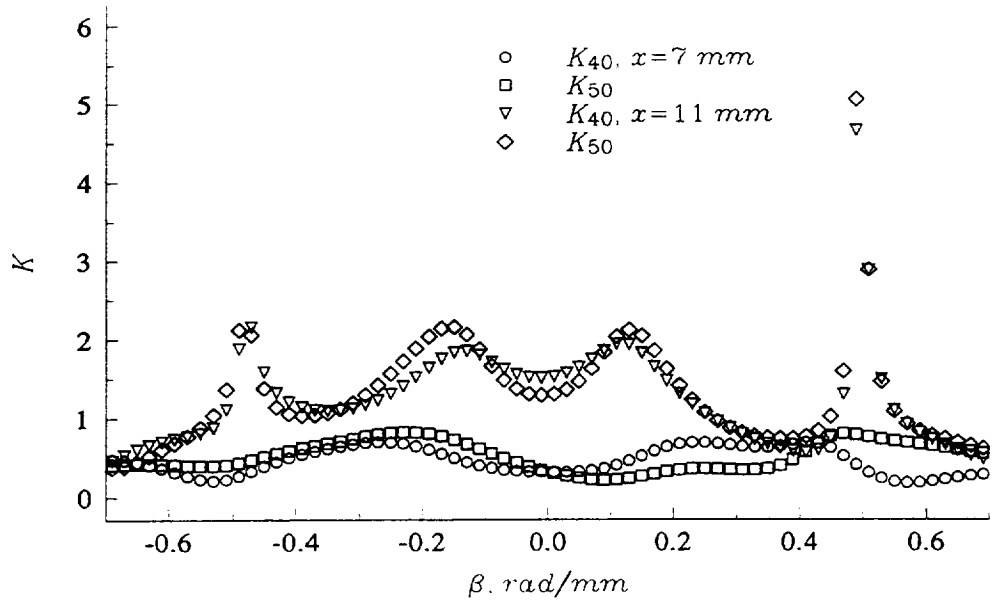

Fig.4.36. Transformation coefficients of disturbances $K(\beta)$ excited by different radiation zones at M=2

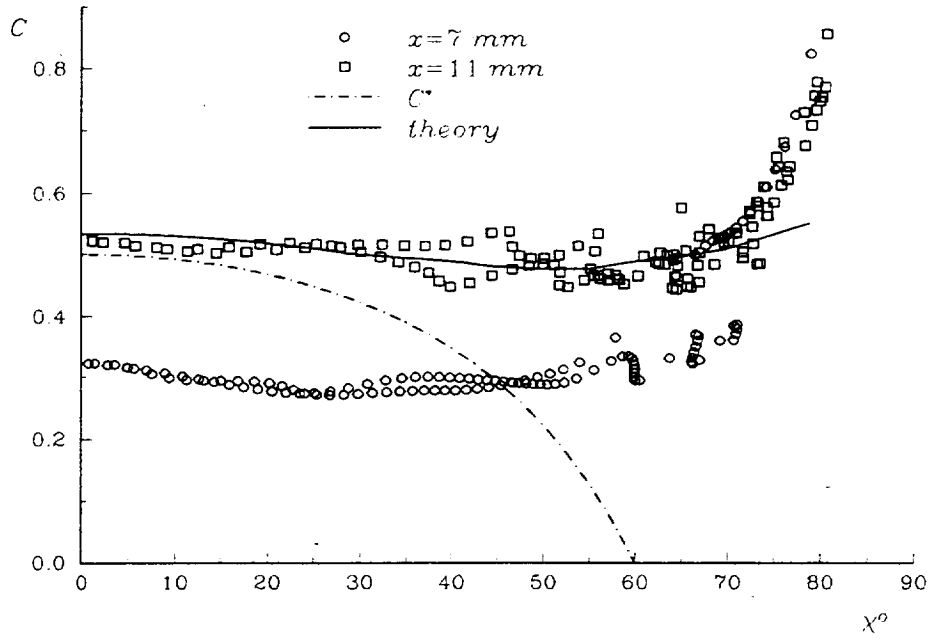

Fig.4.37. Phase velocities of disturbances in the boundary layer excited by acoustic disturbances

5. Blunted leading edge receptivity

To obtain more detailed experimental data we restricted ourselves to the tests at M=2.

5.1. Experiment objectives

The experiments were carried out at Mach number M=2 and unit Reynolds number $Re_1=10^7 m^{-1}$. The controlled disturbances of frequency f=20 kHz ($F=0.26\times10^{-4}$) were generated by electric discharge in chamber. The initial amplitude of controlled disturbances from the local source were fixed during these experiments. Measurements of controlled disturbances were accompanied by calibration tests in order to estimate the pulsation magnitude. Measurements were performed using new hot-wire anemometer and modernized automated data system.

5.2. Flat plates

Experimental set-up was similar to shown in figs.3.1-3.3. The plate *1* with the local disturbance source was the same as in the previous experiments described in item 4. The distance from the plate *1* to the wall of the test section was a=76 mm. The plate *1* was placed below the plate 2. In this case the generation of disturbances in the boundary layer by external controlled acoustic field took place near the leading edge of the plate 2. The plate *2* was fastened to pylon at 116 mm distance from the wall of the test section T-325. The size of the plate *2* were 280 mm length, 160 mm width at top and 80 mm at basis, 7 mm thick. The radius of the leading edge bluntness was r=2.5 mm.

5.3. Results at Mach number M=2

The modernized automated data system sufficiently increased the velocity of information collection and improved the measurement accuracy. It allowed us to carry out more detailed studies of the field of controlled disturbances in a free

stream.

5.3.1. Initial data

More detailed information on initial data is necessary for understanding and estimating of receptivity factors.

The initial field of controlled fluctuations was measured in a free stream in the plane of the plate *2* at the distance y_1=40 mm from the surface of the plate *1* (the plate *2* was placed further downstream). In this case the plate *2* was used as a support for traversing mechanism. The initial amplitude of controlled disturbances from the local source was measured during fluctuation field measurements versus *x, y, z* coordinates. A simplified physical model of disturbance generation in the source vicinity was used for the analysis of experimental data that was described above. Such physical model is based on distributions, similar to shown in fig.5.1, where amplitudes and phases of controlled disturbances $A(x)$, $\Phi(x)$ versus streamwise coordinate at z=0 are presented.

In the first series of experiments on leading edge receptivity (Kosinov et al. 1996, Semionov et al. 1996) three characteristic zones in distributions $A(x)$ and $\Phi(x)$ were distinguished. It seems like we need to add one zone more, which corresponds to the radiation of disturbances directly from the aperture of the source, arising during the ignation of discharge. So in the given work four zones were allocated. The first zone corresponds to acoustic waves, radiated by the source of disturbances, which propagate upwards in the boundary layer of the plate *1* (in fig.5.1 this zone corresponds approximately to the area of the first maximum (24 mm < x < 27 mm), where the phase decrease with coordinate x increasing). The second zone corresponds to radiation of disturbances directly from the aperture of the source (area of the second maximum in fig.5.1). For this area the phase of disturbances is practically constant. The third zone corresponds to radiation from a vortex behind of the aperture (in fig.5.1 this zone approximately corresponds to the area of the third maximum at 30 mm < x < 35 mm). And the fourth zone is observed for x > 35 mm as a radiation from TS waves.

Spanwise variation of controlled disturbances. $A(x)$, $\Phi(x)$ measurements in the free stream allowed to determine the boundary in x of the area of the forced disturbances and to begin more detailed measurements of initial disturbance field, necessary for understanding of receptivity process. For this purpose measurements of spanwise distribution of amplitude and phase $A(z)$, $\Phi(z)$ of controlled disturbance were carried out. This was made in the plane of the plate *2* for streamwise coordinates from x=24 mm (i.e. from the boundary of the forced radiation) up to x=40 mm with 1 mm step. Fig.5.2 shows the isolines of artificial disturbance amplitudes measured in this case. On the basis of these data it is possible to make a conclusion that our simplified physical model is well justified. Vortex structures are formed before and in the vicinity (28 <x< 30 mm) of discharge. The edges of disturbances from before discharge vortexes merge at x=36 mm. The radiation propagate inside the Mach cone from the source. In fig. 5.3 the same data are shown as three-dimensional disturbance amplitude surfaces $A(x, z)$ for more descriptive presentation.

Figs.5.4-5.7 show the distributions $A(z)$, $\Phi(z)$ for four cited zones of radiation: upstream propagating disturbances (fig.5.4); radiation of disturbances directly from the source aperture (fig.5.5); radiation from a vortex behind of the source aperture (fig.5.6); radiation from TS waves (fig.5.7). The behavior of amplitudes and phases of controlled disturbances in a free stream is inherent for each zone of radiation. Only the data at section x=27 mm look like transitive from the first to the second zone.

Normal - to - the wall distributions of controlled disturbances. The results of controlled disturbance field measurements in normal - to - the wall direction are shown in figs. 5.8-5.9. Amplitude and phase distributions of controlled disturbances $A(y)$, $\Phi(y)$ versus y are shown at various x positions and z=0 in fig.5.8 (position y=0 corresponds to the plane of the plate *2*). The values of coordinate x are chosen to correspond to four various zones of radiation (maxima in distribution $A(x)$ in fig.5.1). It is obvious, that the distributions $A(y)$ are similar and remind distributions $A(x)$, presented in fig.5.1. The distribution $A(y)$ at x=38 mm is not measured completely because of restriction on movement of hot-wire. In fig.5.9a a trajectory of the

maximum in distribution *A(y)*, (marked as a circle in fig.5.8a) is shown. The received straight line coincides with Mach line with a high accuracy.

Wave number spectra. The wave spectra over β for the mentioned above zones were obtained by discrete Fourier - transformation. These spectra are shown in figs.5.10a-d for *x* values, corresponding to four various zones of radiation. The waves are observed only in interval (-0,5; 0,5) rad/mm. For the first and the second zone there is a maximum at β=0 in amplitude spectra, for two other zones the rate of increase for three-dimensional waves even grows.

5.3.2. Boundary layer response

Spanwise distributions of controlled disturbances in the boundary layer. To study the disturbance field in the boundary layer, excited by external controlled fluctuations, the plate *2* was mounted in such a way that the leading edge was placed consequently in streamwise positions where distribution *A(x)* has maximum in all zones of radiation (i.e., *x*-coordinate of the leading edges was *x*=26, 29, 31 and 38 mm). The distributions *A(z)* and $\Phi(z)$ in the boundary layer of the plate *2* were measured at two x^* positions (x^*=40 and 50 mm, where x^* is a distance from the leading edge of the plate *2*). The measurements were carried out at position y/δ=const where natural disturbances reach the maximum in normal direction. Obtained amplitude distributions are presented as mass flux fluctuations in figs.5.11-5.14.

Wave number spectra. Amplitude and phase β-spectra of forced oscillations in the boundary layer are shown in figs.5.15-5.18. The amplitude of forced oscillations in the boundary layer are close to external disturbance amplitudes. It seems like oblique waves are excited more easy than two-dimensional waves. However, it is necessary to check this circumstance by determination of corresponding transfer factors that would be made below.

Presented data allow to receive the mean values of mass flux fluctuations, excited in the boundary layer by external controlled disturbances. Total mass flux fluctuations are the following: 0,25% for the first zone, 0,58 % for the second zone

and 0,47 % for the third zone.

Measurements of controlled disturbances in a free stream over the surface of the plate 2. In contrast to the experiments for sharp leading edge, presented here experiments for blunted leading edge have shown that external controlled disturbances easily penetrate into the flow after the shock wave generated at the blunted leading edge. In figs.5.19-5.22 the data are presented which were measured in spanwise and normal directions for four different positions of the plate 2. All of these measurements allow to make conclusion that intensive controlled pulsations exist into viscous layer. As we have mentioned in the second year report, it was not possible to detect them for sharp leading edge case.

The data presented in figs.5.19b-5.22b were measured at the distance x^*=50 mm from the leading edge. The data shown in fig.5.19a were obtained at y=5.4 mm, in fig.5.22a — at y=1.5 mm. All these data corresponds to z=0. Modulated behavior of streamwise amplitude distributions (figs.5.19a-5.21a) was found. First maximum in amplitude distributions appear when hot wire moved through shock wave from blunted leading edge. Mean phase velocities calculations using these data give value C=0.79 for the first zone, C=0.82 for the second zone, C=0.74 for the third zone and C=0.93 for the fourth zone. That means that streamwise phase velocities of controlled disturbances are not characteristic for acoustic waves. They are about 1.5 times more than those in the free flow without flat plate with blunted leading edge. In order to understand these data it is necessary to produce a theoretical model for propagation of acoustic waves through shock wave close to the bluntness. Probably in this case we have a resonator between shock wave and blunted leading edge. Thus, we can conclude that in these experiments excited disturbances were found everywhere in the flow above flat plate in the region of Mach cone.

5.3.3. Transfer factors

Regardless the fact that excited disturbances were found everywhere, we shall estimate transfer factors for each of described above cases in boundary layer. It is necessary to do this for each x^* position. Relevant data are shown in figs.5.23-

5.26. Only for the first zone transfer ratio demonstrates a smooth behavior. For the second and the third zones there are some peaks in these dependencies. Maybe this is because the initial wave spectra contain peaks too. Obtained experimental data correlate with data, received by Gaponov (1995). Probable reason for such behavior of transfer ratio in the last zones may be thought as improper determination of these ratios without determination of β-spectra of external disturbances. For linear case of transformation of external fluctuations into boundary layer unstable disturbances it is necessary to consider disturbances with the identical wave characteristics (Gaponenko et al. 1996).

Considering obtained transfer factors as mean values over β, we see that these factors increase from 2 (for the first zone) to about 6 (for the fourth zone) times. In another hand, using mean total values of mass flux fluctuations obtained in the free stream and in the boundary layer, we can determine mean transfer ratio for each case. Relevant data are presented in Table 5.1. Comparing these data with those obtained for sharp leading edge, we conclude that mean transfer factors are 2-3 times more for boundary layer on blunted flat plate. As transfer factors decrease with increasing x^*, it means that the excited pulsations enter the stable zone of boundary layer on blunted flat plate.

Table 5.1.

	x=26 mm			x=29 mm			x=31 mm			x=38 mm		
	$\langle m\rangle_{fs}$ %	$\langle m\rangle_{bl}$ %	K_1	$\langle m\rangle_{fs}$ %	$\langle m\rangle_{bl}$	K_2	$\langle m\rangle_{fs}$ %	$\langle m\rangle_{bl}$ %	K_3	$\langle m\rangle_{fs}$ %	$\langle m\rangle_{bl}$ %	K_4
x^*=40 mm	0.108	0.254	2.36	0.164	0.242	1.48	0.15	0.386	2.51	0.116	0.636	5.5
x^*=50 mm	0.108	0.199	1.85	0.164	0.219	1.33	0.15	0.304	2.03	0.116	0.611	5.29

To show which disturbances are generated by external controlled fluctuations in the boundary layer, we consider phase velocity of waves. The data are shown in fig.5.27. Here the solid line which corresponds to critical phase velocity $C^*=1-1/(M^*\cos(\chi))$, distinguishes waves of discrete and continuos spectra.

5.4. Figures

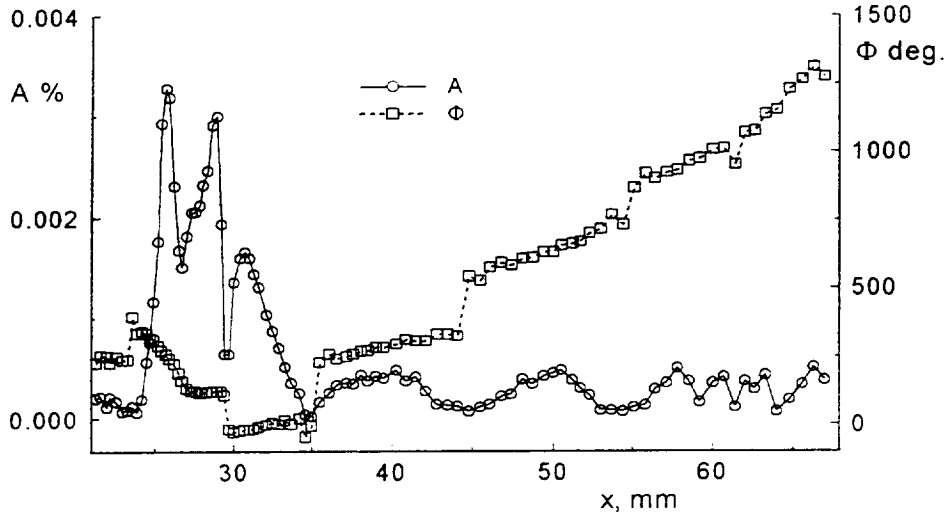

Fig.5.1. Distribution of amplitude and phase of mass flow fluctuation over x for controlled disturbances at frequency 20 kHz

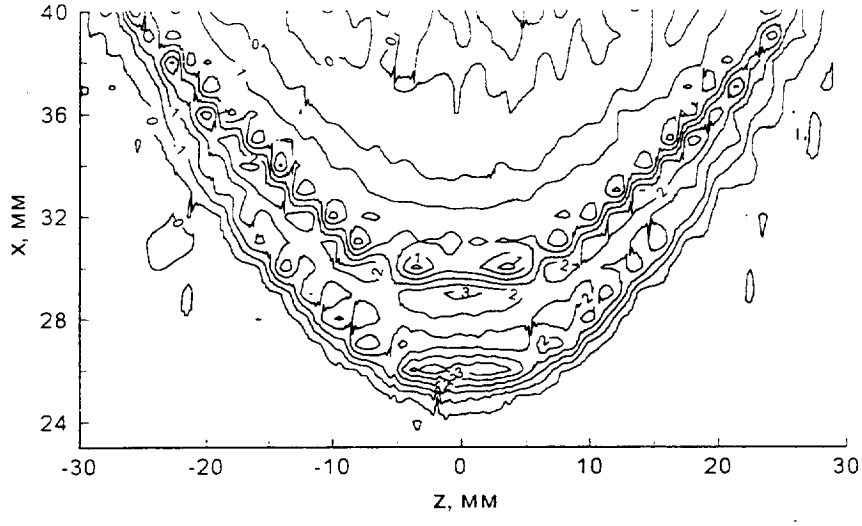

Fig.5.2. Isolines of disturbances amplitude from the local source in free stream

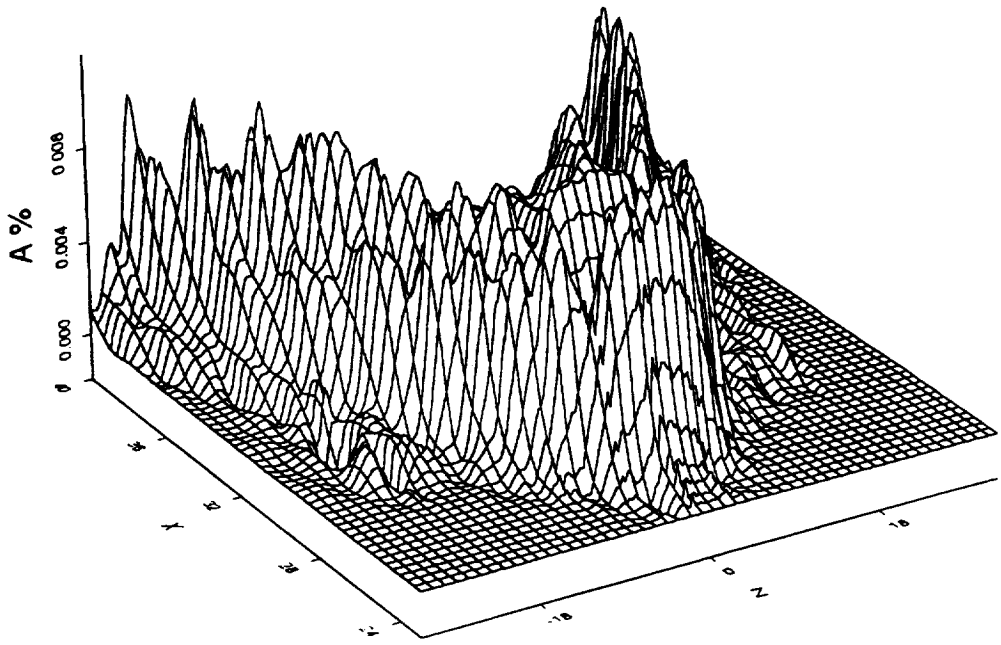

Fig.5.3. View of mass flow fluctuations from the local source in free stream

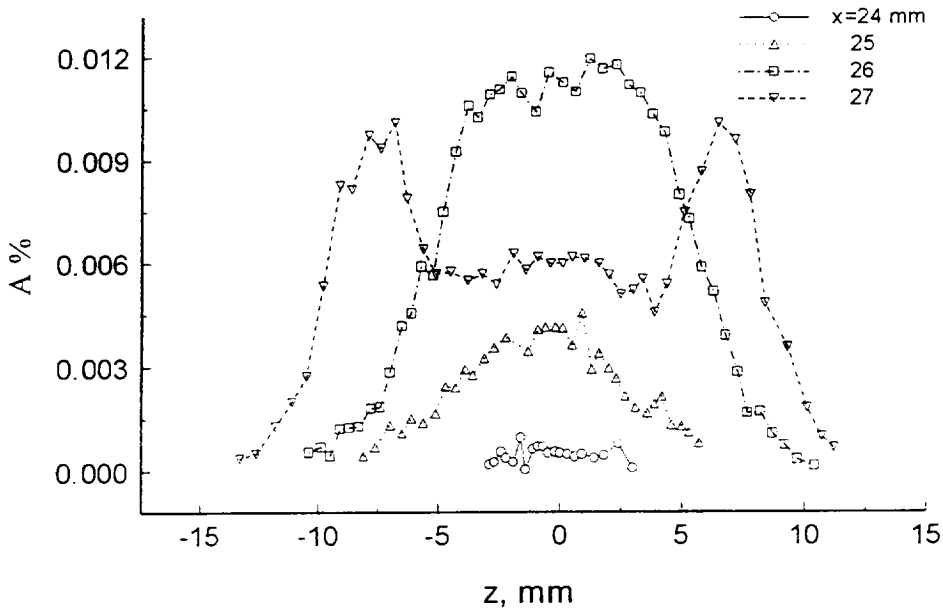

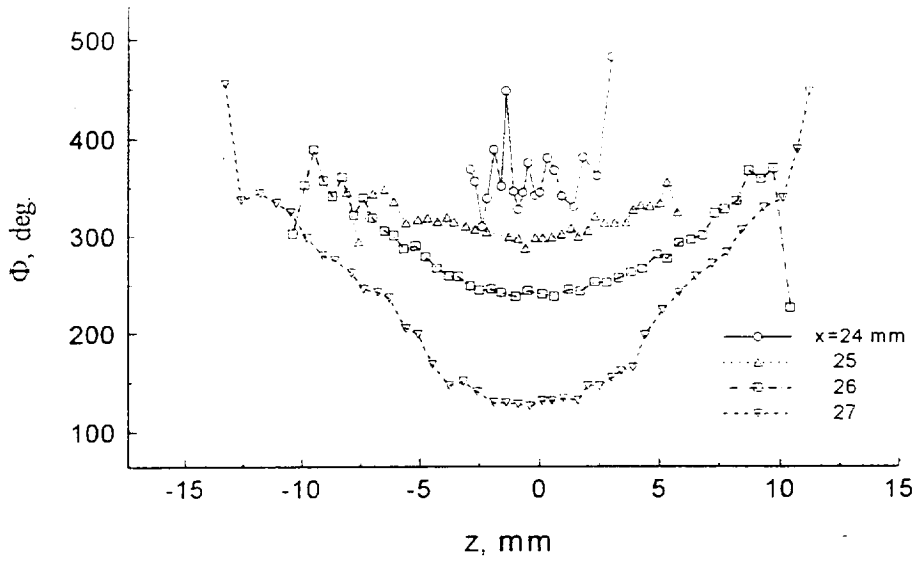

Fig.5.4. Amplitude and phase distributions of mass flow pulsations over spanwise direction

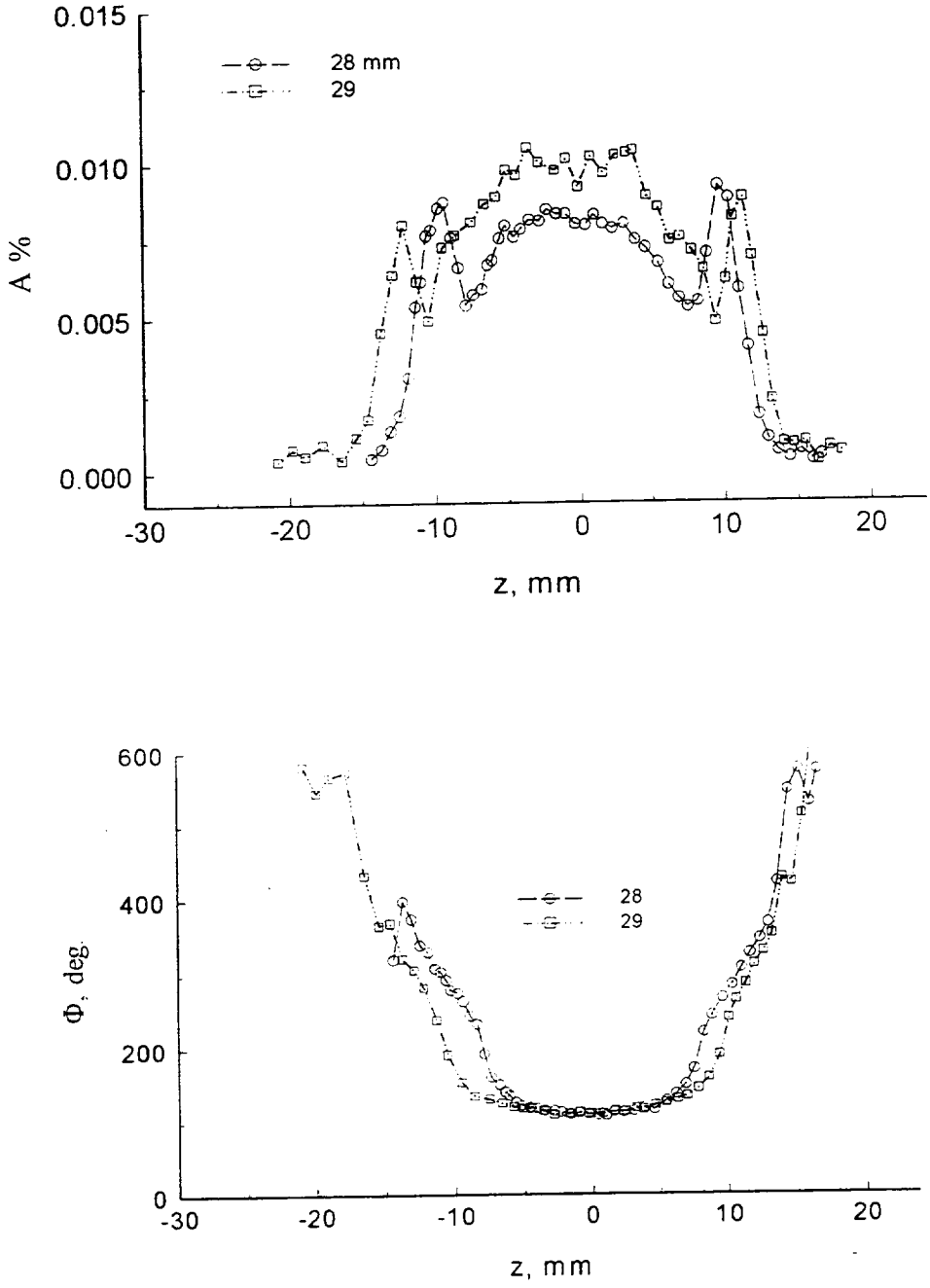

Fig.5.5. Amplitude and phase distributions of mass flow pulsations over spanwise direction

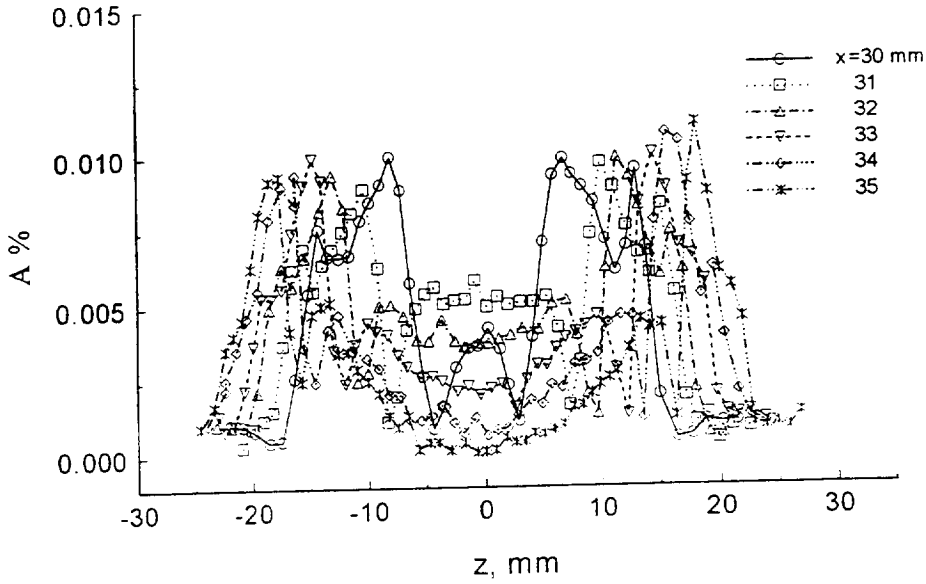

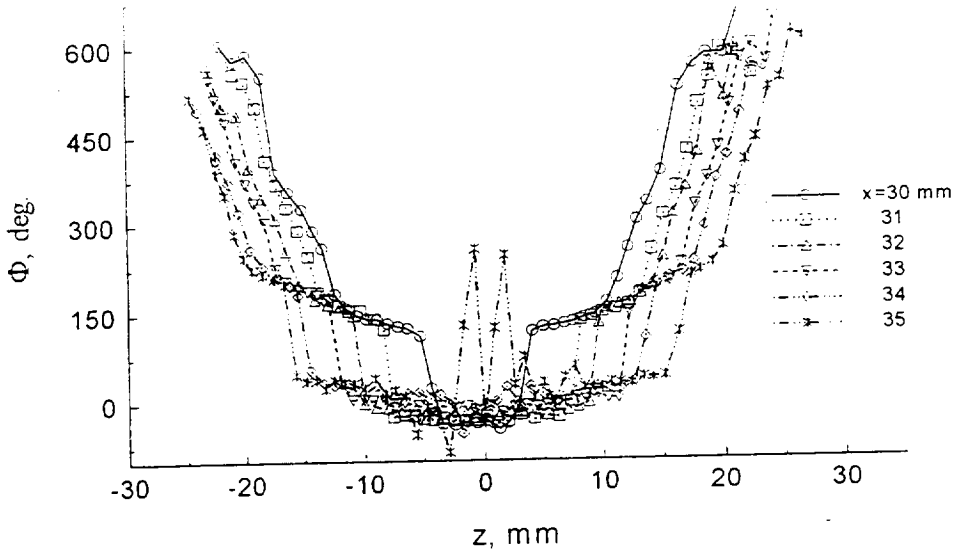

Fig.5.6. Amplitude and phase distributions of mass flow pulsations over spanwise direction

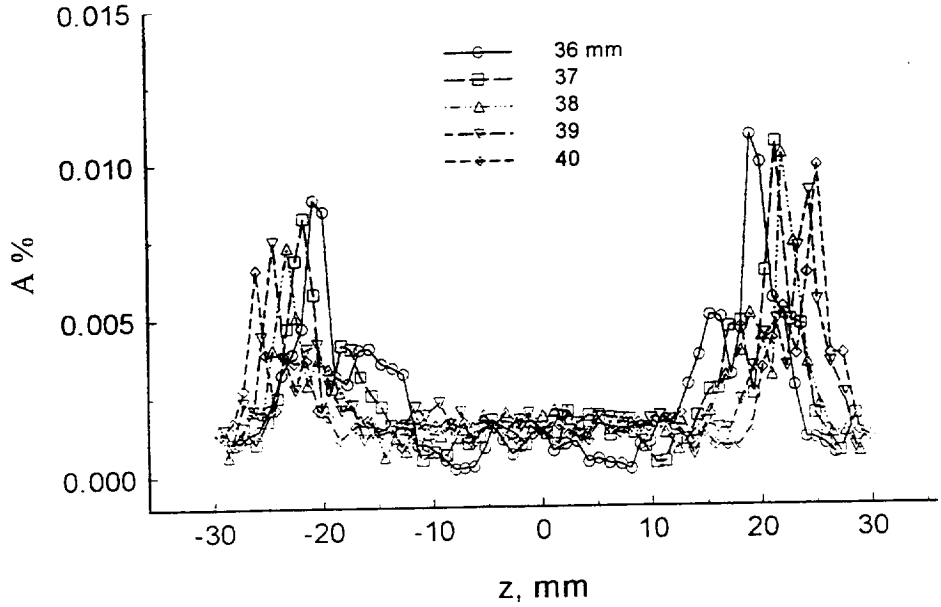

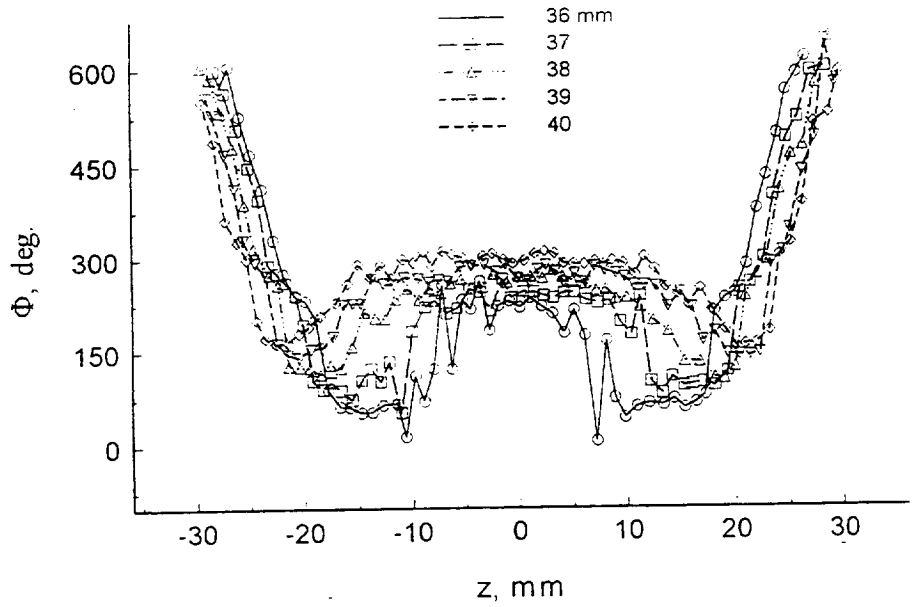

Fig.5.7. Amplitude and phase distributions of mass flow pulsations over spanwise direction

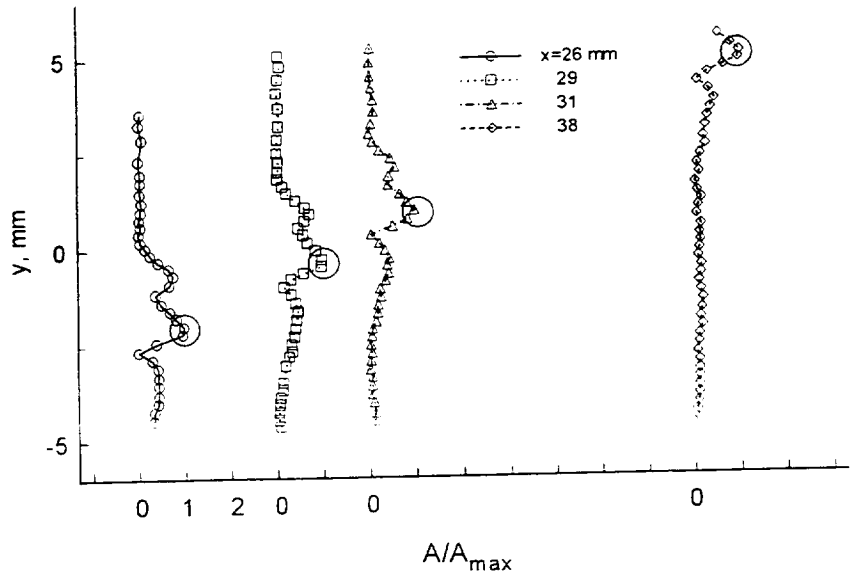

Fig.5.8.a. Examples of amplitude evolution of the radiation boundary

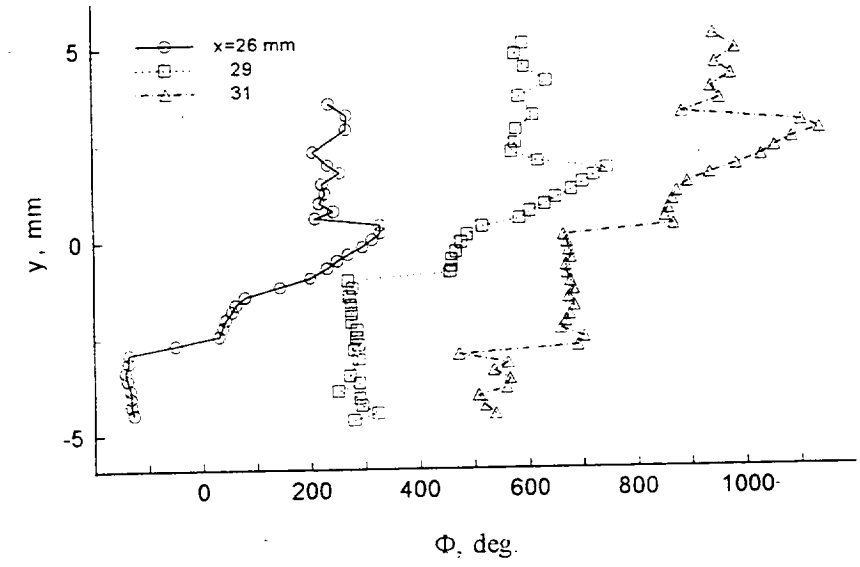

Fig.5.8.b. Examples of phase evolution of the radiation boundary

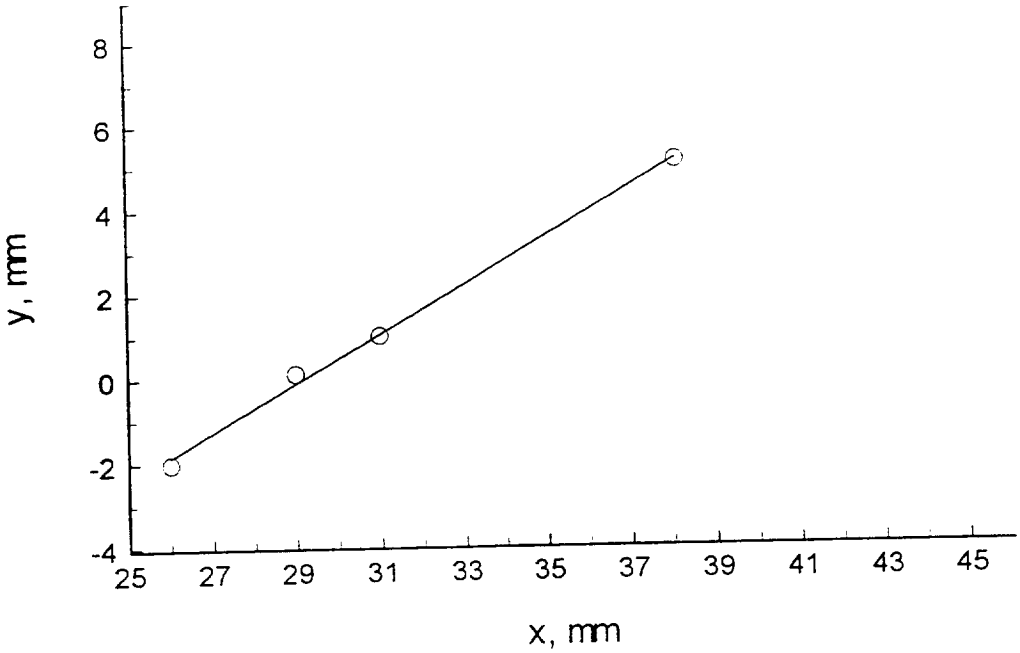

Fig.5.9.a. Mach line from source. Reconstruction over radiation boundary

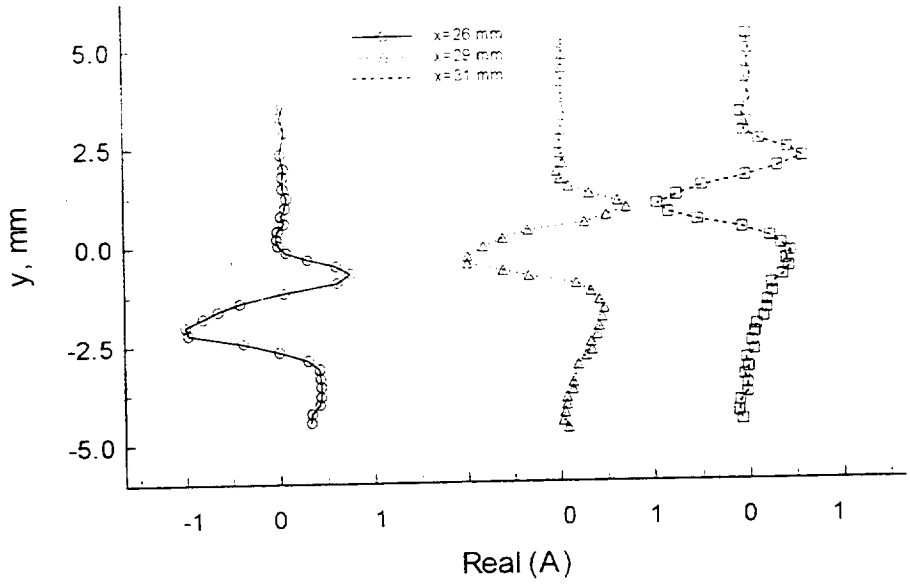

Fig.5.9.b. Real part evolution downstream of mass flow fluctuations from local source. Radiation boundary, z=0

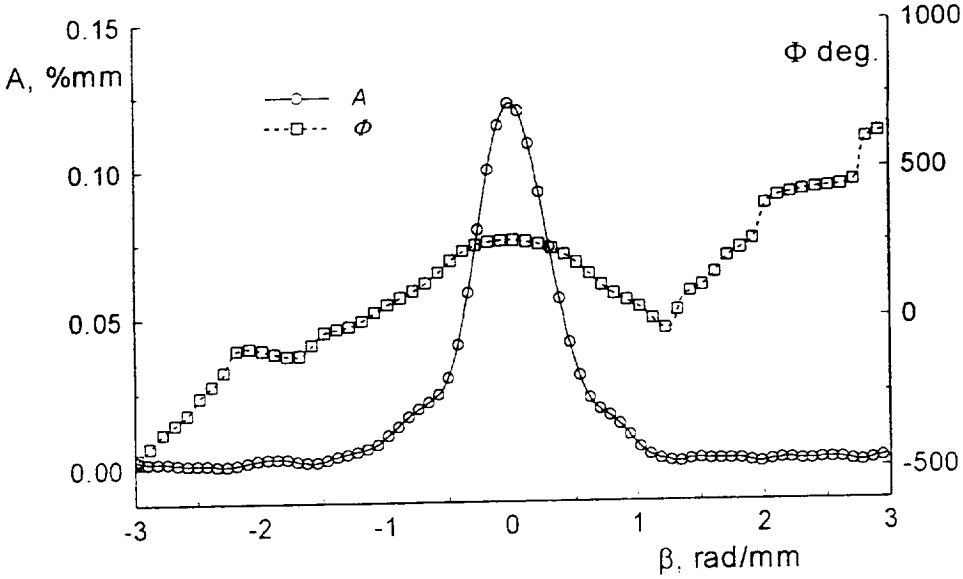

Fig.5.10.a. Initial amplitude and phase β-spectra at x=26 mm

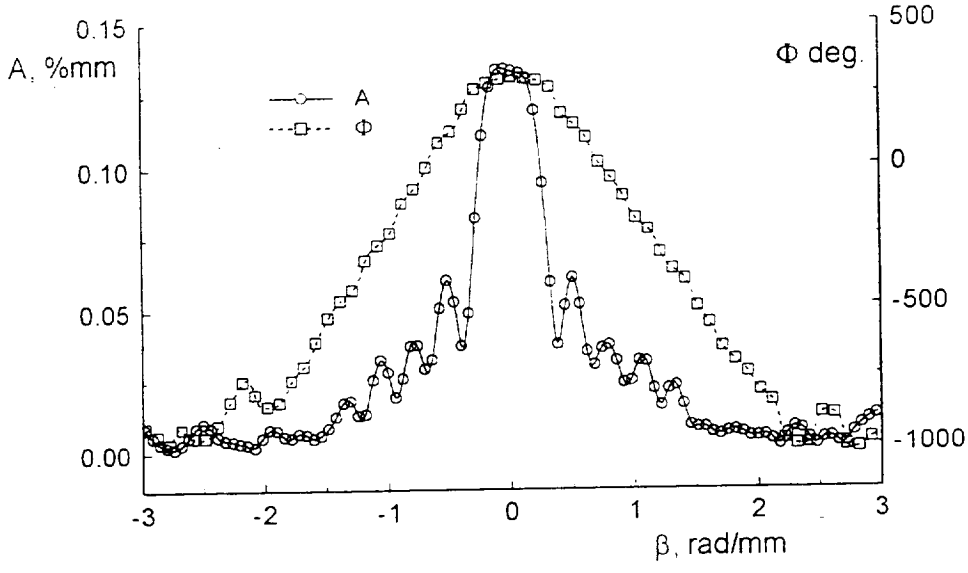

Fig.5.10.b. Initial amplitude and phase β-spectra at x=29 mm

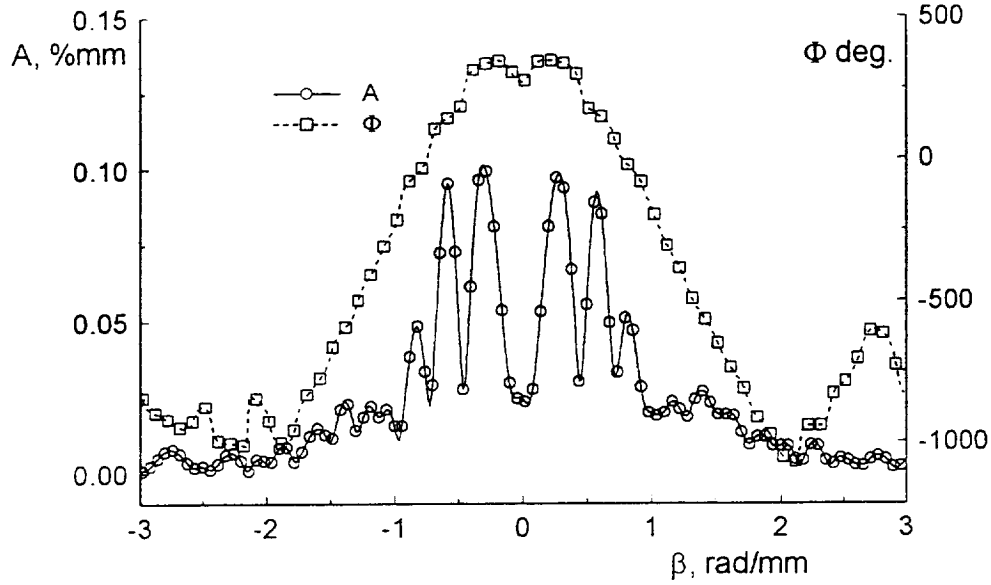

Fig.5.10.c. Initial amplitude and phase β-spectra at x=31 mm

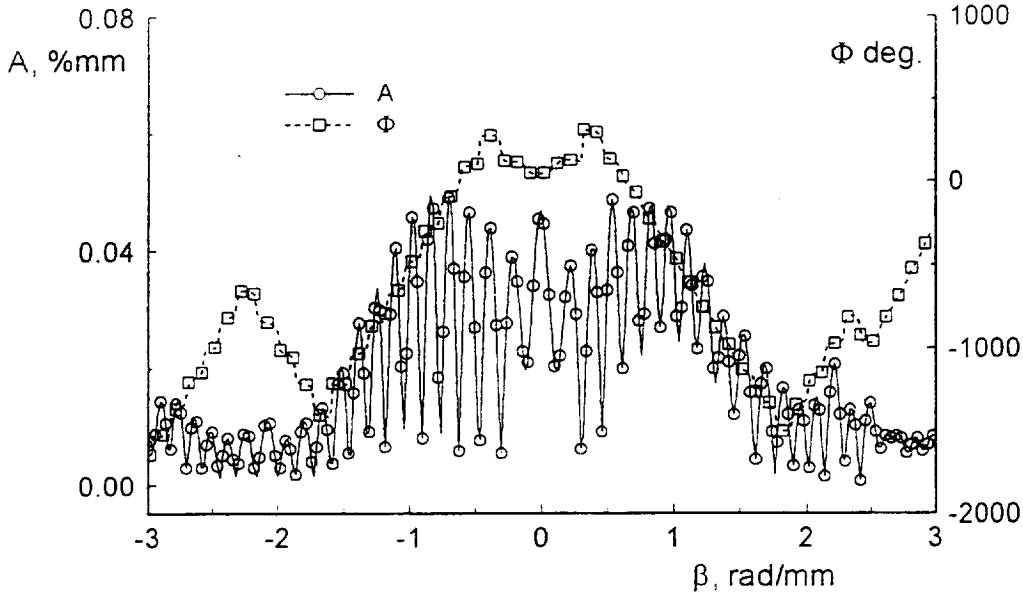

Fig.5.10.d. Initial amplitude and phase β-spectra at x=38 mm

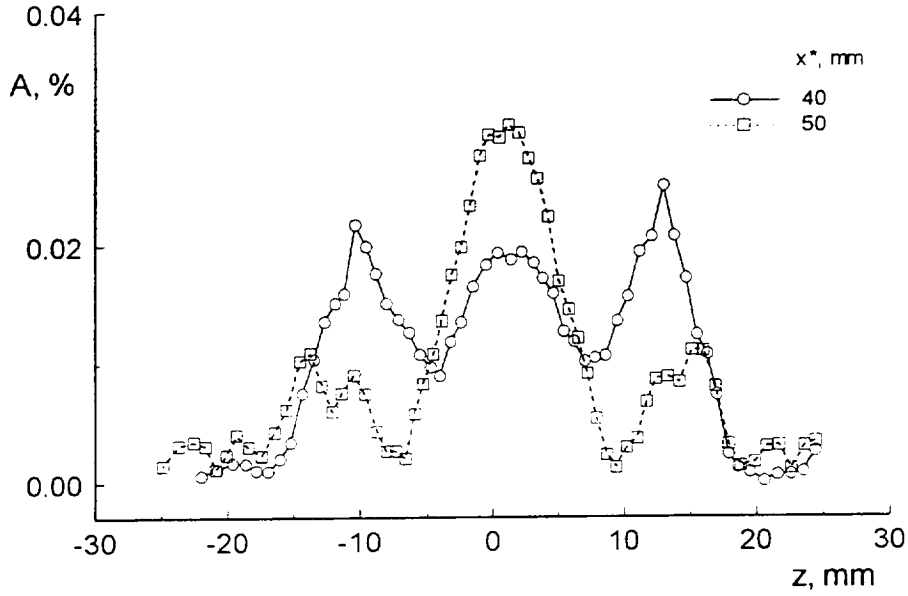

Fig.5.11.a. Boundary layer response from the first zone (x=26 mm)

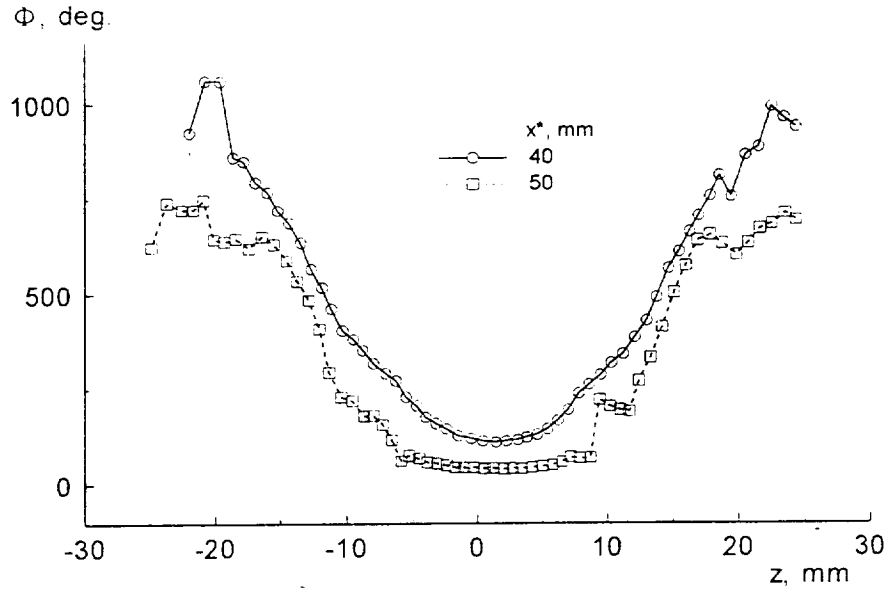

Fig.5.11.b. Boundary layer response from the first zone (x=26 mm)

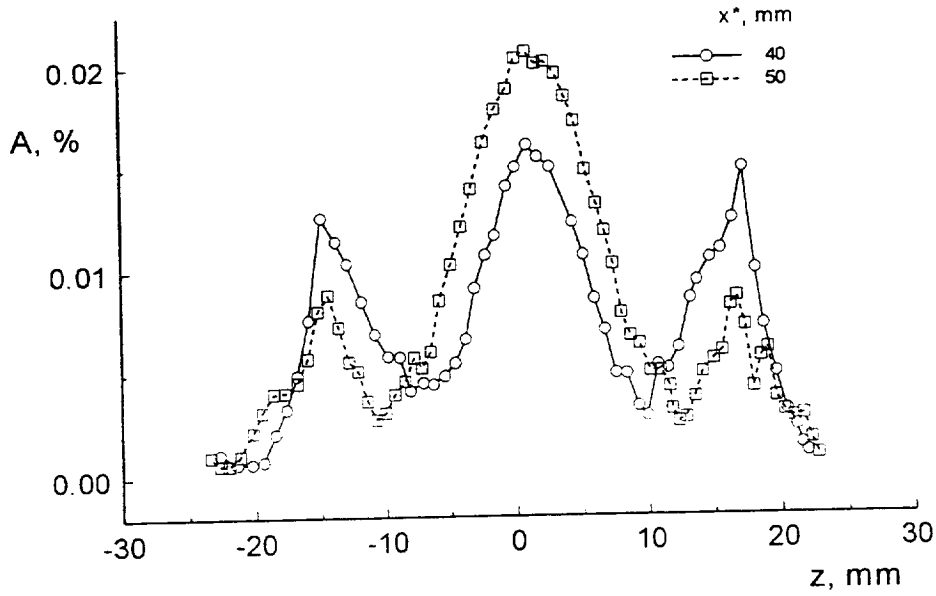

Fig.5.12.a. Boundary layer response from the second zone (x=29 mm)

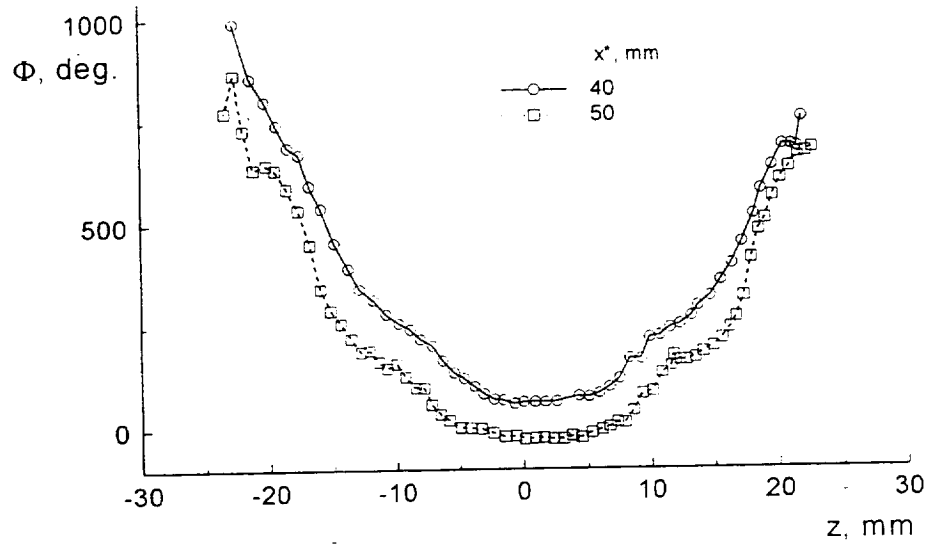

Fig.5.12.b. Boundary layer response from the second zone (x=29 mm)

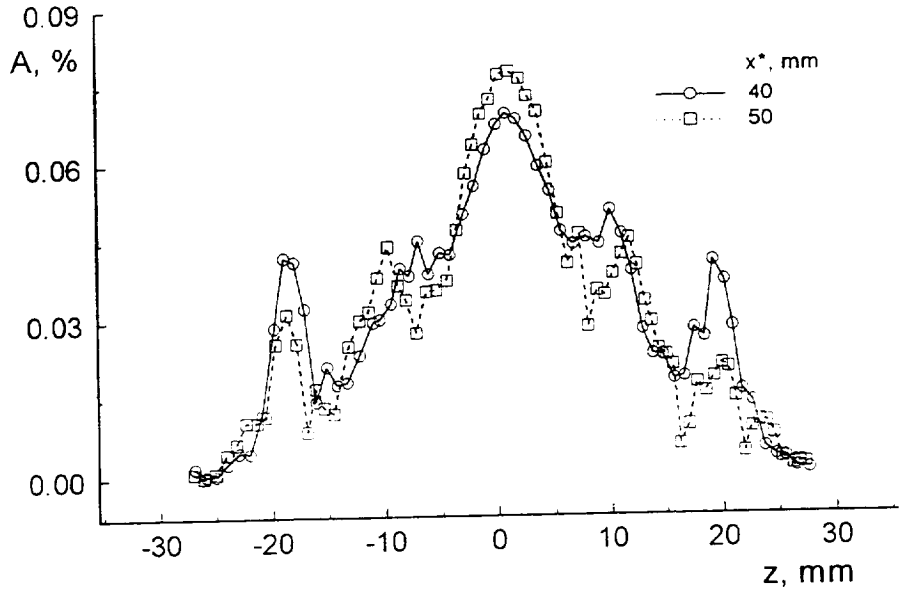

Fig.5.13.a. Boundary layer response from the third zone (x=31 mm)

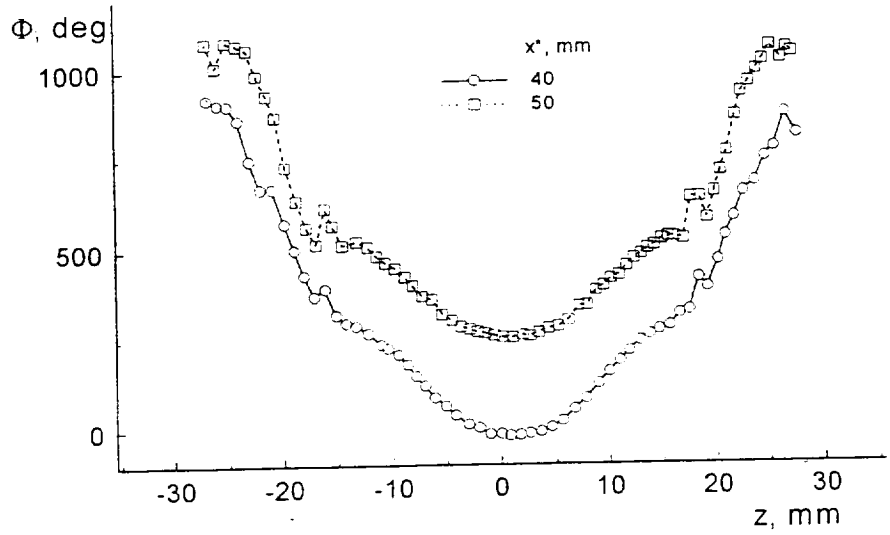

Fig.5.13.b. Boundary layer response from the third zone (x=31 mm)

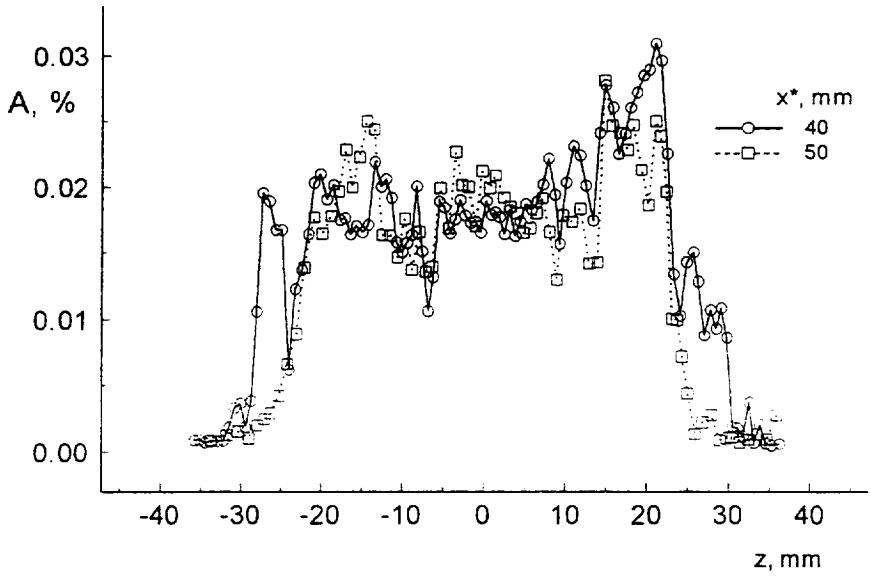

Fig.5.14.a. Boundary layer response from the fourth zone (x=38 mm)

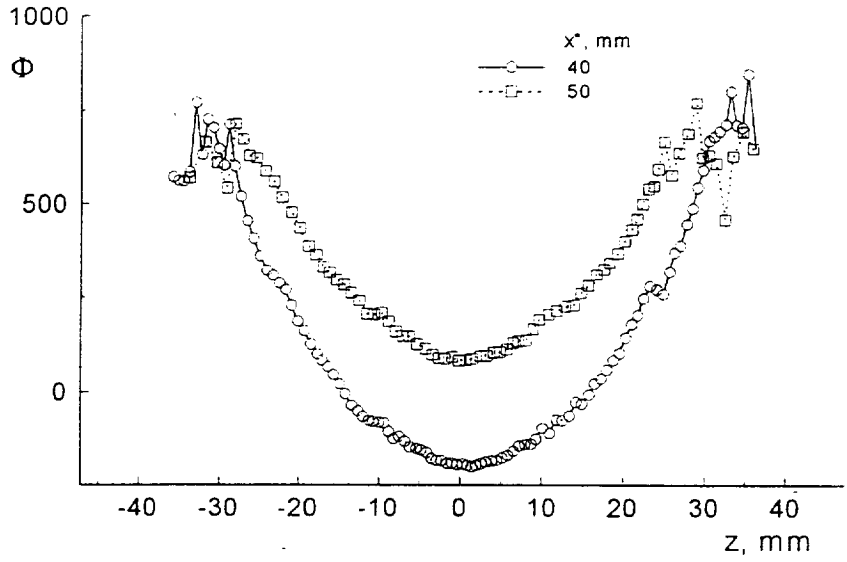

Fig.5.14.b. Boundary layer response from the fourth zone (x=38 mm)

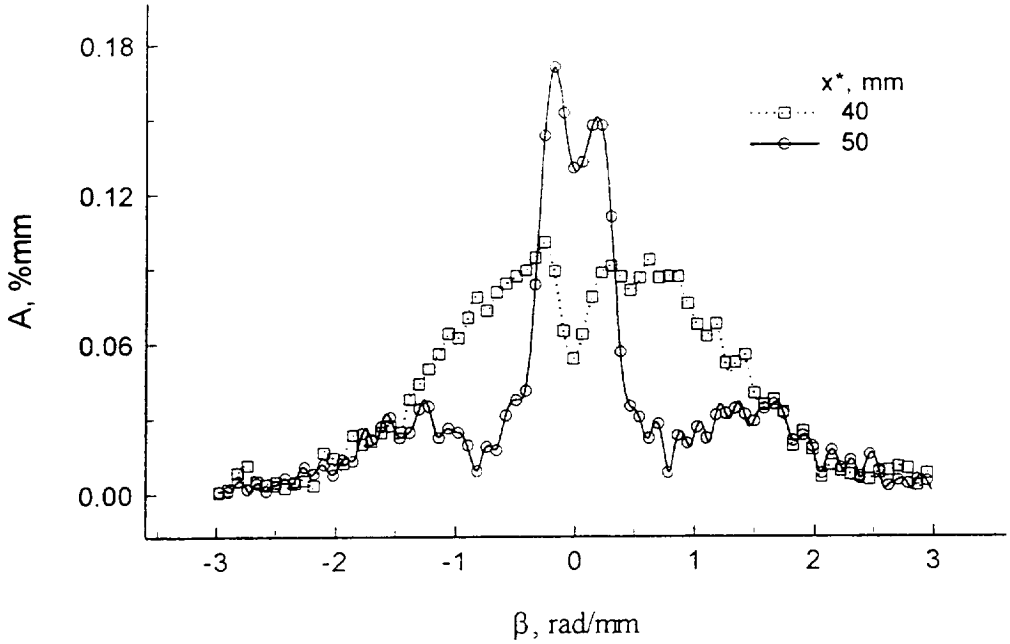

Fig.5.15.a. Amplitude β-spectra excited disturbances in the boundary layer from the first zone

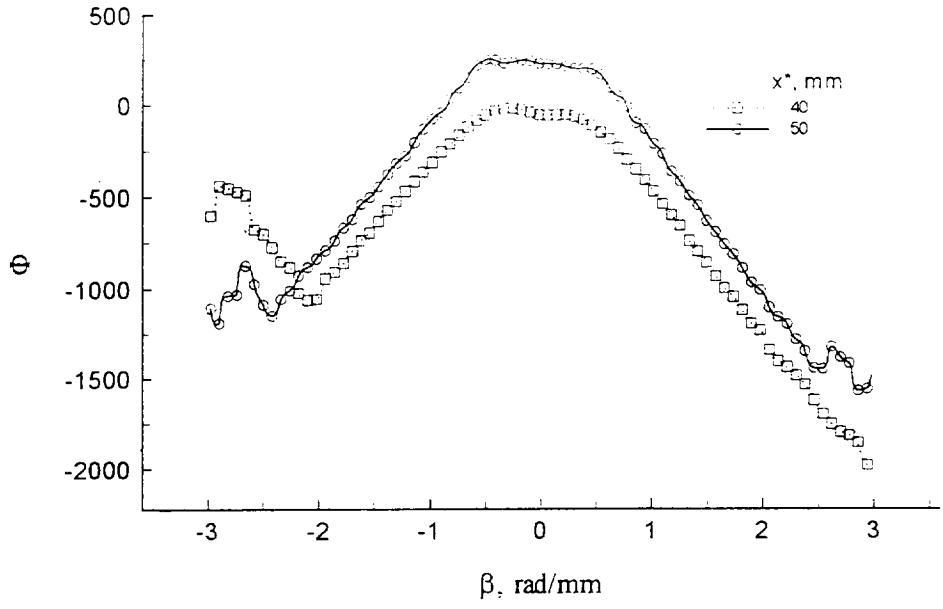

Fig.5.15.b. Phase β-spectra excited disturbances in the boundary layer from the first zone

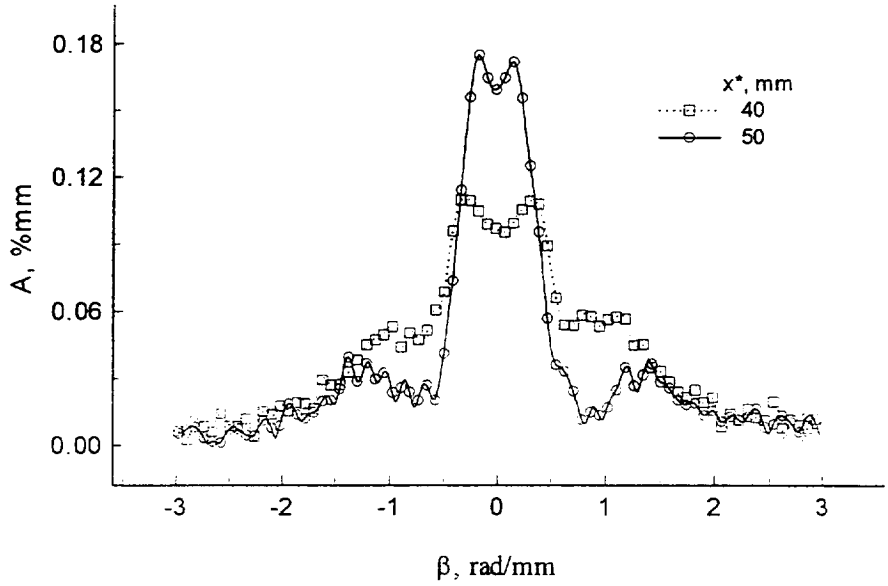

Fig.5.16.a. Amplitude β-spectra excited disturbances in the boundary layer from the second zone

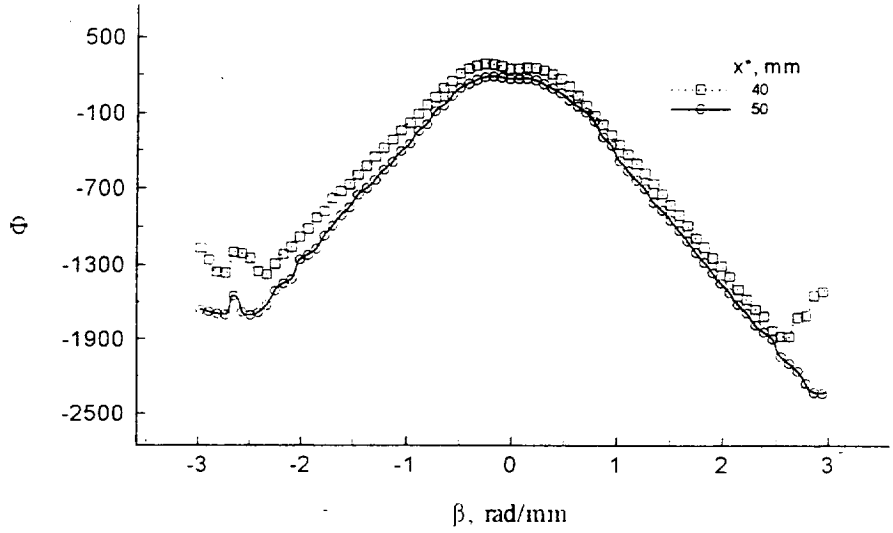

Fig.5.16.b. Phase β-spectra excited disturbances in boundary layer from second zone

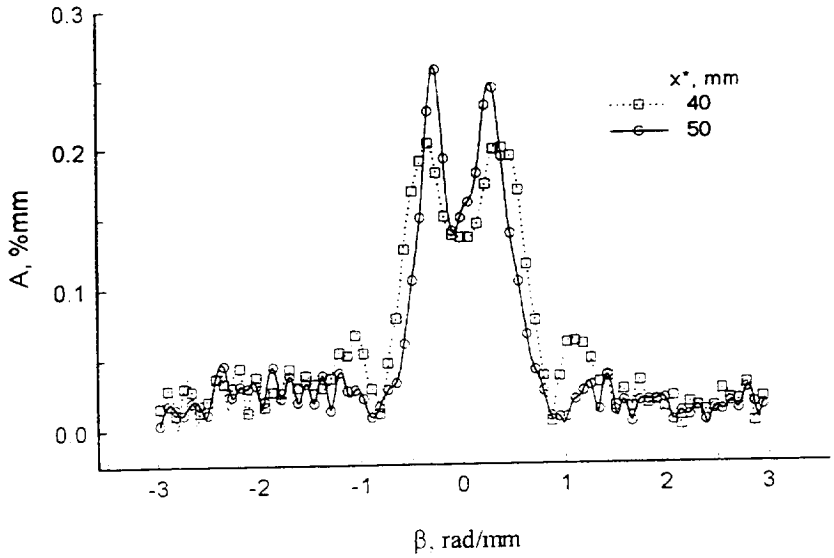

Fig.5.17.a. Amplitude β-spectra excited disturbances in boundary layer from third zone

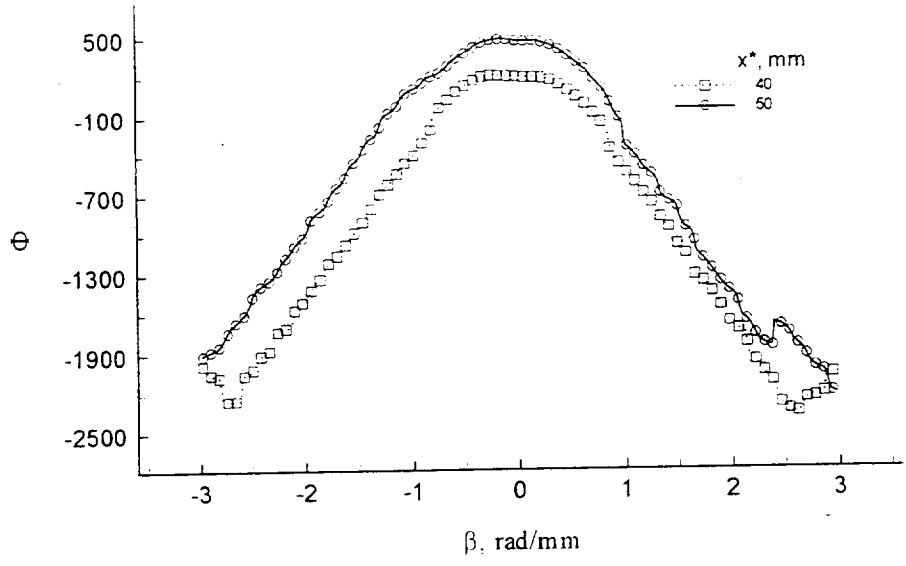

Fig.5.17.b. Phase β-spectra excited disturbances in boundary layer from third zone

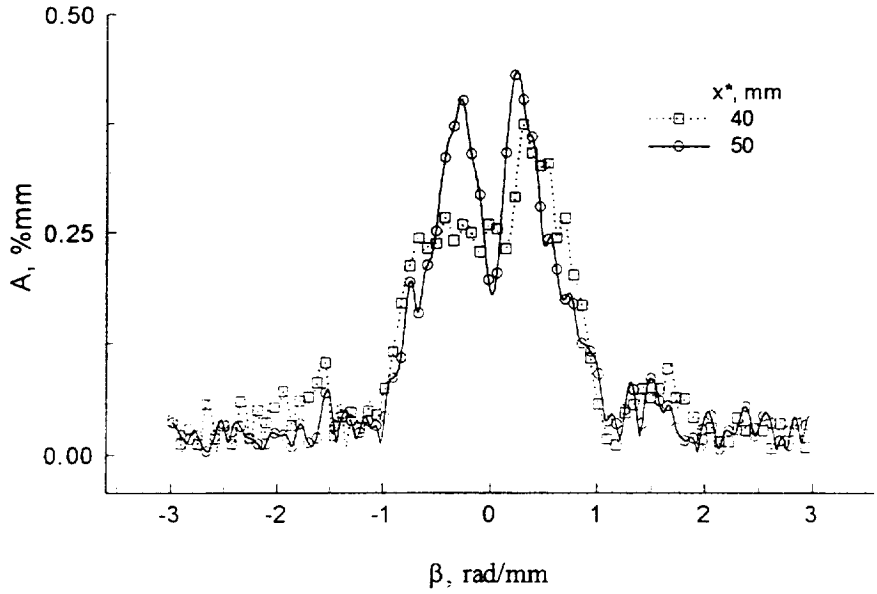

Fig.5.18.a. Amplitude β-spectra excited disturbances in boundary layer from fourth zone

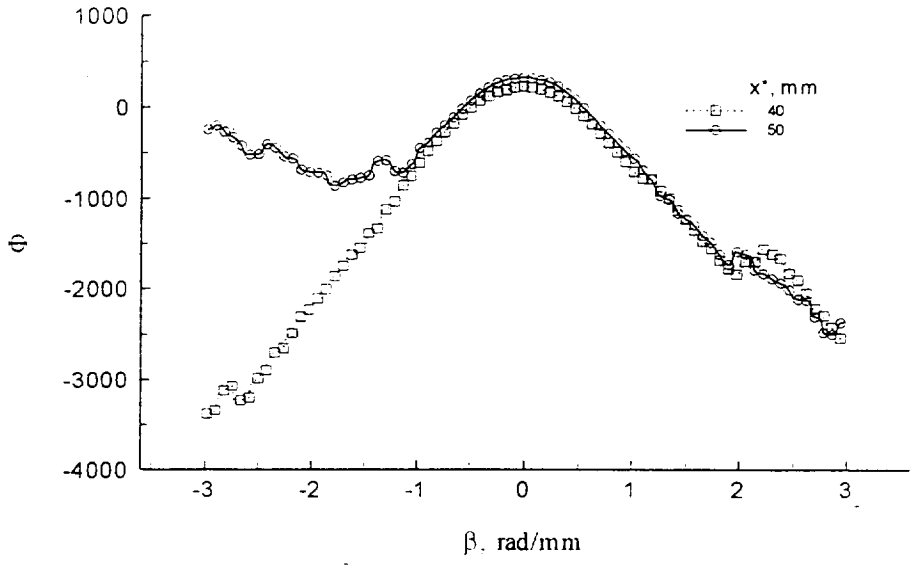

Fig.5.18.b. Phase β-spectra excited disturbances in boundary layer from fourth zone

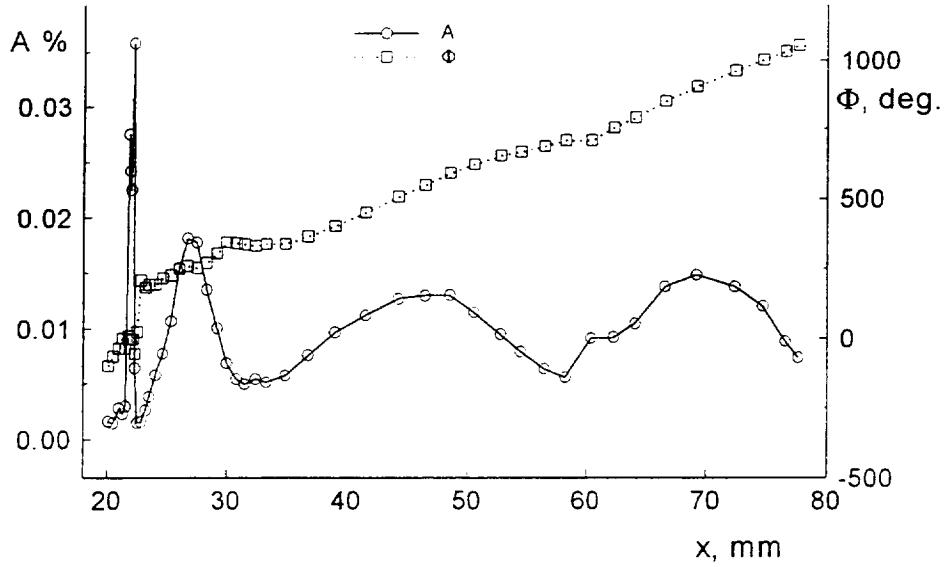

Fig.5.19.a. Streamwise distribution of controlled disturbances at y_1=5.4 mm

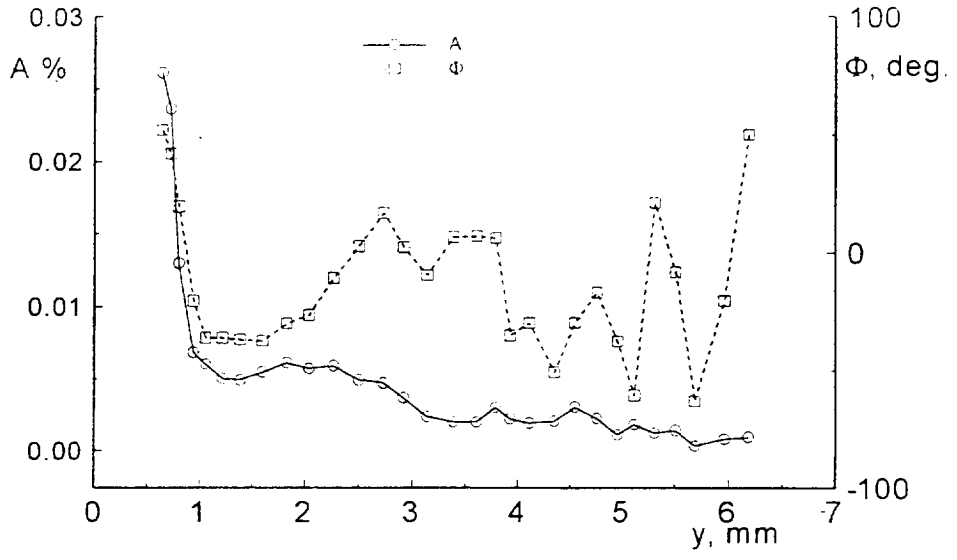

Fig.5.19.b. Normal to plate distribution of controlled disturbances at x^*=50 mm

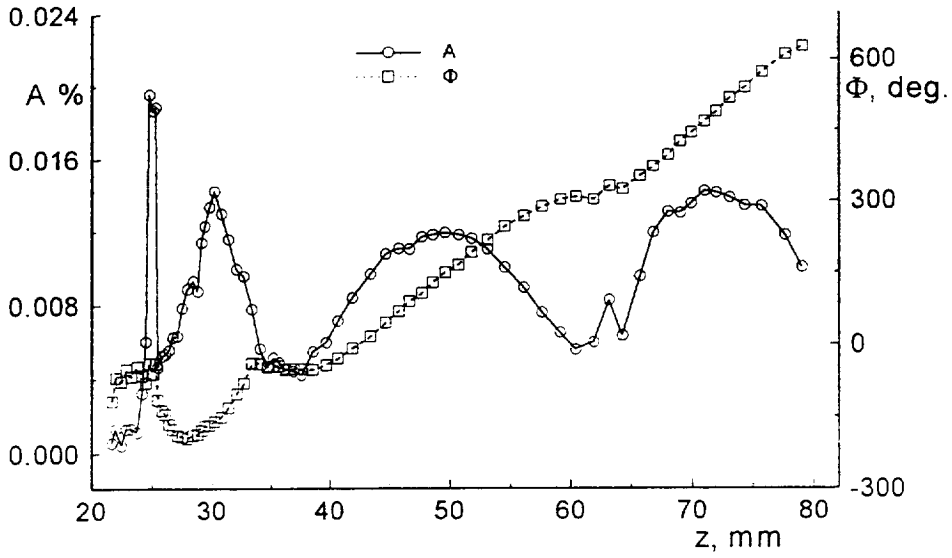

Fig.5.20.a. Streamwise distribution of controlled disturbances at y_1=1.5 mm

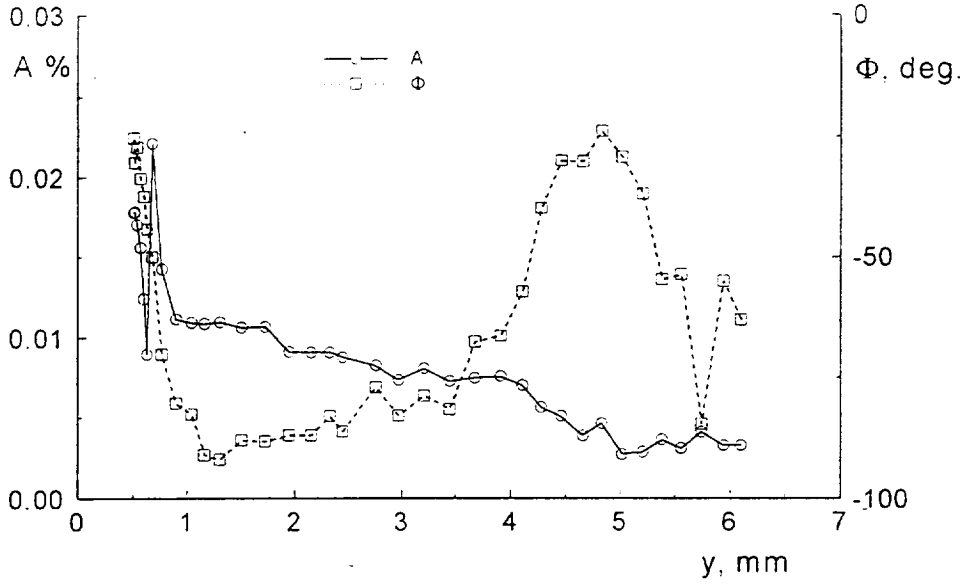

Fig.5.20.b. Normal to plate distribution of controlled disturbances at x^*=50 mm

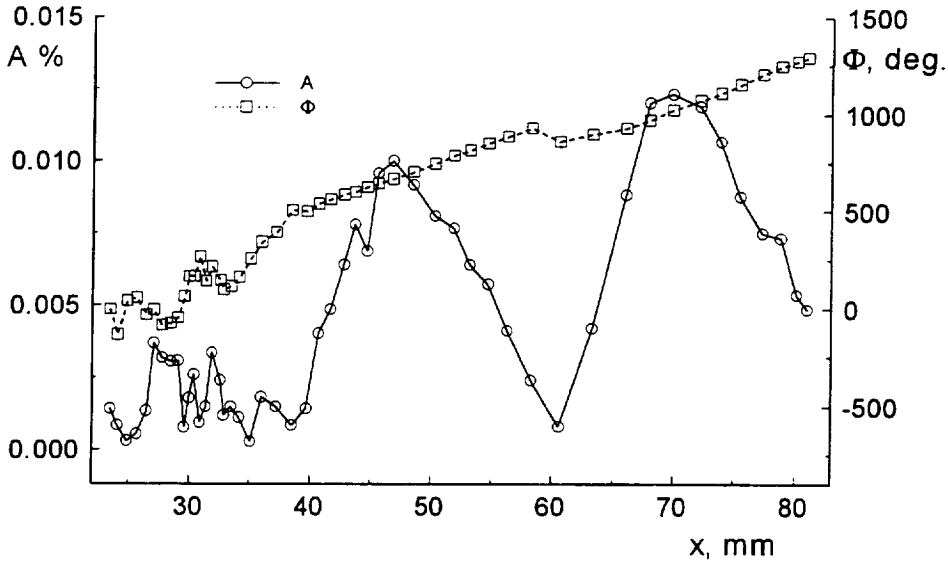

Fig.5.21.a. Streamwise distribution of controlled disturbances at y_1=1.5 mm

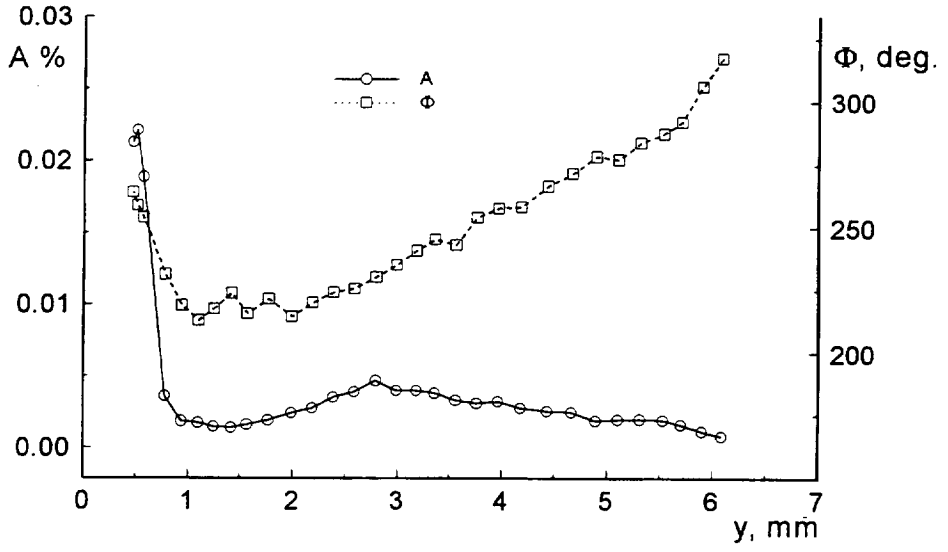

Fig.5.21.b. Normal to plate distribution of controlled disturbances at x^*=50 mm

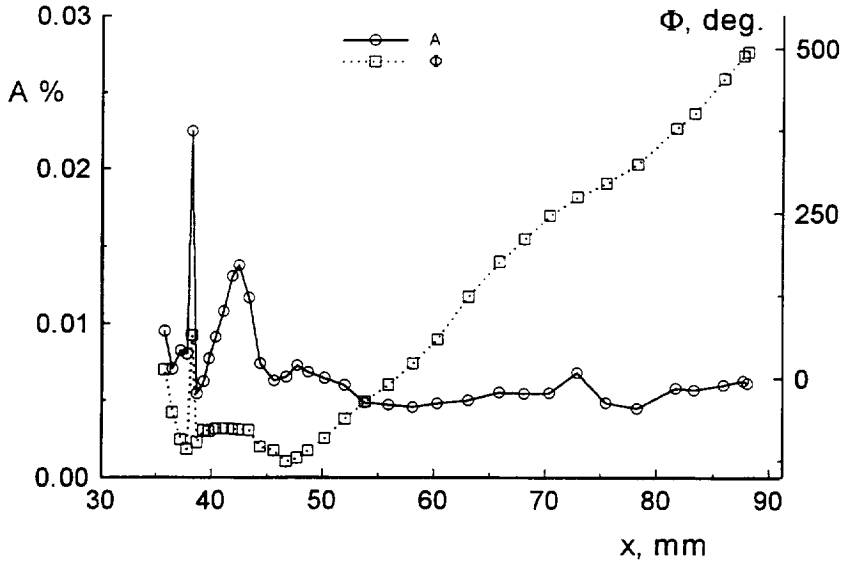

Fig.5.22.a. Streamwise distribution of controlled disturbances at y_1=1.5 mm

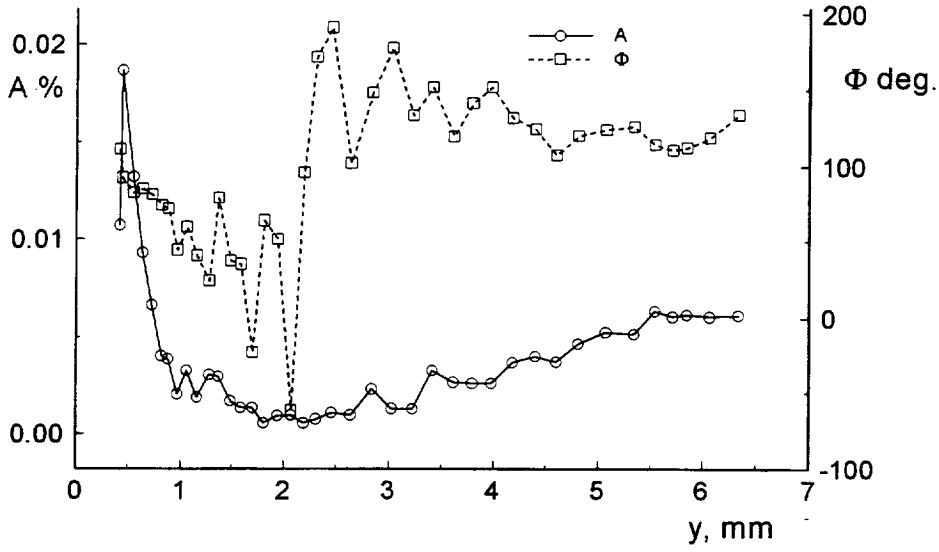

Fig.5.22.b. Normal to plate distribution of controlled disturbances at x^*=50 mm

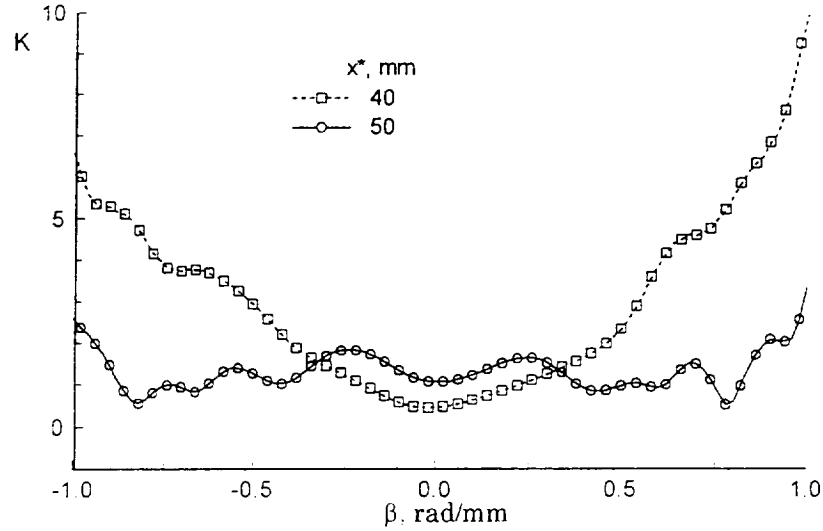

Fig.5.23. Transformation coefficients for disturbances excited from first zone

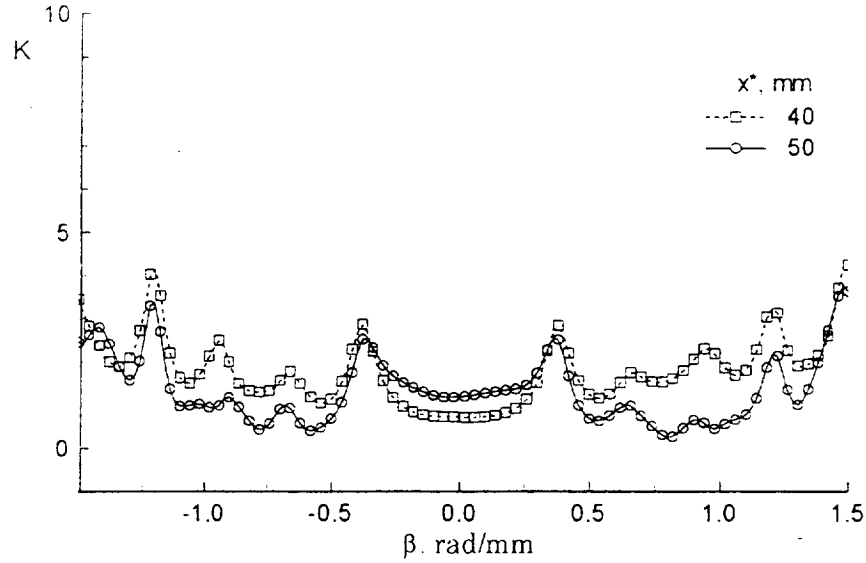

Fig.5.24. Transformation coefficients for disturbances excited from second zone

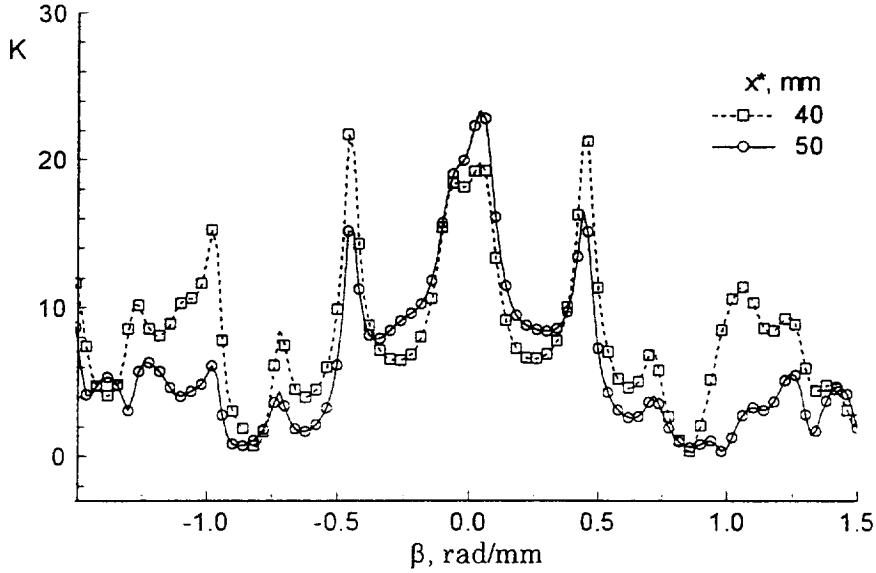

Fig.5.25. Transformation coefficients for disturbances excited from third zone

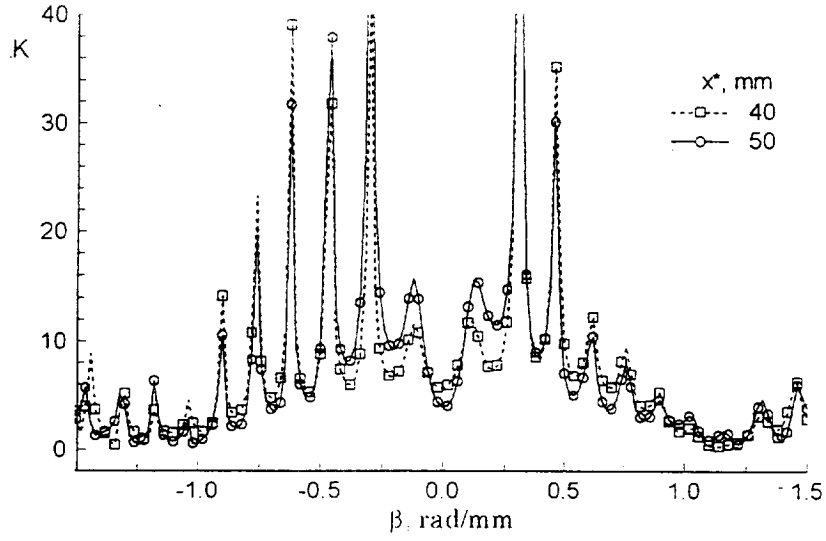

Fig.5.26. Transformation coefficients for disturbances excited from fourth zone

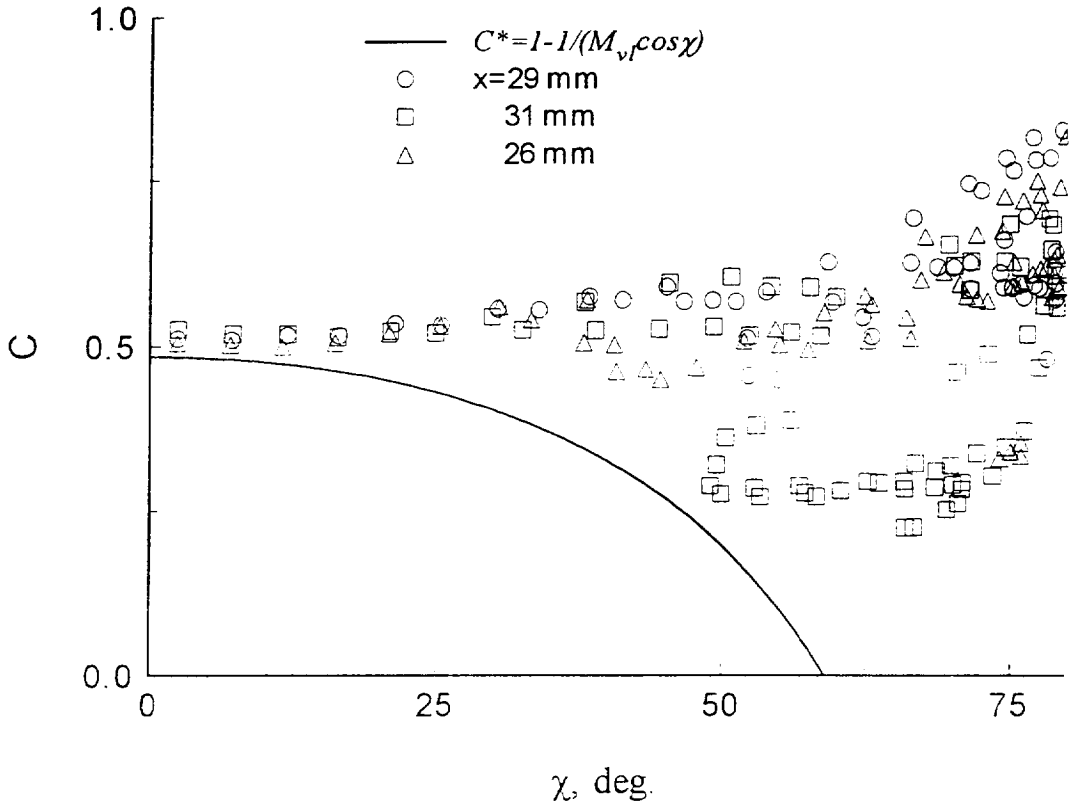

Fig.5.27. Phase velocities excited disturbances

6. Discussion

First of all the we emphasize that an excitation of disturbances in the boundary layer at M=3.5 occurs considerably more intensive compared with M=2 case. According to the theoretical results, obtained by (Fedorov & Khohlov 1992; Gaponov 1995), the intensity of excited disturbances in the boundary layer depends on the spatial orientation of external acoustic waves and grows with inclination angle of waves decreasing in the normal to the model plane. The intensity of the excited disturbances have the maximum when the inclination angle of sound waves in the normal to model plane is zero. However it is necessary to carry out the theoretical analysis of Mach number effect on the transformation of forced sound waves to unstable boundary layer disturbances. We should consider the possible reasons of this difference concerning our experiments.

1. One reason for such difference in the transformation coefficients may be explained from the features of these experiments and the wind tunnel. The neutral stability curves for disturbances with various inclination angles at M=2 and M=3.5, calculated by B. V. Smorodsky, are presented in figs.6.1 and 6.2. On these plots the positions correspond to the experiments are depicted by symbols. The measurements were carried out in unstable area. It is well known, that for supersonic boundary layer in the plate leading edge vicinity there is an area of acoustic disturbances amplification, which expands with Mach number increasing. The experimental data for acoustic branch of neutral stability curve, obtained in our tests for natural disturbances in T-325 wind tunnel are presented in fig.6.3. Expansion of amplification area for acoustic disturbances in the vicinity of the leading edge of the plate with Mach number increasing is obvious for M>2. Also it was obtained, that at M=3.5 and M=4 these areas of acoustic instability and instability region for TS waves cross in a broad band of frequencies. It causes a monotonous growth of disturbances in the boundary layer at M=4.5 immediately from the leading edge, that was obtained by Kendall (1975) too. This also promotes an increase of transformation coefficients K for M=3.5 as compared with M=2 case.

2. A nonlinear effect may be thought as the second reason. All submitted results were considered from the view-point of linear interaction of external acoustic field with supersonic boundary layer in the vicinity of the leading edge of the model. If process of interaction is nonlinear, the direct energy transfer from external low-frequency background into boundary layer eigenoscillations by means of parametric resonance mechanism is possible. In Gaponov et al. 1997, the influence of weakly nonlinear interaction on excitation of unstable modes by acoustic waves was investigated in comparison with linear case. It was obtained there, that nonlinear effects for the disturbance generation is weak in T-325 wind tunnel at M=2. This weak influence is connected with (a) large difference between forced and natural frequencies and (2) a small amplitude of the forced sound waves. But with Mach number increasing the nonlinear receptivity mechanism may occur possibly due to changing of forced disturbance spectra in the wind tunnel. We are sure now that it is not possible in T-325 because a noise level in T-325 test section is too small for this.

3. The main problem in experimental determination of receptivity factors is the indetermination of α_r -spectra of initial controlled disturbances. A separation of radiation field into different zones is rather conventional. It may be proposed to investigate the boundary layer response with more accuracy with the plate *2* continuously moving through radiation field without separation into zones. However this work is very hard. For practical use it may be proposed to use the mean receptivity factors or the maximal value.

The experiments with moving flat plate *2* were performed in this work during the third year. The plate *2* was trapezoidal shaped with sharp leading edge mounted on traversing mechanism with hot-wire at fixed coordinates x^*=50 mm, z=0. The plate *2* moved downstream starting from unforced flow. The data are presented in fig.6.4. for two different intensities of controlled disturbance source. We notice that boundary layer response was observed firstly even if Mach line from controlled disturbance source occurred downstream from the leading edge. The data shown in fig.6.4 are similar to the data presented in figs.3.20, 4.21, 5.1. These data also demonstrate few peaks in amplitude distributions depending on amplitude and phase variation. However, these variations occur more slowly in x-direction. Phase

reduction (from 30 mm to 37 mm) can be explained by the increasing of phase velocity of excited disturbances that shown in fig.4.37. Then phase velocity of excited pulsations is almost constant and for the data presented in fig.6.4 we have growth downstream of phase. Disturbance amplitude increasing from 25 mm to 32 mm let conclude that occur growth of boundary layer receptivity.

Probably the creation of the source of longitudinal controlled disturbances is necessary for the subsequent research of influence of Mach number receptivity and to obtain receptivity factors more precisely. We are discussing a possibility to find the compromise between the theoretical approaches and used here experimental method to reexamine the leading edge receptivity. The goal of future experiments to estimate the receptivity factors more precisely with respect to a concrete theoretic model.

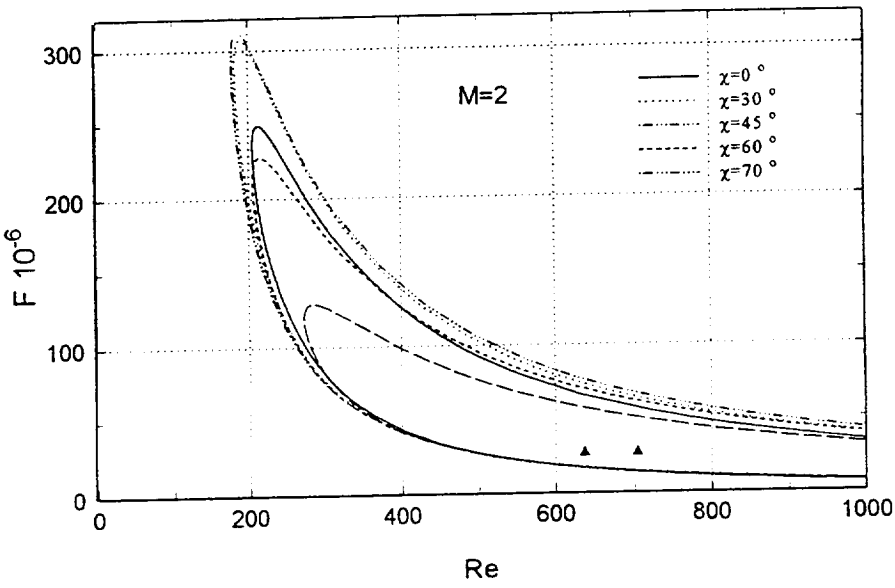

Fig.6.1 Theoretical neutral stability curves for different wave's angle inclination

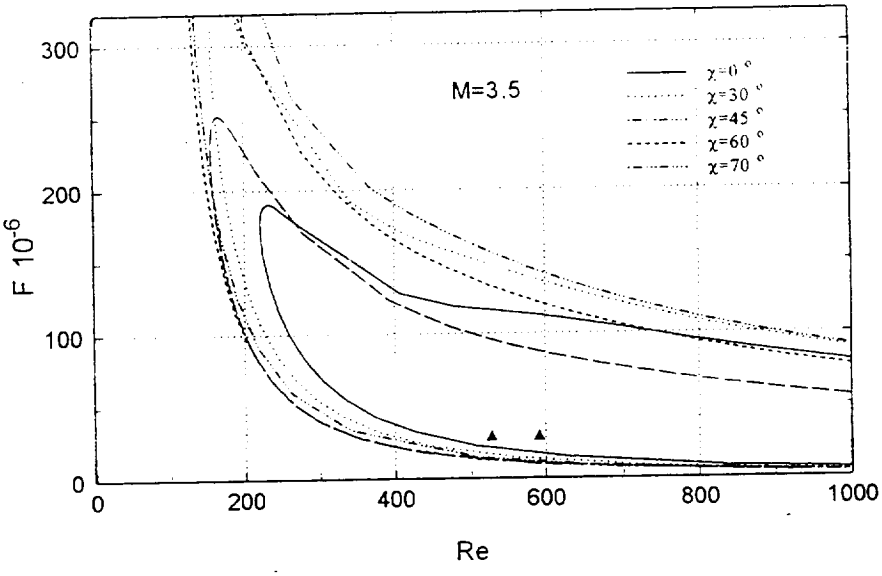

Fig.6.2. Theoretical neutral stability curves for different wave's angle inclination

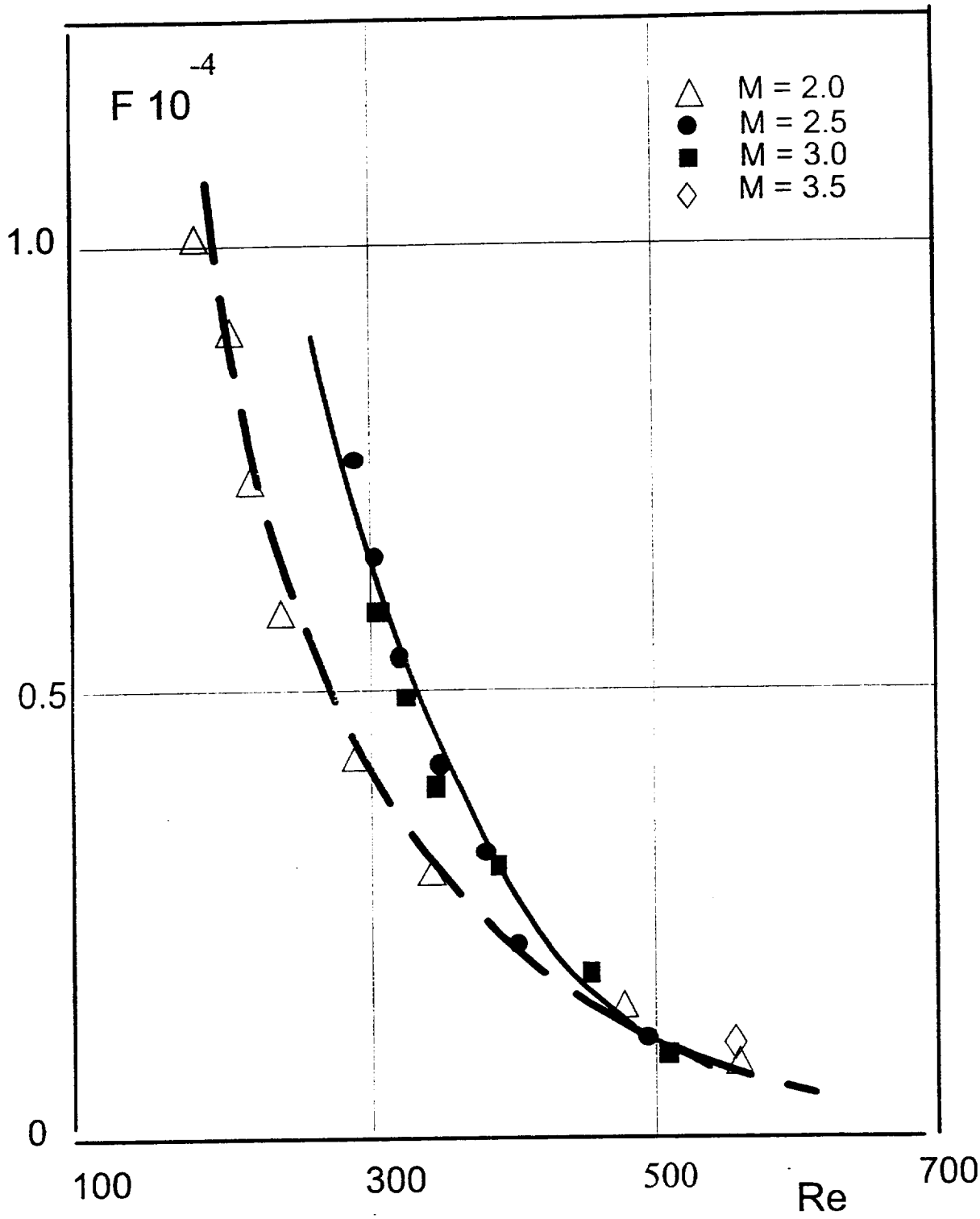

Fig.6.3. Experimental neutral stability curves for natural acoustic disturbances at different Mach numbers

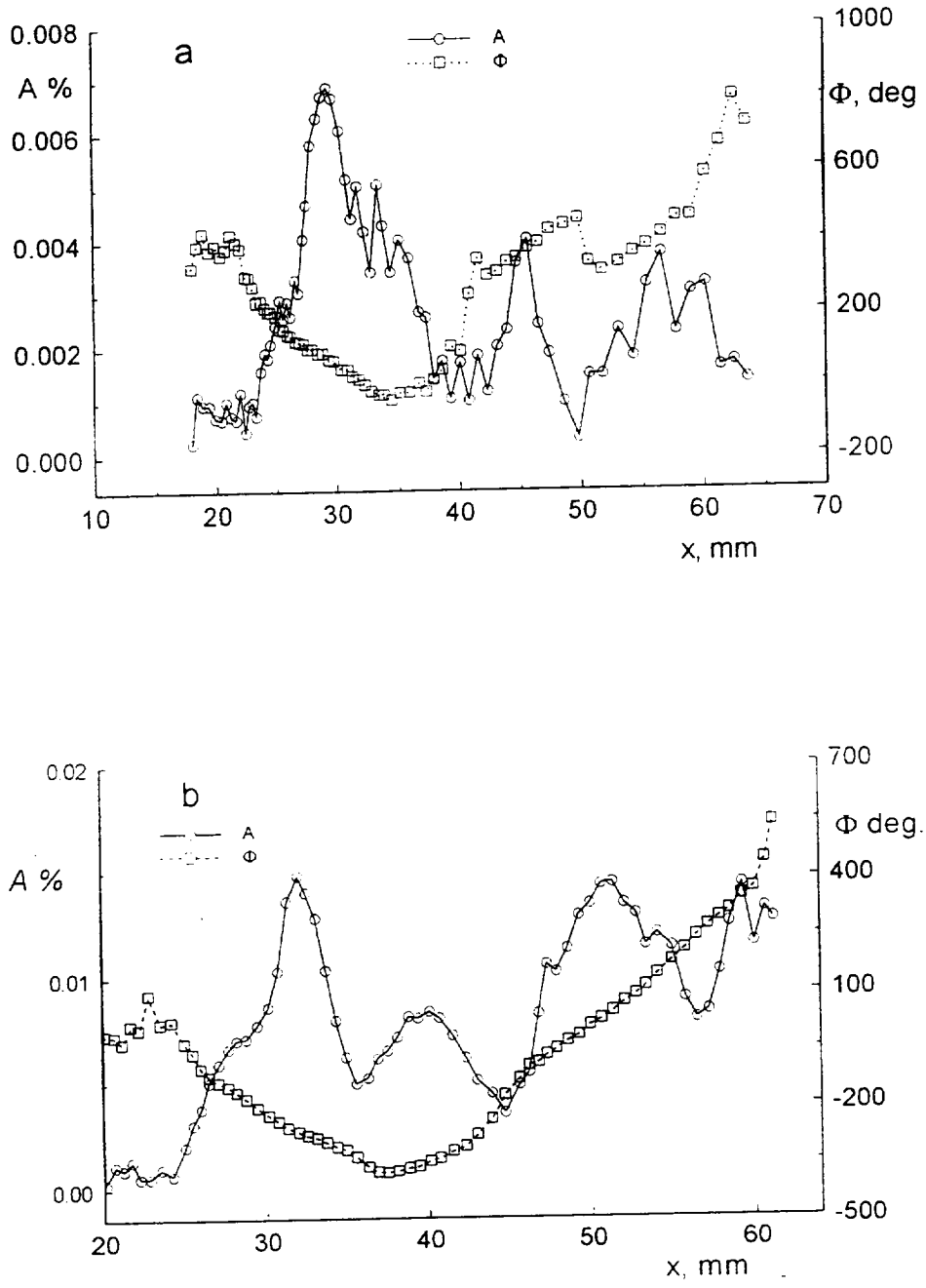

Fig.6.4. Boundary layer response at moving plate through controlled disturbances field

7. Conclusion

According to the Agreement about the cooperation between ITAM SD RAS and NASA (USA) on research of leading edge receptivity at Mach numbers 2 and 3.5, experiments are completed. Hot-wire measurements were carried out and the level and separation of natural fluctuations into modes in free stream of supersonic T-325 ITAM SD RAS wind tunnel were determined at Mach numbers 2 and 3.5 as well as the level of the controlled disturbances field introduced in free stream using a local disturbances source was defined using Kovasznay's method. For fulfillment of these experiments the technical works were carried out to reduce noise level in the test section. For introduction of the controlled disturbances in free stream the disturbances source was improved, to ensure a smooth adjustment of intensity of the excited disturbances. We should emphasis the following results:

During the fist year:

1. It was obtained that mass flux fluctuations increased from 0.07% to 0.2% in the test section at Mach number M=2 in the range of unit Reynolds numbers Re_1 from 7.0×10^6 to 30×10^6 m^{-1}.

2. For M=3.5 and Re_1=7.0×10^6 m^{-1} case the mass flux fluctuations were about 0.15% in the test section.

3. The controlled fluctuations field was investigated in the test section at M=2, Re_1=9.9×10^6 m^{-1} and F=0.25×10^{-4}. It was obtained that disturbances introduced in the free stream are acoustic waves.

4. The controlled fluctuations field was investigated in the test section at M=3.5, Re_1=7.0×10^6 m^{-1} and F=0.28×10^{-4}. It was obtained that disturbances introduced in free stream are acoustic waves too.

During the second year:

5. Leading edge receptivity at Mach numbers M=2 and 3.5 was studied. Experimental study of the controlled disturbances field, introduced into free stream with the help of the local source of disturbances was carried out. Disturbances in the

flat plate boundary layer, excited by external controlled acoustic oscillations in a vicinity of leading edge were measured.

6. Quantitative comparison was carried out between initial level of acoustic free stream disturbances and supersonic boundary layer fluctuations, caused by them. Transformation coefficients of acoustic disturbances into supersonic boundary layer oscillations were obtained.

7. It was found that the excitation of disturbances in the boundary layer by external disturbances occurs considerably more heavily at M=3.5 than at M=2. Transformation coefficients for oblique waves in the boundary layer are higher than for $\beta \approx 0$ waves.

During the third year:

8. After nozzles polishing we found that the mass flux fluctuations increased from 0.05% to 0.08% in the test section at Mach number M=2 in the range of unit Reynolds numbers Re_1 from 6.0×10^6 to 34×10^6 m^{-1}

9. Experimental study of the controlled disturbances field, introduced into free stream with the help of the local source of disturbances, was carried out at M=2. Disturbances in the flat plate boundary layer, excited by the external controlled acoustic oscillations in the vicinity of the blunted leading edge, were measured.

10. Quantitative comparison was made between initial level of acoustic disturbances in free stream and supersonic boundary layer fluctuations, caused by them in the vicinity of blunted leading edge. The transformation coefficients of acoustic disturbances into supersonic boundary layer oscillations were obtained. It was found, that the excitation of disturbances in the boundary layer by external disturbances occurs considerably more heavily in blunted leading edge case than in sharp leading edge case.

11. In these experiments controlled disturbances were found everywhere in the flow above blunted flat plate in the Mach cone region.

These data will serve as a background for the subsequent theoretical research of the leading edge receptivity.

8. Acknowledgment

We are very thankful to Dr. D. Bushnell for support of this work and Dr. J.M. Kendall for the help in development of measuring system. The authors are indebted to Dr. I. I. Maslennikova and Dr. B. V. Smorodsky for stability calculations. This work was supported by NASA, Agreement number NCCW-74 for thefirst year, Agreement number NCC-1-240 for the second and third years.

9. References

Aizin L.B., Polyakov N.F. 1979 Acoustic generation of Tollmien-Schlichting waves over local unevenness of surface immersed in stream. *Preprint ITAM SD RAS №17*, Novosibirsk. (in Russian).

Balakumar P., Malik M.R. 1992 Discrete modes and continuous spectra in supersonic boundary layers. *J. Fluid Mech.* **239,** 631-656.

Bertolotti F.P. 1995 A partial simulation of receptivity and transition in 3-D boundary layers. In *Laminar-Turbulent Transition* (ed. R.Kobayashi). Berlin: Springer-Verlag, pp.491-498.

Bushnell D.M. 1990 Notes on initial disturbances fields for the transition problem. In *Instability and Transition* (eds. M.Y.Hussaini, R.G.Voigt), Springer-Verlag. V.1, pp.217-232.

Bushnell D.M. 1989 Notes on initial disturbances fields for the transition problem. *NASP TM 1051.*

Bushnell D.M., Malic M.R. 1985 Applications of stability theory to laminar flow control. In *Proc. Symp. On the Stability of Time Dependent and Spatially Varying Flows.* (eds. Dwoyer D.L., Hussaini M.Y.), Springer, NY. 1-17.

Choudhari M., Street C.L. 1990 Boundary Layer Receptivity Phenomena in Three-Dimensional and High-Speed Boundary Layers. *AIAA Paper 90-5258.*

Choudhari M., Street C.L. 1992 A finite Reynolds-number approach for the prediction of boundary layer receptivity in localized regions. *Phys. Fluids A.* V.4. No.11, 2495-2514.

Choudhari M., Street C.L. 1993 Interaction of a high speed boundary layer with unsteady freestream disturbances. In *FED - vol.151, Transitional and Turbulent Compressible Flows.* (eds. L.D.Kral, T.A.Zang), ASME, 15-28.

Crouch J.D. 1994 Distributed excitation of Tollmien-Schlichting waves by vortical free-stream disturbances. *Phys. Fluids A.* **6**, 217-223.

Crouch J.D., Spalart P.R. 1995 A study of nonparallel and nonlinear effects on the localized receptivity of boundary layers. *J. Fluid Mech.* **290,** 29-37.

Duck P.W. 1990 The response of a laminar boundary layer in supersonic flow to small amplitude progressive waves. *J. Fluid Mech.* **219,** 423-448.

Duck P.W., Lesseigne D.G., Hussaini M.Y. 1997 The effect of tree-dimensional freestream disturbances on the supersonic flow past a wedge. *Physics of Fluids*, **9**, 456-467.

Fedorov A.V., Khohlov A.P. 1991 Excitation of unstable modes in a supersonic boundary layer by acoustic waves. *Izv. Akad. Sci. USSR. Zh. Mech. Zhid. G.* **4**, 67-74 (in Russian).

Fedorov A.V., Khohlov A.P. 1992 Supersonic boundary layer receptivity to the acoustic disturbances. *Izv. Akad. Sci. USSR. Zh. Mech. Zhid. G.* **1**, 40-47 (in Russian).

Gaponenko V.R., Ivanov A.V., Kachanov Y.S. 1996 Experimental study of 3-D boundary layer receptivity to surface vibration. In *Nonlinear Instability and Transition in Three-Dimensional Boundary Layers*, (eds. P.W.Duck & P.Hall), Kluwer Academic Publishers, pp.389-398.

Gaponov S.A. 1977 Interaction of a supersonic boundary layer with acoustic disturbances. *Izv. Akad. Sci. USSR. Zh. Mech. Zhid. G.* **6,** 51-56 (in Russian).

Gaponov S.A. 1995 On the interaction of a supersonic boundary layer with acoustic waves. *J. Thermophysics and Aeromechanics.* **3,** 181-189.

Gaponov S.A., Maslov A.A. 1980 *Development of disturbances in compressed flows.* Novosibirsk: Nauka Publ.

Gaponov S.A., Maslennikova I.I., Tyushin V.Yu. 1997 Weakly nonlinear interaction of supersonic boundary layer eigen oscillations with external low-frequency acoustic field. In *The thesis of reports IV Siberian seminar «Stability of flows of homogeneous and heterogeneous fluids»*, Novosibirsk, April 23-25, pp.35-36.

Goldstein M.E. 1983 The evolution of Tollmien-Schlichting waves near a leading edge. *J.Fluid Mech.* **127**, 59-81.

Goldstein M.E., Hultgren L.S. 1989 Boundary-layer receptivity to long-wave free-stream disturbances. *Annual Rev. Fluid Mech.* **21**, 137-166.

Heinrich R.A.E., Choudhari M., Kerschen E.J. 1988 A comparison of boundary layer receptivity mechanisms. *AIAA Paper 88-3758.*

Herbert Th., Stukert G.K., Esfahanian V. 1993 Effects of free-stream turbulence on boundary layer transition. *AIAA Paper 93-0488.*

Kachanov Yu.S., Kozlov V.V., Levchenko V.Ya. 1981 *Beginning of turbulence in boundary layer.* Novosibirsk: Nauka Publ. 152 p.

Kachanov Y.S. 1996 Generation development and interaction of instability modes in swept-wing boundary layers. In *Nonlinear Instability and Transition in Three-Dimensional Boundary Layers*, (eds. P.W.Duck & P.Hall), Kluwer Academic Publishers, pp.115-132.

Kendall J.M. 1975 Wind tunnel experiments relating to supersonic and hypersonic boundary-layer transition. *AIAA J.* **13**, N 3, 290-299.

Kendall J.M. 1990 Boundary layer receptivity to freestream turbulence. *AIAA Paper 90-1504.*

Kendall J.M. 1998 Experiments on boundary layer receptivity to freestream turbulence. *AIAA Paper 98-0530.*

Klebanoff P.S. 1971 Effect of freestream turbulence on the laminar boundary layer. Bull. Amer. Phys. Soc., v.10, No.11, pp.1323.

Kobayashi R., Fukunishi Y., Nishikawa T., Kato T. 1995 The receptivity of flat-plate boundary-layers with two-dimensional roughness elements to freestream sound and its control. In *Laminar-Turbulent Transition* (ed. R.Kobayashi). Berlin: Springer-Verlag, pp.507-514.

Kosinov A.D., Maslov A.A., Semionov N.V. 1983 Methods of artificial disturbances introduction in a supersonic flow. *Preprint ITAM SD RAS* №*34-83,* Novosibirsk. (in Russian).

Kosinov A.D., Maslov A.A., Semionov N.V., Shevelkov S.G. 1990 Wave structure of artificial disturbances in a supersonic boundary layer on a flat plate. *J. AMTP.* **31**, 250-252.

Kosinov A.D., Maslov A.A., Semionov N.V. 1994 Methods of controlled disturbances generation for experimental investigation of supersonic boundary layer

receptivity. In *Proceedings of International Conference on the Methods of Aerophysical Research*. Novosibirsk, pp.138-144.

Kosinov A.D., Maslov A.A., Semionov N.V. 1996 Modified method of experimental study of supersonic boundary layer receptivity. In *Proc. Int. Conf. on the Methods of Aerophys. Research*, Novosibirsk, vol.3. 161-166.

Kosinov A.D., Maslov A.A., Shevelkov S.G. 1990 Experiments on the stability of supersonic laminar boundary layer. *J. Fluid Mech.* **219**, 621-633.

Kosinov A.D., Semionov N.V., Shevelkov S.G. 1992 Special features of generation and development of a harmonical wave in supersonic boundary layer. In *Recent Advances in Experimental Fluid Mechanics*. IAP Beijing, pp.53-58.

Kosinov A.D., Semionov N.V., Shevelkov S.G., Zinin O.I. 1994 Experiments of the nonlinear instability of supersonic boundary layers. In *Nonlinear Instability of Nonparallel Flows* (eds. S.P.Lin, W.R.C.Phillips, D.T.Valentine). Berlin: Springer-Verlag, pp.196-205.

Kosorygin V.S., Radeztsky R.H., Jr., Saric W.S. 1995 Laminar-boundary layer, sound receptivity and control. In *Laminar-Turbulent Transition* (ed. R.Kobayashi). Berlin: Springer-Verlag, pp.517-524.

Kovasznay L.S.G. 1950 The Hot-wire anemometer in supersonic flow. *J. Aero Sciences*. **17**, 565-573.

Kovasznay L.S. 1953 Turbulence in supersonic flow. *J. Aero Sciences*. **20**, 657-674.

Mack L.M. 1969 Boundary layer stability theory. *Document 900-277*. Pasadena: California, JPL.

Mack L.M. 1975 Linear stability theory and the problem of supersonic boundary layer transition. *AIAA J.* **13**, 423-448.

Maslov A.A., Semionov N.V. 1986 Excitation of eigen boundary layer oscillations by external acoustic field. *Izv. Akad. Sci. USSR. Zh. Mech. Zhid. G.* **3**, 74-78 (in Russian).

Maslov A.A., Semionov N.V. 1987 Acoustic disturbances and supersonic boundary layer. In *Problems of Nonlinear Acoustics*. Novosibirsk, pp.132-134.

Maslov A.A., Semionov N.V. 1987 Radiation of acoustic oscillations from the supersonic boundary layer. *Izv. SO AN USSR. Seria Tech. Nauk.* **7**, vyp.2, 58-63 (in Russian).

Maslov, A.A., Semionov, N.V. 1989 Structure of artificial disturbances, caused by the external acoustic field, in the supersonic boundary layer. *Izv. Akad. Sci. USSR. Zh. Mech. Zhid. G.* **3**, 113-117. (Russian).

Maslov A.A., Shiplyuk A.N., Sidorenko A.A., Arnal D. 1998 Leading edge receptivity of the hypersonic boundary layer on a flat plate. *Preprint ITAM SD RAS №1-98*, Novosibirsk.

Morkovin M.V. 1969 Critical evaluation of transition from laminar to turbulent shear layers with emphasis on hypersonically traveling bodies. *AFFDL-TR-68-149.* Air Force Flight Dynamics Laboratory, Wright-Patterson AFB, OH.

Nayfeh A.H., Ashour O.N. 1994 Acoustic receptivity of the boundary layer to Tollmien-Schlichting waves resulting from a finite-height hump at finite Reynolds numbers. *Phys. Fluids.* **6**, N 11, 3705-3716.

Nishioka M., Morkovin M.V. 1986 Boundary-layer receptivity to unsteady pressure gradients: experiments and overview. *J.Fluid Mech.* **171**, 219-261.

Reshotko E. 1976 Boundary layer stability and transition. *Annual Review of Fluid Mechanics.* **8**, 311-349.

Reshotko E. 1994 Boundary layer instability, transition and control. *AIAA Paper 94-0001.*

Saric W.S., Reed H.L., Kerschen E.J. 1994 Leading-edge receptivity to sound: Experiments, DNS, theory. *AIAA Paper 94-2222.*

Schmisseur J.D., Schnider S.P., Collicott S.H. Receptivity of the Mach-4 boundary layer on an elliptic cone to laser-generated localized free stream perturbations. *AIAA Paper 98-0532.*

Semionov N.V. 1998 Structure of external controlled disturbances used at receptivity studing of supersonic boundary layer.

Semionov N.V., Kosinov A.D., Maslov A.A. 1996 Experimental investigation of supersonic boundary layer receptivity. In *Transitional Boundary Layers in Aeronautics.* Noth-Holland, Amsterdam, 413-420.

Semionov N.V., Kosinov A.D., Maslov A.A. 1997 Experimental study of boundary layer receptivity at M=3.5. *Stability and Transition of Boundary Layer Flows*, Abstracts. EUROMECH Colloquium 359.

Smits A.J., Hayakawa K., Muck K.C. 1983 Constant temperature hot-wire anemometer practice in supersonic flows. *Experiments in Fluids.* **1**, 83-92.

Westin K.J.A., Boiko A.V., Klingmann G.B., Kozlov V.V., Alfredsson P.H. 1994 Experiments in a boundary layer subjected to free stream turbulence. Part 1. Boundary layer structure and receptivity. *J.Fluid Mech.* **281**, 193-218.

Xiaolin Zhong 1997 Direct numerical simulation of hypersonic boundary layer transition over blunt leading edge, part II: receptivity to sound. *AIAA Paper 97-0756.*

Zinovjev V.N., Lebiga V.A. 1990 Hot-wire measurements in compressible flow. *Izv. SO AN USSR. Seria Tech. Nauk.* **5**, 22-31 (in Russian).

REPORT DOCUMENTATION PAGE

Form Approved
OMB No. 0704-0188

1. AGENCY USE ONLY *(Leave blank)*	2. REPORT DATE	3. REPORT TYPE AND DATES COVERED
	June 1998	Contractor Report

4. TITLE AND SUBTITLE
Supersonic Leading Edge Receptivity

5. FUNDING NUMBERS
NCC1-240
282-10-01-01

6. AUTHOR(S)
Anatoly A. Maslov

7. PERFORMING ORGANIZATION NAME(S) AND ADDRESS(ES)
Institute of Theoretical and Applied Mechanics (ITAM)
Siberian Division
Russian Academy of Sciences
Novosibirsk, 630090, Russia

8. PERFORMING ORGANIZATION REPORT NUMBER

9. SPONSORING/MONITORING AGENCY NAME(S) AND ADDRESS(ES)
National Aeronautics and Space Administration
Langley Research Center
Hampton, VA 23681-2199

10. SPONSORING/MONITORING AGENCY REPORT NUMBER
NASA/CR-1998-208445

11. SUPPLEMENTARY NOTES
Langley Technical Monitor: Dennis M. Bushnell

12a. DISTRIBUTION/AVAILABILITY STATEMENT
Unclassified–Unlimited
Subject Category 02 Distribution: Standard
Availability: NASA CASI (301) 621-0390

12b. DISTRIBUTION CODE

13. ABSTRACT *(Maximum 200 words)*
This paper describes experimental studies of leading edge boundary layer receptivity for imposed stream disturbances. Studies were conducted in the supersonic T-325 facility at ITAM and include data for both sharp and blunt leading edges. The data are in agreement with existing theory and should provide guidance for the development of more complete theories and numerical computations of this phenomena.

14. SUBJECT TERMS
Viscous flow; Boundary layer transition; Receptivity; Supersonic flow

15. NUMBER OF PAGES
145

16. PRICE CODE
A07

17. SECURITY CLASSIFICATION OF REPORT	18. SECURITY CLASSIFICATION OF THIS PAGE	19. SECURITY CLASSIFICATION OF ABSTRACT	20. LIMITATION OF ABSTRACT
Unclassified	Unclassified	Unclassified	

NSN 7540-01-280-5500

Standard Form 298 (Rev. 2-89)
Prescribed by ANSI Std. Z39-18
298-102